HIGGS PHENOMENOLOGY AND NEW PHYSICS BEYOND THE STANDARD MODEL

by

Bin He

A dissertation submitted to the Faculty of the University of Delaware in partial fulfillment of the requirements for the degree of Doctor of Philosophy in Physics

Summer 2015

HIGGS PHENOMENOLOGY AND NEW PHYSICS BEYOND THE STANDARD MODEL

by

Bin He

Approved: ______________________________

Edmund R. Nowak, Ph.D.
Chair of the Department of Physics

Approved: ______________________________

George H. Watson, Ph.D.
Dean of the College of Arts and Sciences

Approved: ______________________________

James G. Richards, Ph.D.
Vice Provost for Graduate and Professional Education

I certify that I have read this dissertation and that in my opinion it meets the academic and professional standard required by the University as a dissertation for the degree of Doctor of Philosophy.

Signed: ____________________

Qaisar Shafi, Ph.D.
Professor in charge of dissertation

I certify that I have read this dissertation and that in my opinion it meets the academic and professional standard required by the University as a dissertation for the degree of Doctor of Philosophy.

Signed: ____________________

Stephen Barr, Ph.D.
Member of dissertation committee

I certify that I have read this dissertation and that in my opinion it meets the academic and professional standard required by the University as a dissertation for the degree of Doctor of Philosophy.

Signed: ____________________

John Gizis, Ph.D.
Member of dissertation committee

I certify that I have read this dissertation and that in my opinion it meets the academic and professional standard required by the University as a dissertation for the degree of Doctor of Philosophy.

Signed: ____________________

Edward Lyman, Ph.D.
Member of dissertation committee

I certify that I have read this dissertation and that in my opinion it meets the academic and professional standard required by the University as a dissertation for the degree of Doctor of Philosophy.

Signed: ______________________________

Nobuchika Okada, Ph.D.
Member of dissertation committee

ACKNOWLEDGEMENTS

I would like to express my sincere thanks to my adivosor, Prof. Qaisar Shafi, for his excellent guidance and continuous support for my PhD study. I would never have been able to finish this dissertation without his support.

I am also grateful to Ilia Gogoladze, who has provided extraordinary help any time I needed it. His patience and knowledge has helped me overcome all the difficulties in my research.

I would also like to thank my colleagues Adeel Ajaib, Matt Civiletti, Rizwan Khalid, Fariha Nasir, Shabbar Raza, Mansoor Rehman and Cem Salih. I have been inspired and sustained by collaborating with them throughout my PhD.

I owe heartfelt thanks to my family and all my friends at Delaware for their unwavering love, support and encouragement.

Finally, I would like to express gratitude to my dissertation committee members, Prof. Stephen Barr, Prof. John Gizis, Prof. Edward Lyman, and Prof. Nobuchika Okada, for their valuable time and insightful comments.

TABLE OF CONTENTS

LIST OF TABLES

LIST OF FIGURES

ABSTRACT

The existence of the Higgs boson was predicted in the 1960's. The discovery of the Higgs boson in 2012 at the Large Hadron Collider (LHC) has been a remarkable triumph of the Standard Model (SM) and particle physics. However, there are still fundamental questions that cannot be answered by the SM. A variety of extensions to the SM have been proposed to explain these mysteries. In this thesis we explore the Higgs boson mass in several extensions to the SM. We first study the impact of vectorlike fermions on the SM Higgs mass bounds. The presence of these fermions significantly modifies the vacuum stability and perturbativity bounds on the mass of the SM Higgs boson. The new vacuum stability bound in this extended SM is estimated to be 117 GeV, to be compared with the SM prediction of about 129 GeV.

The non-minimal gravitational coupling $\xi H^\dagger H \mathcal{R}$ between the SM Higgs doublet H and the curvature scalar $\mathcal{R}$ opens up a very intriguing scenario for inflationary cosmology. In the presence of this coupling, the effective ultraviolet cutoff scale is given by $\Lambda \approx m_P/\xi$, where m_P is the reduced Planck mass, and $\xi \gtrsim 1$ is a dimensionless coupling constant. In type I and type III seesaw extended SM, we investigate the implications of this non-minimal gravitational coupling for the SM Higgs boson mass bounds based on vacuum stability and perturbativity arguments. A lower bound on the Higgs boson mass close to 120 GeV is realized with type III seesaw and $\xi \sim 10 - 10^3$.

Supersymmetry is by far the most compelling extension of the SM. We consider extensions of the Next-to-Minimal Supersymmetric Standard Model (NMSSM) in which the observed neutrino masses are generated through a TeV scale inverse seesaw mechanism. The new particles associated with this mechanism can have sizable couplings to the Higgs field which can yield a large contribution to the mass of the

lightest CP-even Higgs boson. With this new contribution, a 126 GeV Higgs is possible along with order of 200 GeV masses for the stop quarks for a broad range of $\tan\beta$.

Finally we study the implications of the inverse seesaw mechanism on the sparticle spectrum in the Constrained Minimal Supersymmetric Standard Model (CMSSM) and Non-Universal Higgs Model (NUHM2). Employing the maximal value of the Dirac Yukawa coupling involving the up type Higgs doublet provides a 2-3 GeV enhancement of the lightest CP-even Higgs boson mass. This effect permits one to have lighter colored sparticles in the CMSSM and NUHM2 scenarios with LSP neutralino, which can be tested at LHC14.

Chapter 1

INTRODUCTION

Our picture of the universe is based on elementary particles and the interactions between them. After efforts of several generations of physicists, they are summarized in a theory called the Standard Model (SM) of particle physics [1]. The SM is based on the gauge symmetry groups $SU(3)_C \times SU(2)_L \times U(1)_Y$. In the SM, there are two kinds of particles: fermions and gauge bosons. The fermions have spin $\frac{1}{2}$. They are the elementary particles that matter is made of in nature. They fall into two different categories: quarks and leptons. The fermions and their quantum numbers in the SM are listed in Table 1.1. u, d, c, s, t and b stand for up-, down-, charm-, strange-, top- and bottom-type quark. e, μ and τ stand for electron, muon and tau lepton. ν stands for neutrino. The subscripts L and R stand for left- and right-handed.

	Symbol	Particle			$SU(3)$	$SU(2)_L$	$U(1)_Y$
Quarks	q_L^i	$\begin{pmatrix} u_L \\ d_L \end{pmatrix}$	$\begin{pmatrix} c_L \\ s_L \end{pmatrix}$	$\begin{pmatrix} t_L \\ b_L \end{pmatrix}$	3	2	$\frac{1}{6}$
	u_R^i	u_R	c_R	t_R	$\overline{3}$	1	$-\frac{2}{3}$
	d_R^i	d_R	s_R	b_R	$\overline{3}$	1	$\frac{1}{3}$
Leptons	l_L^i	$\begin{pmatrix} \nu_e \\ e_L \end{pmatrix}$	$\begin{pmatrix} \nu_\mu \\ \mu_L \end{pmatrix}$	$\begin{pmatrix} \nu_\tau \\ \tau_L \end{pmatrix}$	1	2	$-\frac{1}{2}$
	e_R^i	e_R	μ_R	τ_R	1	1	1

Table 1.1: Feimions and their quantum numbers in the SM.

The gauge bosons are the force carriers that mediate the interactions between the fermions in the SM. There are three kinds of interactions in the SM: electromagnetic, weak and strong interactions. The corresponding gauge bosons are listed in Table 1.2. The photon and gluons are massless. However, the W and Z bosons are massive. Actually, they are very heavy compared to other particles in the SM. This mystery was not well understood until the emergence of the Higgs mechanism. The Higgs mechanism is a mathematical model proposed in the 1960's by Higgs, Brout, Englert, Guralnik, Hagen and Kibble [2]. By introducing a pair of complex scalar fields, it provides an explanation for the masses of W and Z bosons in the SM through spontaneous electroweak symmetry breaking (EWSB). The fermions in the SM also receive masses through a Yukawa interaction with the Higgs field. A detailed review on the Higgs mechanism in the SM can be found in Ref. [3].

	Gauge boson	Symbol
Electromagnetic interactions	photon	γ
Weak interactions	W boson	W^+, W^-
	Z boson	Z
Strong interactions	gluon	g

Table 1.2: Gauge bosons and their quantum numbers in the SM.

The SM has been the most successful theory in human's history. However, it is not a complete theory of elementary particles. There are fundamental physical phenomena in nature that the SM cannot explain. Below I list several deficiencies of the SM:

1. Neutrino masses:

   Neutrinos are massless in the SM. However, solar and atmospheric neutrino oscillation experiments have established that at least two neutrino states are massive [4]. Adding neutrino mass terms in the SM will spoil the gauge symmetries of the theory. The seesaw mechanism is a simple and promising extension of the SM to incorporate the neutrino masses and mixings observed in solar and atmo-spheric neutrino oscillations. A detailed review on seesaw mechanims can be found in Ref. [5].

2. Gravity:

   Although the SM has explained three fundamental interactions between elementary particles very well, it has failed to include another fundamental interaction: gravity. The most successful theory of gravity to date is Einstein's general relativity. However, the SM is a theory based on quantum mechanics, which is unfortunately incompatible with general relativity. This conflict is actually a central problem of modern physics. Numerous attempts have been made to resolve this conflict, and a number of theories have been proposed. For example, string theory, loop quantum gravity, group field theory, *etc.*

3. Dark matter and dark energy:

   Cosmological observations have provided strong evidence for the existence of dark matter and dark energy. It turns out that the fermions in the SM only accounts for 4.9% of the matter/energy of the universe [7]. Determining the nature of dark matter and dark energy is one of the challenges in particle physics.

Supersymmetry is by far the most compelling extension of the SM. The study of supersymmetry is motivated by solving the hierarchy problem in the SM. Supersymmetry also offers gauge coupling unification and a dark matter candidate. A comprehensive review on supersymmetry can be found in Ref. [6].

In this chapter I will present a brief introduction to the Higgs mechanism, seesaw mechanism and supersymmetry, which are most relevant to my research.

1.1 The Higgs Mechanism

Let us start with a complex scalar field ϕ with the following Lagrangian

$$\mathscr{L} = (\partial_\mu \phi\ )^* (\partial^\mu \phi) - V(\phi)\ ,\ V(\phi) = -\mu^2 (\phi^* \phi) + \frac{1}{2}\lambda (\phi^* \phi)^2 \tag{1.1}$$

This Lagrangian is invariant under the global $U(1)$ phase transformation

$$\phi \to e^{i\alpha}\phi. \tag{1.2}$$

If $\mu^2 < 0$, If $\mu^2 > 0$, the field ϕ acquires a non-zero vacuum expectation value (VEV), and the $U(1)$ symmetry is spontaneously broken. The minimum of the potential occurs at

$$\langle \phi^2 \rangle = \frac{\mu^2}{\lambda}. \tag{1.3}$$

The potential is illustrated in Fig.(1). Let us expand the Lagrangian about a particular ground state

$$\mathrm{Re}(\phi) = \sqrt{\frac{\mu^2}{\lambda}}, \qquad \mathrm{Im}(\phi) = 0. \tag{1.4}$$

If we define

$$\frac{\eta}{\sqrt{2}} \equiv \mathrm{Re}(\phi) - \sqrt{\frac{\mu^2}{\lambda}}, \qquad \frac{\xi}{\sqrt{2}} \equiv \mathrm{Im}(\phi), \tag{1.5}$$

The Lagrangian can be rewritten as the following:

$$\begin{aligned} \mathscr{L} &= \left[\frac{1}{2}\left(\partial_\mu \eta\right)\left(\partial^\mu \eta\right) - \mu^2\eta^2\right] + \left[\frac{1}{2}\left(\partial_\mu \xi\right)\left(\partial^\mu \xi\right)\right] \\ &+ \left[-\frac{\sqrt{2}}{2}\mu\sqrt{\lambda}\eta^3 - \frac{\sqrt{2}}{2}\mu\sqrt{\lambda}\eta\xi^2 - \frac{1}{8}\lambda\eta^4 - \frac{1}{4}\lambda\eta^2\xi^2 - \frac{1}{8}\lambda\xi^4 + \frac{1}{2}\frac{\mu^4}{\lambda}\right]. \end{aligned} \tag{1.6}$$

The scalar field η acquires a mass term $m_\eta = \sqrt{2}\mu$, but the other scalar field ξ is massless. It has been shown that for every spontaneously broken continuous symmetry, the theory must contain a massless particle. These massless particles are called Goldstone bosons.

If the scalar filed ϕ is coupled to a massless gauge field A_μ, the Lagrangian can be made invariant under the local $U(1)$ transformation

$$\phi \rightarrow e^{i\alpha(x)}\phi, \tag{1.7}$$

by introducing the covariant derivative:

$$\mathscr{D}_\mu = \partial_\mu + iqA_\mu, \tag{1.8}$$

where q is the conserved charge. The Lagarangian involving the scalar field ϕ and the gauge field A_μ is

$$\mathscr{L} = \left(\mathscr{D}_\mu\phi\right)^* \mathscr{D}^\mu\phi - V(\phi) - \frac{1}{4}F^{\mu\nu}F_{\mu\nu}, \tag{1.9}$$

where $F_{\mu\nu} \equiv \partial_\mu A_n u - \partial_\nu A_m u$. We can rewrite the Lagrangian in terms of the scalar fields η and ξ as before:

$$\begin{aligned}
\mathscr{L} &= \left[\frac{1}{2}\left(\partial_\mu \eta\right)\left(\partial^\mu \eta\right) - \mu^2\eta^2\right] + \left[\frac{1}{2}\left(\partial_\mu \xi\right)\left(\partial^\mu \xi\right)\right] \\
&+ \left[-\frac{1}{4}F^{\mu\nu}F_{\mu\nu} + \frac{q^2\mu^2}{\lambda}A^\mu A_\mu\right] \\
&+ \left[-\frac{\sqrt{2}}{2}\mu\sqrt{\lambda}\eta^3 - \frac{\sqrt{2}}{2}\mu\sqrt{\lambda}\eta\xi^2 - \frac{1}{8}\lambda\eta^4 - \frac{1}{4}\lambda\eta^2\xi^2 - \frac{1}{8}\lambda\xi^4 + \frac{1}{2}\frac{\mu^4}{\lambda}\right] \\
&+ \sqrt{2}qA^\mu\left[\frac{\mu}{\sqrt{\lambda}}\partial_\mu\xi + \frac{1}{\sqrt{2}}\left(\eta\partial_\mu\xi - \xi\partial_\mu\eta\right)\right] \\
&+ q^2A_\mu A^\mu\left[\sqrt{2}\frac{\mu}{\sqrt{\lambda}}\eta + \frac{1}{2}\left(\eta^2 + \xi^2\right)\right].
\end{aligned} \tag{1.10}$$

As in Eq.(1.6), the first two lines represent a massive scalar particle and a massless Goldstone boson. However, the third line shows that the gauge field has acquired a mass term $m_A^2 = \frac{2q^2\mu^2}{\lambda}$ after the local $U(1)$ symmetry is spontaneously broken.

The other terms describe couplings between the fields η, ξ and A_μ.

1.2 The Higgs Mechanism in the Standard Model

The Standard Model is based on the gauge symmetry groups $SU(3)_C \times SU(2)_L \times U(1)_Y$. The symmetry group $SU(2)_L \times U(1)_Y$ will be spontaneously broken once we introduce a complex doublet under $SU(2)_L$:

$$\phi = \begin{pmatrix} \phi^\dagger \\ \phi^0 \end{pmatrix}, \tag{1.11}$$

and the following terms in the Lagrangian:

$$\mathscr{L} = \left(\mathscr{D}_\mu \phi\right)^\dagger\left(\mathscr{D}^\mu \phi\right) - V(\phi)\ ,\ V(\phi) = -\mu^2\left(\phi^\dagger\phi\right) + \frac{1}{2}\lambda\left(\phi^\dagger\phi\right)^2, \tag{1.12}$$

where

$$\begin{aligned}
\mathscr{D}_\mu &= \partial_\mu - ig_2W_\mu^a\tau^a - i\frac{1}{2}g_1B_\mu \\
&= \begin{pmatrix} \partial_\mu - \frac{i}{2}(g_2W_\mu^3 + g_1B_\mu) & -\frac{i}{2}g_2(W_\mu^1 - iW_\mu^2) \\ -\frac{i}{2}g_2(W_\mu^1 + iW_\mu^2) & \partial_\mu + \frac{i}{2}(g_2W_\mu^3 - g_1B_\mu) \end{pmatrix}
\end{aligned} \tag{1.13}$$

Here W_μ^a and B_μ are $SU(2)$ and $U(1)$ gauge bosons, and g_2 and g_1 are the corresponding coupling constants.

The symmetry of the system is spontaneously broken when the field ϕ acquires the following VEV:

$$\langle\phi\rangle = \frac{1}{\sqrt{2}}\begin{pmatrix} 0 \\ v \end{pmatrix}. \tag{1.14}$$

The field ϕ can be parametrized around the VEV in the following way:

$$\phi = e^{-i\theta_a\tau^a}\frac{1}{\sqrt{2}}\begin{pmatrix} 0 \\ v+h \end{pmatrix} \tag{1.15}$$

We can use a gauge transformation to eliminate the phase factor from ϕ:

$$\phi \to e^{i\theta_a\tau^a}\phi = \frac{1}{\sqrt{2}}\begin{pmatrix} 0 \\ v+h \end{pmatrix} \tag{1.16}$$

This is called the Unitary Gauge.

Let us expand $(\mathscr{D}_\mu\phi\ )^\dagger(\mathscr{D}^\mu\phi)$ and the potential in the Unitary Gauge:

$$\begin{aligned}(\mathscr{D}_\mu\phi\ )^\dagger(\mathscr{D}^\mu\phi) &= \frac{1}{2}(\partial_\mu h)^2 + \frac{1}{8}g_2^2(v+h)^2\left[(W_\mu^1)^2+(W_\mu^2)^2\right] \\ &+ \frac{1}{8}(v+h)^2(g_2W_\mu^3 - g_1B_\mu)^2. \end{aligned} \tag{1.17}$$

$$V = \mu^2h^2 + \lambda v h^3 + \frac{1}{4}\lambda h^4. \tag{1.18}$$

The Lagrangian then becomes

$$\begin{aligned}\mathscr{L} &= (\mathscr{D}_\mu\phi\ )^\dagger(\mathscr{D}^\mu\phi) - V(\phi) \\ &= \frac{1}{2}(\frac{1}{2}g_2v)^2\left[(W_\mu^1)^2+(W_\mu^2)^2\right] + \frac{1}{2}(\frac{1}{2}\sqrt{g_1^2+g_2^2}v)^2\left[(W_\mu^1)^2+(W_\mu^2)^2\right] \\ &- \mu^2h^2 - \lambda v h^3 - \frac{1}{4}\lambda h^4 \\ &+ \frac{1}{8}g_2^2(v^2+2vh)\left[(W_\mu^1)^2+(W_\mu^2)^2\right] + \frac{1}{8}(v^2+2vh)(g_2W_\mu^3-g_1B_\mu)^2 \end{aligned} \tag{1.19}$$

We can define three new gauge fields $W_\mu^\pm$ and Z_μ in the following way:

$$W_\mu^\pm = \frac{1}{\sqrt{2}}(W_\mu^1 \mp iW^2), \quad Z_\mu = \frac{1}{\sqrt{g_1^2+g_2^2}}(g_2W_\mu^3 - g_1B_\mu), \tag{1.20}$$

and a gauge field A_μ orthogonal to Z_μ

$$A_\mu = \frac{1}{\sqrt{g_1^2 + g_2^2}}(g_2 W_\mu^3 + g_1 B_\mu). \tag{1.21}$$

Substituting these new fields in the Lagrangian, we obtain

$$\begin{aligned}\mathscr{L} &= \frac{1}{2}m_W^2 W^{+\mu}W_\mu^+ + \frac{1}{2}m_W^2 W^{-\mu}W_\mu^- + \frac{1}{2}m_Z^2 Z^\mu Z_\mu \\ &- \mu^2 h^2 - \lambda v h^3 - \frac{1}{4}\lambda h^4 \\ &+ \cdots \end{aligned} \tag{1.22}$$

where $m_W = \frac{1}{2}g_2 v$, $m_Z = \frac{1}{2}\sqrt{g_1^2 + g_2^2}v$, and $m_h = \sqrt{2}\mu$. After the symmetry breaking, the gauge fields $W_\mu^\pm$ and Z_μ acquire masses, while A_μ remains massless. We also obtain a massive scalar field h. This is the Higgs boson in the SM.

It is conventional to define the weak mixing angle θ_w:

$$\cos\theta_w = \frac{g_2}{g_1^2 + g_2^2} \tag{1.23}$$

The fermions in the SM also receive masses from the spontaneous symmetry breaking. We can introduce the following gauge invariant Yukawa terms in the Lagrangian:

$$\mathscr{L}_{Yukawa} = -y_e \overline{L}\phi e_R - y_u \overline{Q}_L \phi^\dagger u_R - y_d \overline{Q}_L \phi d_R \tag{1.24}$$

After the Higgs field ϕ acquires a VEV, the Yukawa terms become

$$\mathscr{L}_{Yukawa} = -\frac{1}{\sqrt{2}}y_e v \overline{e}_L e_R - \frac{1}{\sqrt{2}}y_u v \overline{u}_L u_R - \frac{1}{\sqrt{2}}y_d v \overline{d}_L d_R + h.c. + \cdots \tag{1.25}$$

The fermions receive standard mass terms:

$$m_e = \frac{1}{\sqrt{2}}y_e v, \quad m_u = \frac{1}{\sqrt{2}}y_u v, \quad m_d = \frac{1}{\sqrt{2}}y_d v. \tag{1.26}$$

The Higgs mechanism has generated the masses of the weak bosons $W^\pm$, Z and all the fermions in the SM. The gauge symmetries $SU(2)_L \times U(1)_Y$ are spontaneously broken, while the eletromagnetic symmetry $U(1)_{EM}$ and color symmetry $SU(3)_C$ stay unbroken.

1.3 Theoretical Constraints on the Higgs Boson Mass

The mass of the Higgs boson is an unknown parameter in the SM. However, there are some theoretical constraints on the Higgs mass. Below I outline the most relevant constraints to my research.

1.3.1 Vacuum Stability Bound

As we have seen in the Higgs potential, if the quartic coupling λ is negative, the vacuum is not stable since it has no minimum. In order to keep the Higgs potential bounded from below, λ must remain positive up to the cut-off scale Λ at which SM breaks down. This puts a lower bound on the Higgs boson mass, which depends on the cut-off scale. This is called the vacuum stability bound. If one adopts the reduced Planck scale ($M_P \simeq 2.4 \times 10^{18}$ GeV) as the cut-off scale, the vacuum stability bound is about 129 GeV.

1.3.2 Perturbativity Bound

On the other hand, the quartic coupling λ cannot be arbitrarily large since it may spoil the perturbation theory in the SM. This has seen discussed with different Higgs decays [8, 9]. For example, the partial Higgs decay width into gauge bosons is given by [8]

$$\Gamma_{\text{total}} \simeq \Gamma_{\text{Born}} \left[1 + 3\hat{\lambda} + 62\hat{\lambda}^2 + \mathcal{O}(\hat{\lambda}^3) \right], \tag{1.27}$$

where $\hat{\lambda} = \lambda/(4\pi)^2$. If λ is too large so that the one loop term becomes close to the Born term, *i.e.* $3\hat{\lambda} \sim 1$, the perturbative series will not converge.

Following Ref. [10], the perturbativity bound on the Higgs boson mass can be calculated using the condition $\lambda(\Lambda) = 4\pi$, which corresponds to a two-loop correction to β_λ of about 50%. If one adopts the reduced Planck scale ($M_P \simeq 2.4 \times 10^{18}$ GeV) as the cut-off scale, the perturbativity bound is about 175 GeV.

1.4 Seesaw Mechanism

One problem in the SM is that neutrinos are massless. However, solar and atmospheric neutrino oscillation experiments have established that at least two neutrino states are massive [4]. The seesaw mechanism is a simple and promising extension of the SM to incorporate the neutrino masses and mixings observed in solar and atmospheric neutrino oscillations. The key idea is to introduce a dimension-five operator [11]:

$$\frac{y_5 LL\phi\phi}{M_R}. \tag{1.28}$$

This operator violates lepton number by two units, and generates Majorana masses for neutrinos in the SM after spontaneous symmetry breaking. To achieve the correct neutrino mass, the seesaw scale M_R is required to be $\sim \mathcal{O}(10^{15}$ GeV), if the Yukawa coupling y_5 is assumed to be of order 1. There are three main seesaw extensions of the SM, type I [12], type II [13], and type III [14], in which singlet right-handed neutrinos, $SU(2)$ triplet scalar, and $SU(2)$ triplet right-handed neutrinos, respectively, are introduced to form a dimension-five operator. Below I outline type I and type III seesaw mechanisms which are relevant to my research.

1.4.1 Type I Seesaw

The simplest way to form a dimension-five operator is to introduce right-handed singlet fermions ν_R. The relevant terms in the Lagrangian are given by

$$\mathscr{L}_\nu = -Y_\nu \overline{L}\phi\nu_R - M_R\overline{\nu_R^c}\nu_R \tag{1.29}$$

For simplicity, we can assume the three right-handed neutrinos are degenerate in mass (M_R). At energies below M_R, the heavy right-handed neutrinos are integrated out and the effective dimension-five operator can be generated. After electroweak symmetry breaking, the light neutrino mass matrix is obtained as

$$\mathbf{M}_\nu = m_D M_R^{-1} m_D^T, \tag{1.30}$$

where $m_D = Y_\nu v/\sqrt{2}$ is the Dirac mass matrix for the neutrinos after the Higgs field gets the VEV v. If one assumes $M_R \gg m_D$, the eigenvalues of $\mathbf{M}_\nu$ can be very small.

Therefore, the presence of heavy right-handed neutrinos will generate the light neutrino masses in the SM, and this mechanism is called the seesaw mechanism. The scenario where heavy right-handed singlet fermions are introduced is called the Type I seesaw.

1.4.2 Type III Seesaw

The basic structure of type III seesaw is similar to type I seesaw, except that instead of the singlet right-handed neutrinos, three generations of fermions which transforms as (3,0) under the electroweak gauge group $SU(2)_L \times U(1)_Y$ are introduced:

$$\Sigma_R = \frac{\sigma^i}{2}\Sigma_R^i = \begin{pmatrix} \Sigma_R^0/\sqrt{2} & \Sigma_R^\dagger \\ \Sigma_R^- & -\Sigma_R^0/\sqrt{2} \end{pmatrix}. \tag{1.31}$$

With canonically normalized kinetic terms for the triplet fermions, we replace the SM-singlet right-handed neutrinos of type I seesaw in Eq. (3.3) by these SU(2) triplet fermions. The relevant terms in the Lagrangian are given by

$$\mathscr{L}_\Sigma = -\overline{L}\sqrt{2}Y_\Sigma^\dagger \Sigma \widetilde{\phi} - \widetilde{\phi}\overline{\Sigma}\sqrt{2}Y_\Sigma L - \frac{1}{2}\mathrm{Tr}\left[\overline{\Sigma} M_\Sigma \Sigma\right] \tag{1.32}$$

The light neutrino mass matrix via type III seesaw mechanism is obtained as

$$\mathbf{M}_\nu = m_D M_\Sigma^{-1} m_D^T, \tag{1.33}$$

where $m_D = Y_\Sigma v/\sqrt{2}$ is the Dirac mass matrix for the neutrinos after the Higgs field gets the VEV v. Eq. (1.33) has the same form as Eq. (1.30). Therefore, the light neutrino masses can be obtained if $M_\Sigma \gg m_D$. This is known as the Type III seesaw mechanism.

1.5 Supersymmetry

The study of supersymmetry is motivated by solving the hierarchy problem in the SM. The SM Higgs boson mass is subject to large quantum corrections due to its interactions with other particles in the SM. For example, the correction from a fermion is given by

$$\Delta m_h^2 = -\frac{\lambda_f^2}{8\pi^2}\Lambda^2 + \cdots , \tag{1.34}$$

where Λ is the cutoff scale at which SM breaks down and new physics appears to modify the behavior of the theory. If Λ is the Planck mass M_P, this quantum correction is much larger the required Higgs boson mass $m_h \sim \mathcal{O}(100\text{ GeV})$. One solution to this problem is to propose there exists a scalar particle that couples to the Higgs field with the term $-\lambda_S h^2 S^2$. The Higgs boson mass will receive a correction from the scalar:

$$\Delta m_h^2 = \frac{\lambda_S}{16\pi^2}\left[\Lambda^2 - 2m_S^2 \ln\left(\frac{\Lambda}{m_S}\right)\right] + \cdots \tag{1.35}$$

If for each fermion in the SM, there exist two corresponding complex scalars with $\lambda_S = \lambda_f^2$, the terms proportional to Λ^2 in Eq. (1.1) will be exactly canceled.

Supersymmetry is a proposed symmetry motivated by this solution. In supersymmetry, a bosonic state can be transformed into a fermionic state, and vice versa. Therefore, for each fermion / boson in the SM, we can introduce a superpartner with spin differing by 1/2 unit, which serves to cancel the large quantum corrections to the Higgs boson mass.

1.5.1 Minimal Supersymmetric Standard Model

The Minimal Supersymmetric Standard Model (MSSM) is a minimal supersymmetric extension to the SM. For each quark / lepton in the SM, there is a superpartner called squark / slepton with spin 0. The W, B bosons (see section 1.2) and gluons have superparters with spin $\frac{1}{2}$, and they are called winos, binos and gluinos. There are two Higgs fields in the MSSM: h_u and h_d, which couple to the up type quarks and down type quarks, respectively. Their spin $\frac{1}{2}$ superparters are called Higgsinos. The particle content of MSSM is shown in Table 1.3. The SM particle and its corresponding superpartner form a supermultiplet. The supermultiplets in the MSSM are summarized in Table 1.4. These supermultiplets can be described by the superfield in the superspace, which we will discuss next.

1.5.2 Superfields and Lagrangian

It is very convenient to study supersymmetry using superspace and superfields. A detailed discussion can be found in Ref. [6]. Superspace is an enlarged space with

SM Particle		Symbol	Spin	Superpartner	Symbol	Spin
Fermions	Quark	$q_L,\ u_R,\ d_R$	$\frac{1}{2}$	Squark	$\widetilde{q}_L,\ \widetilde{u}_R,\ \widetilde{d}_R$	0
	Lepton	$l_L,\ e_R$	$\frac{1}{2}$	Slepton	$\widetilde{l}_L,\ \widetilde{e}_R$	0
Bosons	W boson	W	1	Wino	$\widetilde{W}$	$\frac{1}{2}$
	B boson	B	1	Bino	$\widetilde{B}$	$\frac{1}{2}$
	Gluon	g	1	Gluino	$\widetilde{g}$	$\frac{1}{2}$
Higgs bosons	Higgs	h_u	0	Higgsino	$\widetilde{h}_u$	$\frac{1}{2}$
	Higgs	h_d	0	Higgsino	$\widetilde{h}_d$	$\frac{1}{2}$

Table 1.3: Particle content in the MSSM.

coordinates $(x_\mu, \theta^\alpha, \theta^\dagger_{\dot\alpha})$, where θ^α and $\theta^\dagger_{\dot\alpha}$ are complex anticommuting two-component spinors. Each field in superspace is represented by these coordinates, *i. e.* $\Phi(x_\mu, \theta^\alpha, \theta^\dagger_{\dot\alpha})$. Such a field is called a superfield.

One can define a chiral superfield to describe the chiral supermultiplet in the MSSM. The chiral covariant derivatives are defined as

$$D_\alpha = \frac{\partial}{\partial\theta^\alpha} - i(\sigma^\mu\theta^\dagger)_\alpha\partial_\mu, \qquad D^\dagger_{\dot\alpha} = -\frac{\partial}{\partial\theta^{\dagger\dot\alpha}} + i(\theta\sigma^\mu)_{\dot\alpha}\partial_\mu. \tag{1.36}$$

where σ^μ is defined as:

$$\sigma^0 = \begin{pmatrix} 1 & 0 \\ 0 & 1 \end{pmatrix},\ \sigma^1 = \begin{pmatrix} 0 & 1 \\ 1 & 0 \end{pmatrix},\ \sigma^2 = \begin{pmatrix} 0 & -i \\ i & 0 \end{pmatrix},\ \sigma^3 = \begin{pmatrix} 1 & 0 \\ 0 & -1 \end{pmatrix}. \tag{1.37}$$

A chiral superfield $\Phi(x, \theta, \theta^\dagger)$ is a superfield satisfying the following constraint:

$$D^\dagger_{\dot\alpha}\Phi(x, \theta, \theta^\dagger) = 0. \tag{1.38}$$

By solving Eq. (1.38), we can obtain the component form of the chiral superfield:

$$\begin{aligned}\Phi(x, \theta, \theta^\dagger) &= \phi(x) + i\theta^\dagger\overline{\sigma}^\mu\theta\partial_\mu\phi(x) + \frac{1}{4}\theta\theta\theta^\dagger\theta^\dagger\partial_\mu\partial^\mu\phi(x) + \sqrt{2}\theta\psi(x) \\ &- \frac{i}{\sqrt{2}}\theta\theta\theta^\dagger\overline{\sigma}^\mu\partial_\mu\psi(x) + \theta\theta F(x),\end{aligned} \tag{1.39}$$

Supermultiplet	Fermionic State	Bosonic State
Q	q_L	$\widetilde{q}_L$
U	u_R	$\widetilde{u}_R$
D	d_R	$\widetilde{d}_R$
L	l_L	$\widetilde{l}_L$
E	e_R	$\widetilde{e}_R$
H_u	h_u	$\widetilde{h}_u$
H_d	h_d	$\widetilde{h}_d$
$\mathcal{W}$	W	$\widetilde{W}$
$\mathcal{B}$	B	$\widetilde{B}$
$\mathcal{G}$	g	$\widetilde{g}$

Table 1.4: Supermultiplets in the MSSM.

where $\phi(x)$ is a complex scalar field, $\psi(x)$ is a left-handed Weyl spinor (fermion) field, and $F(x)$ is an auxiliary field to keep supersymmetry algebra close off-shell. $\overline{\sigma}^\mu$ is defined as:

$$\overline{\sigma}^0 = \begin{pmatrix} 1 & 0 \\ 0 & 1 \end{pmatrix}, \ \overline{\sigma}^1 = \begin{pmatrix} 0 & -1 \\ -1 & 0 \end{pmatrix}, \ \overline{\sigma}^2 = \begin{pmatrix} 0 & i \\ -i & 0 \end{pmatrix}, \ \overline{\sigma}^3 = \begin{pmatrix} -1 & 0 \\ 0 & 1 \end{pmatrix}. \tag{1.40}$$

It is clear that a chiral superfield can be used to describe a chiral supermultiplet which contains a chiral fermion $\psi(x)$ and its scalar superpartner $\psi(x)$.

Likewise, a vector superfield can be defined to represent the gauge supermultiplet in the MSSM. A vector field $V(x, \theta, \theta^\dagger)$ is a superfield satisfying the following constraint:

$$V(x, \theta, \theta^\dagger) = V^*(x, \theta, \theta^\dagger) \tag{1.41}$$

The component form is the vector superfield is

$$
\begin{aligned}
V(x,\theta,\theta^\dagger) &= a + \theta\xi + \theta^\dagger\xi^\dagger + \theta\theta b + \theta^\dagger\theta^\dagger b^* + \theta^\dagger\overline{\sigma}^\mu\theta A_\mu + \theta^\dagger\theta^\dagger\theta(\lambda - \frac{i}{2}\sigma^\mu\partial_\mu\xi^\dagger) \\
&+ \theta\theta\theta^\dagger(\lambda^\dagger - \frac{i}{2}\overline{\sigma}^\mu\partial_\mu\xi) + \theta\theta\theta^\dagger\theta^\dagger(\frac{1}{2}D + \frac{1}{4}\partial_\mu\partial^\mu a). \qquad (1.42)
\end{aligned}
$$

The vector superfield can be used to represent a guage supermultiplet which contains a gauge boson A_μ and a gaugino λ. Like the chiral auxiliary field F, the gauge auxiliary field D is needed in order that supersymmetry algebra is closed off-shell.

It turns out that the only term contributing to the Lagrangian from a vector superfield is the D-term.

$$
[V]_D = \int d^2\theta d^2\theta^\dagger \, V(x,\theta,\theta^\dagger) = \frac{1}{2}D + \frac{1}{4}\partial_\mu\partial^\mu a. \qquad (1.43)
$$

The term $\frac{1}{4}\partial_\mu\partial^\mu a$ can be dropped in the Lagrangian since it is a total derivative.

The only term contributing to the Lagrangian from a chiral superfield is the F-term.

$$
[\Phi]_F = \int d^2\theta \, \Phi\Big|_{\theta^\dagger=0} = \int d^2\theta d^2\theta^\dagger \, \delta^{(2)}(\theta^\dagger)\,\Phi \; = \; F. \qquad (1.44)
$$

To ensure the action is real, this contribution to the Lagrangian is always accompanied by its complex conjugate:

$$
[\Phi]_F + \text{c.c.} = \int d^2\theta d^2\theta^\dagger \; \left[\delta^{(2)}(\theta^\dagger)\,\Phi + \delta^{(2)}(\theta)\,\Phi^*\right]. \qquad (1.45)
$$

The Lagrangian for the chiral superfields in superspace is given by

$$
\mathscr{L} = [\Phi^{*i}\Phi_i]_D + \left([W(\Phi_i)]_F + \text{c.c.}\right). \qquad (1.46)
$$

Here $W(\Phi_i)$ is a holomorphic function of the chiral superfieds that is called superpotential. Its form varies in different supersymmetric models. For example, in a simple modeld called the Wess-Zumino model, the superpotential is defined as:

$$
W = \frac{1}{2}M^{ij}\Phi_i\Phi_j + \frac{1}{6}y^{ijk}\Phi_i\Phi_j\Phi_k. \qquad (1.47)
$$

Note that the composite superfield $\Phi^{*i}\Phi_i$ in Eq. (1.46) is a vector field since it satisfies the constraint in Eq. (1.41).

The Lagrangian for an Abelian gauge theory involving the chiral superfield and the vector superfield is given by

$$\mathscr{L} = \left[\Phi^{*i} e^{2gq_i V} \Phi_i\right]_D + ([W(\Phi_i)]_F + \text{c.c.}) + \frac{1}{4}([G^\alpha G_\alpha]_F + \text{c.c.}) - 2\kappa[V]_D \tag{1.48}$$

Here q_i is the $U(1)$ charge carried by the chiral superfield Φ_i. G_α is the gauge-invariant Abelian field strength superfield associated with the vector superfield V:

$$G_\alpha = -\frac{1}{4} D^\dagger D^\dagger D_\alpha V. \tag{1.49}$$

κ is a dimensionless parameter and $2\kappa[V]_D$ is called the Fayet-Iliopoulos term. This type of term can play a important role in spontaneous supersymmetry breaking.

The superpotential for the MSSM is given by

$$W_{\text{MSSM}} = \mathbf{Y_u} UQH_u - \mathbf{Y_d} DQH_d - \mathbf{Y_e} ELH_d + \mu H_u H_d\,. \tag{1.50}$$

$\mathbf{Y_u}$, $\mathbf{Y_d}$, and $\mathbf{Y_e}$ are dimensionless Yukawa coupling matrices. Q, U, D, L, E, H_u, and H_d are the chiral superfields corresponding to the supermultiplets in Table 1.4. The term μ has dimensions of [mass]. In order to accommodate a Higgs VEV of 175 GeV, μ has to be of order 10^2 or 10^3 GeV. This is very unnatural, since there is no explanation for why it is many orders of magnitude smaller than the Planck scale. This puzzle is called “the μ problem”.

1.5.3 R-Parity and Matter Parity

There are other gauge invariant terms that are not included in the superpotential in Eq. (1.50). For example, let us examine the following terms:

$$W = \frac{1}{2}\lambda ELL + \lambda' DLQ + \mu' LH_u + \frac{1}{2}\lambda'' UDD. \tag{1.51}$$

These terms are all gauge invariant. However, the first three terms violate lepton number by 1 unit, and the last term violates baryon number by 1 unit. Such terms may cause serious problems in MSSM. For example, if λ' and λ'' were not suppressed, the lifetime of the proton would be extremely short. In order to avoid these terms, one can define a quantum number called "matter parity":

$$P_M = (-1)^{3(\mathrm{B-L})}. \tag{1.52}$$

With this definition, the quark and lepton supermultiplets will have $P_M = 1$. The gauge boson supermutilples do not carry baryon or lepton number, therefore they also have $P_M = 1$. The Higgs supermultiplets H_u and H_d have $P_M = -1$. If one requires that any term in the Lagragian in the MSSM must have $P_M = 1$, the terms in Eq.(1.51) are forbidden, while the terms in Eq. (1.50) are still allowed.

Another widely used parity is called the "R-parity". It is defined as the following:

$$P_M = (-1)^{3(\mathrm{B-L})+2\mathrm{s}}. \tag{1.53}$$

where s is the spin of the particle. Requiring R-parity conservation will have the same effect on the Lagrangian as requiring matter parity conservation. However, the advantage of R-parity is that all SM particles have $P_R = 1$, while all their superpartners have $P_R = -1$. This is very useful in phenomenological studies at colliders.

1.5.4 Soft Supersymmetry Breaking

The fact that none of the superpartners of the SM particles has been discovered so far indicates that supersymmetry must be a broken symmetry. One way to break supersymmetry is to introduce the "soft" supersymmetry breaking terms. "Soft" means that these terms do not disturb the cancellation of the quadratic divergences. To avoid any correction to Δm_h^2 that is proportional to Λ^2, these terms can only contain couplings with positive mass dimension. The soft supersymmetry breaking terms in the MSSM are:

$$\begin{aligned}
\mathscr{L}_{\text{soft}}^{\text{MSSM}} &= -\frac{1}{2}\left(M_1\widetilde{\mathcal{B}}\widetilde{\mathcal{B}} + M_2\widetilde{\mathcal{W}}\widetilde{\mathcal{W}} + M_3\widetilde{\mathcal{G}}\widetilde{\mathcal{G}} + \text{c.c.}\right) \\
&- \left(\mathbf{a_u}\,\widetilde{u}_R\,\widetilde{q}_L\,h_u - \mathbf{a_d}\,\widetilde{d}_R\,\widetilde{q}_L\,h_d - \mathbf{a_e}\,\widetilde{e}_R\,\widetilde{l}_L\,h_d + \text{c.c.}\right) \\
&- \mathbf{m_Q^2}\,\widetilde{q}_L^\dagger\,\widetilde{q}_L - \mathbf{m_L^2}\,\widetilde{l}_L^\dagger\,\widetilde{l}_L - \mathbf{m_u^2}\,\widetilde{u}_R^\dagger\,\widetilde{u}_R - \mathbf{m_d^2}\,\widetilde{d}_R^\dagger\,\widetilde{d}_R - \mathbf{m_e^2}\,\widetilde{e}_L^\dagger\,\widetilde{e}_L \\
&- m_{H_u}^2\,h_u^*\,h_u - m_{H_d}^2\,h_d^*\,h_d - (b\,h_u\,h_d + \text{c.c.})\,.
\end{aligned} \tag{1.54}$$

M_1, M_2, M_3 are the bino, wino, gluino mass terms. a_u, a_d, and a_e are complex 3×3 matrices with dimensions of [mass]. m_Q^2, m_L^2, m_u^2, m_d^2 and m_e^2 are hermition 3×3 matrices. The last four terms contribute to the Higgs potential in the MSSM. These terms break supersymmetry explicitly because they contain only scalars and gauginos but not their superpartners. To provide a Higgs VEV of 175 GeV, we expect

$$M_1,\, M_2,\, M_3,\, a_u,\, a_d,\, a_e \sim m_{\rm soft}, \tag{1.55}$$

$$\mathbf{m_Q^2},\, \mathbf{m_L^2},\, \mathbf{m_u^2},\, \mathbf{m_d^2},\, \mathbf{m_e^2},\, m_{H_u}^2,\, m_{H_d}^2,\, b \sim m_{\rm soft}^2, \tag{1.56}$$

with $m_{\rm soft}$ not much greater than the TeV scale. This is a strong reason for many theoretical physicists to believe that supersymmetry will be discovered at the LHC.

The MSSM introduces a large number (105) of new parameters to the ordinary SM. This makes the phenomenological analysis on the MSSM very complicated. In order to form more viable models, one can make various assumptions to reduce the number of new parameters. For example, it is often assumed that the squark and slepton squared-mass matrices are proportional to the 3×3 identity matrix:

$$\mathbf{m_Q^2} = m_Q^2 I_3, \quad \mathbf{m_L^2} = m_L^2 I_3, \quad \mathbf{m_u^2} = m_u^2 I_3, \quad \mathbf{m_d^2} = m_d^2 I_3, \quad \mathbf{m_e^2} = m_e^2 I_3, \tag{1.57}$$

and each (scalar)^3 couplings matrix is proportional to the corresponding Yukawa coupling matrix:

$$\mathbf{a_u} = A_u\, \mathbf{Y_u}, \quad \mathbf{a_d} = A_d\, \mathbf{Y_d}, \quad \mathbf{a_e} = A_e\, \mathbf{Y_e}. \tag{1.58}$$

A_u, A_d and A_e are called trilinear couplings. The b term is often assumed to be proportional to the μ term.

$$b = B_0 \mu. \tag{1.59}$$

B_0 is called bilinear coupling. These conditions can help minimize the flavor-changing and CP-violating effects in the MSSM.

A well-studied minimal scenario is called the constrained MSSM (CMSSM) or minimal Supergravity (mSUGRA) scenario. The assumptions in this model are the following:

- All gaugino masses are unified at the Grand Unification enerygy scale M_{GUT}:

$$M_1(M_{\mathrm{GUT}}) = M_2(M_{\mathrm{GUT}}) = M_3(M_{\mathrm{GUT}}) = m_{1/2}. \tag{1.60}$$

- All scalar masses are unified at M_{GUT}:

$$m_Q^2 = m_L^2 = m_u^2 = m_d^2 = m_e^2 = m_0^2, \quad m_{H_u}^2 = m_{H_d}^2 = m_0^2. \tag{1.61}$$

- All trilinear couplings are unified at M_{GUT}:

$$A_u = A_d = A_e = A_0. \tag{1.62}$$

The values of μ and b are determined by two minimization conditions of the two-Higgs doublet scalar potential. However, one still needs to specify the ratio of the VEVs of the two neutral Higgs fields at low energy scale, as well as the sign of μ. This leaves a total of four free parameters and an unknown sign:

$$m_{1/2}, \quad m_0, \quad A_0, \quad \tan\beta, \quad \mathrm{sign}(\mu). \tag{1.63}$$

This framework has been used as a benchmark scenario in many phenomenological studies on supersymmetry. It will also be discussed when I present my research results.

Chapter 2

EXTENDED STANDARD MODEL WITH VECTOR LIKE FERMIONS

In this chapter we study the impact of vectorlike fermions on the SM Higgs mass bounds [15]. Unification at $M_{\rm GUT} \sim 3 \times 10^{16}$ GeV of the three SM gauge couplings can be achieved by postulating the existence of a pair of vectorlike fermions carrying SM charges and masses of order 300 GeV – 1 TeV. The presence of these fermions significantly modifies the vacuum stability and perturbativity bounds on the mass of the SM Higgs boson. The new vacuum stability bound in this extended SM is estimated to be 117 GeV, to be compared with the SM prediction of about 128 GeV. An upper bound of 190 GeV is obtained based on perturbativity arguments. The impact on these predictions of type I seesaw physics is also discussed.

2.1 Introduction

Under a somewhat radical assumption that the next energy frontier lies at the reduced Planck scale ($M_P \simeq 2.4 \times 10^{18}$ GeV), it has been found that the SM Higgs boson mass lies in the range 128 GeV $\lesssim m_H \lesssim$ 175 GeV [16]. Here the lower bound of 128 GeV on m_H derives from arguments based on the stability of the SM vacuum. More precisely, that the Higgs quartic coupling does not become negative at any scale between M_Z and M_P. The upper bound of 175 GeV or so on m_H stems from the requirement that the Higgs quartic coupling remains perturbative and does not exceed 4π, say, during its evolution between M_Z and M_P. Thus, it would appear that discovery of a relatively 'light' Higgs boson (with mass well below 128 GeV) may signal the presence of physics beyond the SM.

Supersymmetry is by far the most compelling extension of the SM and its minimal realization (MSSM) predicts a relatively 'light' SM–like Higgs boson with mass

$\lesssim$ 130 GeV. However, in the light of LHC, plausible alternatives to supersymmetry deserve careful investigation. For instance, it was shown in [17] that the new physics between M_Z and M_P associated with type II seesaw [13] around TeV scale or higher can yield a 'light' Higgs boson with mass $\gtrsim$ 114.4 GeV, the LEP II bound. A 'light' Higgs boson is also realized in scenarios of gauge–Higgs unification with a compactification scale below M_P [18].

In this chapter we revisit another extension of the SM, proposed several years ago, in which new TeV scale vectorlike fermions are introduced in order to implement unification at some scale $M_{\rm GUT}$ of the three SM gauge couplings [19]. The new vectorlike fermions carry SM gauge quantum numbers and their presence therefore modifies the SM Higgs mass bounds based on vacuum stability and perturbativity arguments. In particular, by including only a pair of vectorlike fermions for which case $M_{\rm GUT} \simeq 3 \times 10^{16}$ GeV, the vacuum stability bound can be lowered from its conventional value of around 128 GeV to a significantly lower value of about 117 GeV. To keep the discussion as realistic as possible, we also study the possible impact neutrino oscillation physics could have on the Higgs mass predictions. We employ type I seesaw for these considerations [12]. Note that a more complicated scenario containing several new particles (including scalars) can yield $M_{\rm GUT} \simeq M_P$, with a vacuum stability bound as low as 114 GeV.

2.2 New Fermions and the Higgs Boson Mass

Let us start by introducing the following vectorlike fermions:

$$Q\left(3,2,\frac{1}{6}\right) + \overline{Q}\left(\bar{3},2,-\frac{1}{6}\right) + D\left(3,1,\frac{1}{3}\right) + \overline{D}\left(\bar{3},1,-\frac{1}{3}\right), \tag{2.1}$$

where the brackets contain the $SU(3)_c \times SU(2)_L \times U(1)_Y$ quantum numbers of the new particles. The SM Lagrangian is supplemented by additional terms, and the relevant ones are given by

$$\begin{aligned}\mathcal{L}_{new} &= -\kappa_1 \bar{Q}\bar{D}\Phi^c - \kappa_2 QD\Phi - y_1^i Q d_i^c \Phi - y_2^i q_i D\Phi - y_3^i Q u_i^c \Phi^c - M_F(\bar{Q}Q + \bar{D}D) \\ &+ h.c. \end{aligned}\tag{2.2}$$

where Φ denotes the SM higgs doublet, $\Phi^c \equiv i\sigma_2\Phi^*$ its charge conjugate, and we employ the standard notation q_i, u_i^c, d_i^c for the SM quarks, with $i = 1, 2, 3$. The parameters $y^i_{1,2,3}$ and $\kappa_{1,2}$ are dimensionless couplings. We assume, for simplicity, that the new fermions have a common vectorlike mass M_F. As pointed out in [20], most of the $y^i_{1,2,3}$ couplings have to be very small due to constraints from the precision electroweak data. To accommodate this, we will assume that the couplings $y^i_{1,2,3}$ are sufficiently small so that they do not give a significant contribution in the RGE analysis. However, the $y^i\ 's$ allow the new fermions to decay into the SM particles, without creating any cosmological problems.

There are constraints on the $\kappa_{1,2}$ couplings and the masses of the new matter fields. The most important ones arise from the S and T parameters which severely limit the number of additional chiral generations. Consistent with these constraints, one should therefore add new matter which is predominantly vectorlike. In the limit where the vectorlike mass M_F is much heavier than the chiral mass term (arising from Yukawa coupling to the Higgs doublets), the contribution to the T parameter from a single chiral fermion is given by [21]

$$\delta T \approx \frac{N(\kappa_i v)^2}{10\pi \sin^2\theta_W m_W^2}\left[\left(\frac{\kappa_i v}{M_V}\right)^2 + O\left(\frac{\kappa_i v}{M_V}\right)^4\right], \tag{2.3}$$

where κ_i, $i = 1, 2$, are the Yukawa couplings in Eq. (2.2), $v = 246.2$ GeV is the vacuum expectation value (VEV) of the Higgs field, and N counts the number of additional SU(2) doublet pairs, which in our case is 3. From the precision electroweak data $T \leq 0.06(0.14)$ at 95% CL for $m_H = 117$ GeV (300 GeV) [22]. We will take $\delta T < 0.1$ as a conservative bound for our analysis. We see from Eq. (2.3) that with $M_F \sim 500$ GeV, the Yukawa couplings κ_i can be $O(1)$.

For the SM gauge coupling we employ the two renormalization group equation (RGE) [23] :

$$\frac{dg_i}{d\ln\mu} = \frac{b_i}{16\pi^2}g_i^3 + \frac{g_i^3}{(16\pi^2)^2}\left(\sum_{j=1}^{3} B_{ij}g_j^2 - C_i^t y_t^2\right), \tag{2.4}$$

where g_i ($i = 1, 2, 3$) are the SM gauge couplings and y_t is the top Yukawa coupling,

$$b_i^{SM} = \left(\frac{41}{10}, -\frac{19}{6}, -7\right), \quad B_{ij}^{SM} = \begin{pmatrix} \frac{199}{50} & \frac{27}{10} & \frac{44}{5} \\ \frac{9}{10} & \frac{35}{6} & 12 \\ \frac{11}{10} & \frac{9}{2} & -26 \end{pmatrix}, \quad C_i^t = \left(\frac{17}{10}, \frac{3}{2}, 2\right). \tag{2.5}$$

For a renormalization scale $\mu > M_F$, the beta function for gauge couplings receives an additional contribution from the vectorlike fermions,

$$b_i' = \left(\frac{2}{5}, 2, 2\right), \quad B_{ij}' = \begin{pmatrix} \frac{3}{50} & \frac{3}{10} & \frac{8}{5} \\ \frac{1}{10} & \frac{49}{2} & 8 \\ \frac{1}{5} & 3 & \frac{114}{3} \end{pmatrix}, \quad C_i^{\kappa_1} = C_i^{\kappa_2} = \left(\frac{1}{2}, \frac{3}{2}, 2\right), \tag{2.6}$$

where $C_i^{\kappa_1}$ and $C_i^{\kappa_2}$ stand for the contribution which is proportional to the κ_i coupling in the two loop RGE for gauge couplings.

For the top Yukawa coupling, we have [23]

$$\frac{dy_t}{d\ln\mu} = y_t\left(\frac{1}{16\pi^2}\beta_t^{(1)} + \frac{1}{(16\pi^2)^2}\beta_t^{(2)}\right). \tag{2.7}$$

Here the one-loop contribution is

$$\beta_t^{(1)} = \frac{9}{2}y_t^2 - \left(\frac{17}{20}g_1^2 + \frac{9}{4}g_2^2 + 8g_3^2\right), \tag{2.8}$$

while the two-loop contribution is given by

$$\begin{aligned} \beta_t^{(2)} &= -12y_t^4 + \left(\frac{393}{80}g_1^2 + \frac{225}{16}g_2^2 + 36g_3^2\right)y_t^2 + \frac{1187}{600}g_1^4 - \frac{9}{20}g_1^2g_2^2 \\ &\quad + \frac{19}{15}g_1^2g_3^2 - \frac{23}{4}g_2^4 + 9g_2^2g_3^2 - 108g_3^4 + \frac{3}{2}\lambda^2 - 6\lambda y_t^2. \end{aligned} \tag{2.9}$$

In solving Eq. (2.7), the initial top Yukawa coupling at $\mu = M_t$ is determined from the relation between the pole mass and the running Yukawa coupling [24, 25],

$$M_t \simeq m_t(M_t)\left(1 + \frac{4}{3}\frac{\alpha_3(M_t)}{\pi} + 11\left(\frac{\alpha_3(M_t)}{\pi}\right)^2 - \left(\frac{m_t(M_t)}{2\pi v}\right)^2\right), \tag{2.10}$$

with $y_t(M_t) = \sqrt{2}m_t(M_t)/v$ and $\alpha_3 \equiv g_3^2/4\pi$. Here, the second and third terms in parentheses correspond to one- and two-loop QCD corrections, respectively, while the fourth term comes from the electroweak corrections at one-loop level. The numerical values of the third and fourth terms are comparable (their signs are opposite). The electroweak corrections at two-loop level and the three-loop QCD corrections are both comparable and of sufficiently small magnitude [25] to be safely ignored.

For a renormalization scale $\mu > M_F$, according to the Eq. (2.2), the beta function for the top Yukawa coupling receives an additional contribution at one loop level as follows:

$$\delta\beta_t^{(1)} = 3(\kappa_1^2 + \kappa_2^2), \tag{2.11}$$

and the additional two loop contributions are

$$\delta\beta_t^{(2)} = \left(\frac{5}{8}g_1^2 + \frac{45}{8}g_2^2 + 20g_3^2\right)(\kappa_1^2 + \kappa_2^2) - \frac{27}{4}(\kappa_1^4 + \kappa_2^4) - \frac{27}{4}y_t^2(\kappa_1^2 + \kappa_2^2). \tag{2.12}$$

The one and two loop RGEs for the Yukawa couplings κ_1 and κ_2 are given by

$$\frac{d\kappa_1}{d\ln\mu} = \kappa_1\left(\frac{1}{16\pi^2}\beta_{\kappa_1}^{(1)} + \frac{1}{(16\pi^2)^2}\beta_{\kappa_1}^{(2)}\right). \tag{2.13}$$

Here the one loop contribution is

$$\beta_{\kappa_1}^{(1)} = -\frac{1}{4}g_1^2 - \frac{9}{4}g_2^2 - 8g^3 + \frac{9}{2}\kappa_1^2 + 3\kappa_2^2 + 3y_t^2, \tag{2.14}$$

while the two-loop contribution is given by

$$\begin{aligned}\beta_{\kappa_1}^{(2)} \quad = \quad & -\frac{127}{600}g_1^4 - \frac{23}{4}g_2^4 - 108g_3^4 - \frac{27}{20}g_1^2g_2^2 + \frac{31}{15}g_1^2g_3^2 + 9g_2^2g_3^2 - 6\lambda\kappa_1^2 \\ & + \left(\frac{85}{40}g_1^2 + \frac{45}{8}g_2^2 + 20g_3^2\right)y_t^2 + \left(\frac{237}{80}g_1^2 + \frac{225}{16}g_2^2 + 36g_3^2\right){\kappa_1}^2 + \frac{3}{2}\lambda^2 \\ & + \left(\frac{5}{8}g_1^2 + \frac{45}{8}g_2^2 + 20g_3^2\right)\kappa_2^2 - 12\kappa_1^4 - \frac{27}{4}(y_t^4 + \kappa_2^4 + y_t^2\kappa_1^2 + \kappa_1^2\kappa_2^2). \end{aligned} \tag{2.15}$$

The RGE for the Yukawa coupling κ_2 is obtained by making the replacement $\kappa_1 \leftrightarrow \kappa_2$ in Eqs. (2.13)-(2.15). This follows from the various quantum numbers listed in Eq. (2.1). As previously mentioned, we are neglecting mixing terms involving the new vectorlike particles and the SM ones.

The RGE for the Higgs boson quartic coupling is given by [23]

$$\frac{d\lambda}{d\ln\mu} = \frac{1}{16\pi^2}\beta_\lambda^{(1)} + \frac{1}{(16\pi^2)^2}\beta_\lambda^{(2)}, \tag{2.16}$$

with

$$\beta_\lambda^{(1)} = 12\lambda^2 - \left(\frac{9}{5}g_1^2 + 9g_2^2\right)\lambda + \frac{9}{4}\left(\frac{3}{25}g_1^4 + \frac{2}{5}g_1^2g_2^2 + g_2^4\right) + 12y_t^2\lambda - 12y_t^4, \tag{2.17}$$

and

$$\begin{aligned}\beta_\lambda^{(2)} \;=\;& -78\lambda^3 + 18\left(\frac{3}{5}g_1^2 + 3g_2^2\right)\lambda^2 - \left(\frac{73}{8}g_2^4 - \frac{117}{20}g_1^2g_2^2 - \frac{1887}{200}g_1^4\right)\lambda - 3\lambda y_t^4 \\ & + \frac{305}{8}g_2^6 - \frac{867}{120}g_1^2g_2^4 - \frac{1677}{200}g_1^4g_2^2 - \frac{3411}{1000}g_1^6 - 64g_3^2y_t^4 - \frac{16}{5}g_1^2y_t^4 - \frac{9}{2}g_2^4y_t^2 \\ & + 10\lambda\left(\frac{17}{20}g_1^2 + \frac{9}{4}g_2^2 + 8g_3^2\right)y_t^2 - \frac{3}{5}g_1^2\left(\frac{57}{10}g_1^2 - 21g_2^2\right)y_t^2 - 72\lambda^2y_t^2 \\ & + 60y_t^6.\end{aligned} \tag{2.18}$$

We calculate the Higgs boson pole mass m_H from the running Higgs quartic coupling using the one-loop matching condition [26].

According to Eq. (2.2) there are additional contributions to the one and two loop beta function for λ which are proportional to the κ_1 and κ_2 couplings. At one loop we have

$$\delta\beta_\lambda^{(1)} = 12(\kappa_1^2 + \kappa_2^2)\lambda - 12(\kappa_1^4 + \kappa_2^4), \tag{2.19}$$

and for two loop

$$\begin{aligned}\delta\beta_\lambda^{(2)} \;=\;& \left(\frac{8}{5}g_1^2 - 64g_3^2\right)(\kappa_1^4 + \kappa_2^4) - \frac{9}{2}g_2^4(\kappa_1^2 + \kappa_2^2) + 10\lambda\left(\frac{1}{4}g_1^2 + \frac{9}{4}g_2^2 + 8g_3^2\right)(\kappa_1^2 + \kappa_2^2) \\ & + \frac{3}{5}g_1^2\left(\frac{3}{2}g_1^2 + 9g_2^2\right)(\kappa_1^2 + \kappa_2^2) - 72\lambda^2(\kappa_1^2 + \kappa_2^2) - 3\lambda(\kappa_1^4 + \kappa_2^4) \\ & + 60(\kappa_1^6 + \kappa_2^6).\end{aligned} \tag{2.20}$$

We next analyze the two loop RGEs numerically and show how the vacuum stability and perturbativity bounds on the SM Higgs boson mass are altered in the presence of the new TeV scale vectorlike particles.

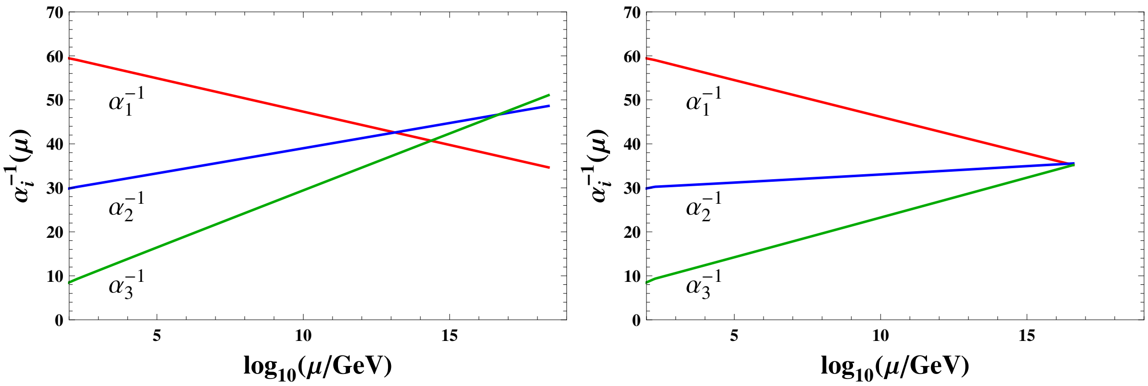

Figure 2.1: Gauge coupling evolution in the SM (left panel) and in the extended SM (right panel). The vectorlike mass is set equal to 500 GeV and the gauge coupling unification scale is $M_{GUT} \simeq 3 \times 10^{16}$ GeV.

We chose the cutoff scale to be M_{GUT}, the scale at which the SM gauge couplings are all equal. This choice is motivated by the following argument. Namely, we want to have as much as possible model independent analysis and in the realistic GUT's we can have very different representation for fields. For instance there are many choice of fileds to break GUT symmetry [27], or if one address the question of flavor structure of fermions in the framework of GUT, or origin of neutrino mass and etc. Also it is well known that in many GUT the cutoff scale has to be very close to the M_{GUT} scale doe to existence of big representation under the GUT gauge symmetry, for instance in SO(10), E(6) etc.

We define the vacuum stability bound as the lowest Higgs boson mass obtained from the running of the Higgs quartic coupling which satisfies the condition $\lambda(\mu) \geq 0$, for any scale between $M_Z \leq \mu \leq M_{\mathrm{GUT}}$. On the other hand, the perturbativity bound is defined as the highest Higgs boson mass obtained from the running of the Higgs quartic coupling with the condition $\lambda(\mu) \leq 4\pi$ for any scale between $M_Z \leq \mu \leq M_{\mathrm{GUT}}$.

In Figure 3.1, we present the evolution of the gauge couplings for the SM (left panel) and for the extended SM (ESM) containing the vectorlike fermions $Q+\bar{Q}+D+\bar{D}$ (right panel). As noted in [19], in ESM model with new vectorlike fermions weighing a 100 GeV or so, one can realize essentially perfect gauge coupling unification at some

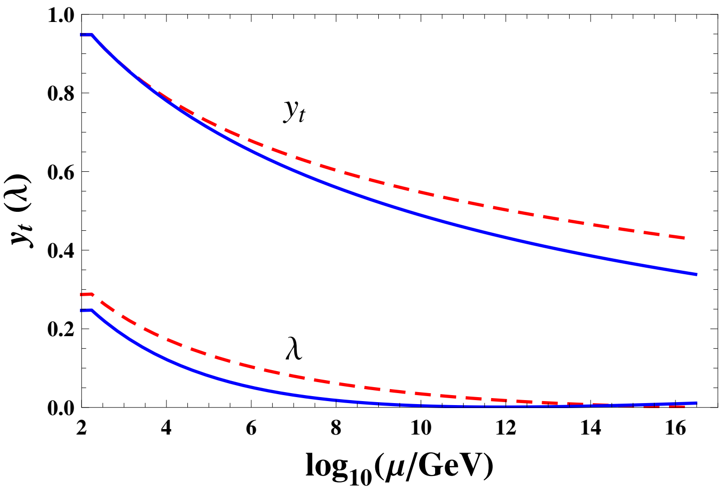

Figure 2.2: Evolution of the top Yukawa coupling in the SM (red dashed line) and in the extended SM (blue solid line). The evolution of the SM Higgs quartic coupling in the two cases are also displayed. We have set $M_F = 500$ GeV and $\kappa_i = 0$.

scale $M_{\rm GUT}$. Furthermore, if we require gauge coupling unification at a level of around 1% or so, then the new vectorlike fermion mass should weigh less than a TeV. For definiteness, we set $M_F = 500$ GeV in our calculation. In this case the SM gauge couplings are unified at $M_{\rm GUT} \simeq 3\times10^{16}$ GeV. As seen in Figure 3.1, the new vectorlike particles help achieve unification by altering the slopes of the three gauge couplings. In particular, the slope of α_3 is changed and it becomes larger at $M_{\rm GUT}$ in comparison to the SM case. The evolution of the top Yukawa coupling is also affected and its value is somewhat smaller at $M_{\rm GUT}$.

In Figure 3.2 we show how the evolution of the two-loop top Yukawa coupling in ESM with $M_F = 500$ GeV. The red dashed line stands for the SM case, and the blue solid line corresponds to the ESM with $\kappa_i = 0$. We also present in Figure 3.2 the evolution of the Higgs quartic coupling. The red dashed line corresponds to the vacuum stability bound for Higgs quartic coupling in the SM, and the blue solid line corresponds to the quartic couplings in the ESM. We see that at $M_{\rm GUT}$, the top Yukawa coupling in the ESM is smaller in comparison to the SM case. On the other hand, it is well known that in the determination of the SM Higgs boson mass vacuum stability bound [16], a crucial role is played by the interplay between the top Yukawa coupling and Higgs quartic coupling, which have comparable and dominant contributions in the RGE for Higgs quartic coupling (See Eq. (2.17)). The negative sign contribution from the top Yukawa coupling makes the Higgs quartic coupling smaller during the evolution. This is how the lower bound for Higgs boson mass is obtained in the SM. So, having in the model a smaller value at $M_{\rm GUT}$ for the top Yukawa coupling means having a milder contribution in the RGE for the Higgs quartic coupling, and this explains why in ESM, somewhat smaller values for the Higgs quartic coupling[1] can satisfy the vacuum stability bound, compared to the SM. In ESM, the lower bound for the SM Higgs boson mass using the one-loop matching condition [26] is found to be $m_H = 117$ GeV, close to the LEP bound of 114.4 GeV [29]. We estimate a theoretical error in this prediction of about 2 GeV, which is in addition to the errors arising from the experimental uncertainties in the determination of the top quark mass and α_3 [30].

As mentioned earlier, the κ_i coupling in Eq. (2.2) can be $O(1)$ if $M_F > 500$ GeV. In Figure 3.3 we present the Higgs boson mass versus κ_i for varying M_F scales. For simplicity, we assume that $\kappa \equiv \kappa_1 = \kappa_2$. The upper solid blue and red curves correspond to the Higgs perturbativity bound, and the lower dashed curves correspond to the vacuum stability bound when the vectorlike particle mass is taken to be 500 GeV (dashed red) and 1 TeV (dashed blue). It is interesting to observe that the perturbativity bound decreases as κ increases from zero to $\kappa \approx 0.6$, and then increases as the value of κ is increased further. We can easily understand this behavior at one loop level. It arises from the interplay between the terms $12\lambda(\kappa_1^2+\kappa_2^2)$ and $-12(\kappa_1^4+\kappa_2^4)$ in Eq. (2.19). Up to $\kappa \approx 0.6$, the term proportional to $\kappa^2\lambda$ dominates over the $\sim \kappa^4$ contribution. So, for $\kappa \leq 0.6$, in the RGE in Eq. (2.16), we have an effective additional contribution with the same sign as the λ coupling, which leads to the decrease of the perturbativity bound. For $\kappa \geq 0.6$ the $\sim \kappa^4$ contribution dominates compared to the term $\kappa^2\lambda$, and we have an effective additional contribution which has the same sign

[1] A similar observation was made in ref. [28] when considering the type III seesaw mechanism for neutrinos.

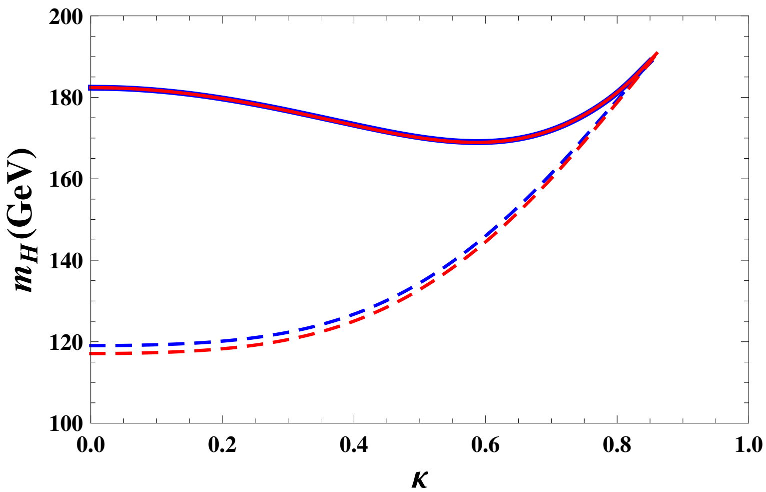

Figure 2.3: Perturbativity (solid) and vacuum stability (dashed) bounds on the Higgs boson pole mass (m_H) versus $\kappa(\equiv \kappa_1 = \kappa_2)$, with vectorlike particle mass $M_F = 500$ GeV (red lines) and $M_F = 1$ TeV (blue lines). The maximum value for the perturbativity bound is $m_H \simeq 191$ GeV when $\kappa = 0.86$. The lower bound for the Higgs mass is $m_H \simeq 117$ GeV, with $\kappa = 0$ and $M_F = 500$ GeV.

contribution as the top quark in Eq. (2.16). This leads to an increasing perturbativity bound as the κ coupling increases. Note that we have an upper bound $\kappa = 0.86$ for $M_F = 500$ GeV, and $\kappa = 0.84$ for $M_F = 1$ TeV. This happens because either the top Yukawa or κ coupling becomes nonperturbative before the GUT scale. Corresponding to the upper bound for κ couplings, we have an upper bound on the Higgs mass: $m_H = 191$ GeV if $M_F = 500$ GeV, and $m_H = 189$ GeV if $M_F = 1$ TeV.

We see in Figure 3.3 that the vacuum stability bound gradually increases as the κ coupling increases. This happens because in the evolution of the Higgs quartic coupling, corresponding to the vacuum stability bound, the contribution proportional to the term $-\kappa^4$ dominates over the $\kappa^2\lambda$ contribution for lower values of κ. So in the RGE for the Higgs quartic coupling (see Eq. (2.16)) we have an additional contribution with the same sign as the top quark. This leads to the explanation why the vacuum stability bound increases when value of κ increases at low scale, and they eventually merge with the vacuum stability bound. We obtain the following results for the Higgs mass corresponding to the vacuum stability bound: $m_H = 117$ GeV when $M_F = 500$ GeV, and $m_H = 119$ GeV when $M_F = 1$ TeV, with $\kappa = 0$.

2.3 Type I Seesaw and the Higgs Boson Mass

We next consider the impact of type I seesaw physics [12] on the Higgs mass bounds found in the previous section. The terms relevant for neutrino oscillations through type I seesaw are given by

$$\mathcal{L}_\nu = -y_D^{ij}\, l_i\, \nu_j^c\, \Phi^c - \frac{1}{2} M_R^{ij} (\nu^c)_i^T \nu_j + h.c., \quad i, j = 1, 2, 3. \tag{2.21}$$

Here l_i is the lepton doublet, ν_i^c the right handed neutrino, y_D^{ij} is neutrino Yukawa coupling and M_R^{ij} denotes the right handed neutrino mass matrix.

Above the scale M_R we have the following one loop RGE for $Y_\nu \equiv y_D^{ij}$,

$$\frac{d\mathbf{Y}_\nu}{d\ln\mu} = \frac{1}{16\pi^2}\mathbf{Y}_\nu \left(3y_t^2 + \mathrm{tr}\left[Y_\nu^\dagger Y_\nu\right] + \frac{3}{2} Y_\nu^\dagger Y_\nu - \left(\frac{9}{20} g_1^2 + \frac{9}{4} g_2^2\right)\right). \tag{2.22}$$

The various beta functions are modified as follows:

$$\begin{aligned}
\beta_t^{(1)} &\to \beta_t^{(1)} + \mathrm{tr}\left[Y_\nu^\dagger Y_\nu\right], \\
\beta_{\kappa_1}^{(1)} &\to \beta_{\kappa_1}^{(1)} + \mathrm{tr}\left[Y_\nu^\dagger Y_\nu\right], \\
\beta_{\kappa_2}^{(1)} &\to \beta_{\kappa_2}^{(1)} + \mathrm{tr}\left[Y_\nu^\dagger Y_\nu\right], \\
\beta_\lambda^{(1)} &\to \beta_\lambda^{(1)} + 4\ \mathrm{tr}[Y_\nu^\dagger Y_\nu]\lambda - 4\ \mathrm{tr}[(Y_\nu^\dagger Y_\nu)^2].
\end{aligned} \tag{2.23}$$

It is certainly interesting to consider realistic cases of the neutrino mass matrix and mixing which reproduce the current neutrino oscillation data. We will consider a scenario in which the light neutrinos form a hierarchical mass spectrum. It was shown in Ref. [28] that the impact on the SM Higgs boson mass from an inverted-hierarchial neutrino mass spectrum is not significantly different from the hierarchial case.

The light neutrino mass matrix is diagonalized by a mixing matrix U_{MNS} such that

$$\mathbf{M}_\nu = \frac{v^2}{2M}\, Y^T Y = U_{MNS} D_\nu U_{MNS}^T, \tag{2.24}$$

with $D_\nu = \mathrm{diag}(m_1, m_2, m_3)$, where we have assumed, for simplicity, that the Yukawa matrix $\mathbf{Y}_\nu$ is real. We further assume that the mixing matrix has the so-called tri-bimaximal form [31]

$$U_{MNS} = \begin{pmatrix} \sqrt{\frac{2}{3}} & \sqrt{\frac{1}{3}} & 0 \\ -\sqrt{\frac{1}{6}} & \sqrt{\frac{1}{3}} & \sqrt{\frac{1}{2}} \\ -\sqrt{\frac{1}{6}} & \sqrt{\frac{1}{3}} & -\sqrt{\frac{1}{2}} \end{pmatrix}, \tag{2.25}$$

which is in very good agreement with the current best fit values of the neutrino oscillation data [32].

For the hierarchical case the diagonal neutrino mass matrix is given by

$$D_\nu \simeq \mathrm{diag}(0, \sqrt{\Delta m_{12}^2}, \sqrt{\Delta m_{23}^2}). \tag{2.26}$$

We fix the input values for the solar and atmospheric neutrino oscillation data as [32]

$$\begin{aligned} \Delta m_{12}^2 &= 8.2 \times 10^{-5}\ \mathrm{eV}^2, \\ \Delta m_{23}^2 &= 2.4 \times 10^{-3}\ \mathrm{eV}^2. \end{aligned} \tag{2.27}$$

Our finding are presented in Figure 3.4 where we plot the vacuum stability (dashed) and perturbativity (solid) bound versus $\kappa (\equiv \kappa_1 = \kappa_2)$, with M_F set equal to 500 GeV. We consider three distinct mass scales for the heavy right handed neutrinos, namely, $M_R = 10^{13}$ GeV (red), 10^{14} GeV (blue) and 10^{15} GeV (green). The general picture of the Higgs mass versus κ coupling is qualitatively the same as in Figure 3.3. Only the initial values for the Higgs mass when $\kappa = 0$ is taken are changed depending on the type I seesaw scale. According to Eq. (2.23) the Dirac neutrino Yukawa coupling Y_ν gives an additional contribution to the Higgs quartic coupling RGE with the same sign as the top quark contribution. It is natural to expect that the vacuum stability bound will increase if the Y_ν coupling is increased. For $M_R = 10^{13}$ GeV, the vacuum stability bound essentially coincides with the corresponding bounds in Figure 3.3. With $M_R = 10^{14}$ GeV the vacuum stability bound is only slightly altered since Y_ν is still not large at that scale in comparison to the top Yukawa coupling. For $M_R = 10^{15}$

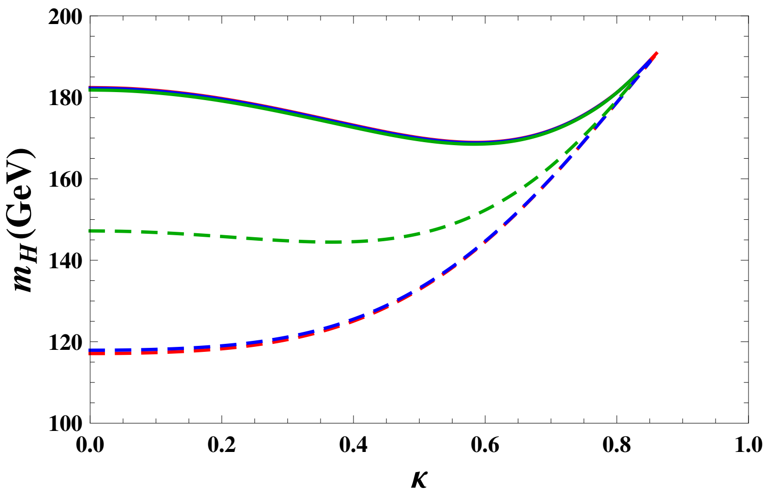

Figure 2.4: Perturbativity (solid) and vacuum stability (dashed) bounds on the Higgs boson pole mass (m_H) versus $\kappa(\equiv \kappa_1 = \kappa_2)$ in the extended SM, including type I seesaw physics. We consider three different type I seesaw scales $M_R = 10^{13}$ GeV (red), 10^{14} GeV (blue) and 10^{15} GeV (green). For our calculation we consider a hierarchical neutrino mass spectrum, and we set $M_F = 500$ GeV. The maximum and minimal values for the Higgs mass corresponding to the perturbativity and vacuum stability bounds are the same as in Figure 3.3.

GeV we see a significant change in the vacuum stability bound since now the coupling Y_ν is larger than the top Yukawa coupling, and the two of them together force the Higgs quartic coupling at low scale to be larger in order to satisfy the vacuum stability bound. Note that there is hardly any impact of type I seesaw on the perturbativity bound. This is due to the fact that above the seesaw scale the Higgs quartic coupling is already larger than Y_ν.

2.4 Conclusion

Following ref. [19], we have considered a plausible extension of the SM in which new vectorlike fermions carrying SM quantum numbers and with masses of order 300 GeV – 1 TeV are introduced. This relatively modest extension of the SM, denoted by ESM in the text, leads to a rather precise unification of the SM gauge couplings at $M_{\rm GUT} \sim 3 \times 10^{16}$ GeV, and it also gives rise to a vacuum stability bound on the SM

Higgs mass of 117 GeV. The perturbativity bound on the Higgs mass is estimated to lie close to 190 GeV. The new vectorlike fermions should be accessible at the LHC.

Chapter 3

SEESAW EXTENDED STANDARD MODEL WITH NON-MINIMAL GRAVITATIONAL COUPLING

In this chapter we examine the impact of the non-minimal gravitational coupling on the SM Higgs mass bounds [33]. In the presence of non-minimal gravitational coupling $\xi H^\dagger H \mathcal{R}$ between the SM Higgs doublet H and the curvature scalar $\mathcal{R}$, the effective ultraviolet cutoff scale is given by $\Lambda \approx m_P/\xi$, where m_P is the reduced Planck mass, and $\xi \gtrsim 1$ is a dimensionless coupling constant. In type I and type III seesaw extended SM, which can naturally explain the observed solar and atmospheric neutrino oscillations, we investigate the implications of this non-minimal gravitational coupling for the SM Higgs boson mass bounds based on vacuum stability and perturbativity arguments. A lower bound on the Higgs boson mass close to 120 GeV is realized with type III seesaw and $\xi \sim 10 - 10^3$.

3.1 Introduction

In general, the non-minimal gravitational coupling between the SM Higgs doublet and the curvature scalar,

$$\xi H^\dagger H \mathcal{R}, \tag{3.1}$$

can be introduced in the SM. This coupling opens up a very intriguing scenario for inflationary cosmology, namely, the possibility that the SM Higgs field may play the role of inflation field, and this has been investigated in several recent papers [34]-[40]. As pointed out in [41], in the presence of the non-minimal gravitational coupling, it is natural to identify the effective ultraviolet cutoff scale as

$$\Lambda \approx \frac{m_P}{\xi}, \tag{3.2}$$

for $\xi \geq 1$, rather than m_P. Note that the cutoff may depend on the background field value which in our case is of order the electroweak scale (see last refs. in [34] and [40]).

In this chapter, we extend previous work on the Higgs boson mass bounds in type I and III seesaw extended SM [28] to the case with non-minimal gravitational coupling. The ultraviolet cutoff scale is taken to be $\Lambda = m_P/\xi$ in our analysis. We will show that the gravitational coupling as well as type I and III seesaw effects can dramatically alter the vacuum stability and perturbativity bounds on the SM Higgs boson mass. In particular, the vacuum stability bound on the Higgs boson mass can be lowered to 120 GeV or so, significantly below the usual lower bound of about 128 GeV found in the absence of seesaw and with $\xi = 0$.

3.2 Non-Minimal Gravitational Coupling and Type I Seesaw Extended Standard Model

In type I seesaw, three generations of SM-singlet right-handed neutrinos $\psi_i (i = 1, 2, 3)$ are introduced. The relevant terms in the Lagrangian are given by

$$\mathcal{L} \supset -y_{ij}\overline{\ell_i}\psi_j H - M_R\overline{\psi_i^c}\psi_i, \tag{3.3}$$

where ℓ_i is the i-th generation SM lepton doublet. For simplicity, we assume in this paper that the three right-handed neutrinos are degenerate in mass (M_R). At energies below M_R, the heavy right-handed neutrinos are integrated out and the effective dimension five operator is generated by the seesaw mechanism. After electroweak symmetry breaking, the light neutrino mass matrix is obtained as

$$\mathbf{M}_\nu = \frac{v^2}{2M_R}\mathbf{Y}_\nu^T\mathbf{Y}_\nu, \tag{3.4}$$

where $v = 246$ GeV is the VEV of the Higgs doublet, and $\mathbf{Y}_\nu = y_{ij}$ is a 3×3 Yukawa matrix.

For a renormalization scale $\mu < M_R$, the heavy fermions are decoupled, and there is no effect on the RGEs for the SM couplings. However, in the presence of the non-minimal gravitational coupling, a factor $s(\mu)$ defined as

$$s(\mu) = \frac{1 + \frac{\xi\mu^2}{m_P^2}}{1 + (6\xi + 1)\frac{\xi\mu^2}{m_P^2}}, \tag{3.5}$$

is assigned to each term in the RGEs associated with the physical Higgs boson loop corrections [34, 35, 38]. In our analysis, we employ 2-loop RGEs for the SM couplings. Since the SM beta functions suitably modified with the s-factor are known only at 1-loop level, we employ the beta functions with the s-factor for 1-loop corrections, while the beta functions for 2-loop corrections are without the s-factor. We have checked that the effects of the s-factor in beta functions for 2-loop corrections are negligible as far as our final results are concerned [36].

The SM REGs with a renormalization scale $\mu < M_R$ are presented in Chapter 2. The Higgs boson pole mass m_H is determined through one-loop effective potential improved by two-loop RGEs. The second derivative of the effective potential at the potential minimum leads to [42]

$$\begin{aligned} m_H^2 &= \lambda\zeta^2 v^2 + \frac{3}{64\pi^2}\zeta^2 v^2 \left\{ g_2^4 \left(\log \frac{g_2^2\zeta^2 v^2}{4\mu^2} + \frac{2}{3} \right) \right. \\ &+ \left. \frac{1}{2}\left(g_2^2 + \frac{3}{5}g_1^2 \right)^2 \left[\log \frac{\left(g_2^2 + \frac{3}{5}g_1^2\right)\zeta^2 v^2}{4\mu^2} + \frac{2}{3} \right] - 8y_t^4 \log \frac{y_t^2\zeta^2 v^2}{2\mu^2} \right\}, \end{aligned} \tag{3.6}$$

where $\zeta = \exp\left(-\int_{M_Z}^{\mu} \frac{\gamma(\mu)}{\mu} d\mu\right)$, with the anomalous dimension γ of the Higgs doublet evaluated at two-loop level. All running parameters are evaluated at $\mu = m_H$, and the Higgs boson mass is determined as the root of this equation. We have checked that our results on the Higgs boson mass bounds for the SM case ($\xi = 0$ and $M_R \to \infty$) coincide with the ones obtained in recent analysis [43].

For the renormalization scale $\mu \geq M_R$, the SM RGEs should be modified to include contributions from the singlet and triplet fermions in type I seesaw, so that the RGE evolution of the Higgs quartic coupling is altered. For simplicity, we consider only one-loop corrections from the heavy fermions.

For $\mu \geq M_R$, the above RGEs are modified as

$$\begin{aligned} \beta_t^{(1)} &\to \beta_t^{(1)} + \mathrm{tr}\left[\mathbf{S}_\nu\right], \\ \beta_\lambda^{(1)} &\to \beta_\lambda^{(1)} + 4\mathrm{tr}\left[\mathbf{S}_\nu\right]\lambda - 4\mathrm{tr}\left[{\mathbf{S}_\nu}^2\right], \end{aligned} \tag{3.7}$$

where $\mathbf{S}_\nu = \mathbf{Y}_\nu^\dagger \mathbf{Y}_\nu$, and its corresponding RGE is given by

$$16\pi^2 \frac{d\mathbf{S}_\nu}{d\ln\mu} = \mathbf{S}_\nu \left[6y_t^2 + 2\ \mathrm{tr}\left[\mathbf{S}_\nu\right] - \left(\frac{9}{10}g_1^2 + \frac{9}{2}g_2^2\right) + (2+s)\mathbf{S}_\nu\right]. \tag{3.8}$$

We analyze the RGEs numerically and show how the vacuum stability and perturbativity bounds on Higgs boson mass are altered in the presence of type I seesaw and the non-minimal gravitational coupling. As previously noted, because of the gravitational coupling, we set the ultraviolet cutoff as $\Lambda = m_P/\xi$ for $\xi \geq 1$ ($\Lambda = m_P$ as usual if $\xi < 1$). We define the vacuum stability bound as the lowest Higgs boson mass obtained from the running of the Higgs quartic coupling which satisfies the condition $\lambda(\mu) \geq 0$ for any scale between $m_H \leq \mu \leq \Lambda$. On the other hand, the perturbativity bound is defined as the highest Higgs boson mass obtained from the running of the Higgs quartic coupling with the condition $\lambda(\mu) \leq 4\pi$ for any scale between $m_H \leq \mu \leq \Lambda$.

In order to see the effects of the neutrino Yukawa coupling on the Higgs boson mass bounds, we first examine a toy model with $\mathbf{Y}_\nu = \mathrm{diag}(0, 0, Y_\nu)$. In Figure 3.1, the vacuum stability and perturbativity bounds on Higgs boson mass as a function of ξ are depicted for various Y_ν values and a fixed seesaw scale $M_R = 10^{13}$ GeV. The results for the perturbativity bound are almost insensitive to Y_ν. On the other hand, for a fixed $\xi < m_P/M_R$, the vacuum instability bound becomes larger, as Y_ν is increased. For a fixed Y_ν, the vacuum instability bound becomes smaller, as ξ is increased. When $\xi > m_P/M_R$ or equivalently $\Lambda < M_R$, the vacuum stability and perturbativity bounds coincides with the SM ones with Λ, as expected. For a fixed cutoff scale $\Lambda > M_R$, the window for the Higgs boson mass between the vacuum stability and perturbative bounds becomes narrower and is eventually closed as Y_ν becomes sufficiently large. This behavior is shown in Figure 3.2 for various values of ξ. Increasing ξ widens the Higgs mass window for a fixed Y_ν.

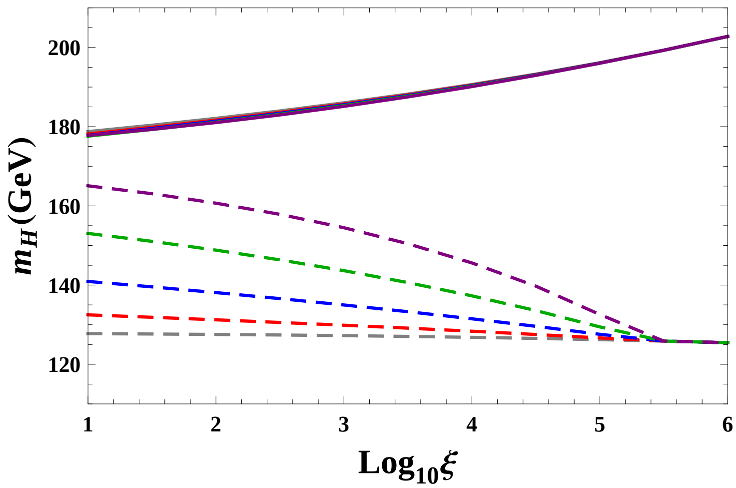

Figure 3.1: Perturbativity and vacuum stability bounds on Higgs boson mass versus ξ for various Y_ν and $M_R = 10^{13}$ GeV for type I seesaw. The gray lines correspond to $Y_\nu = 0$. The red, blue, green and purple lines correspond to $Y_\nu = 0.6, 0.8, 1.0$ and 1.2.

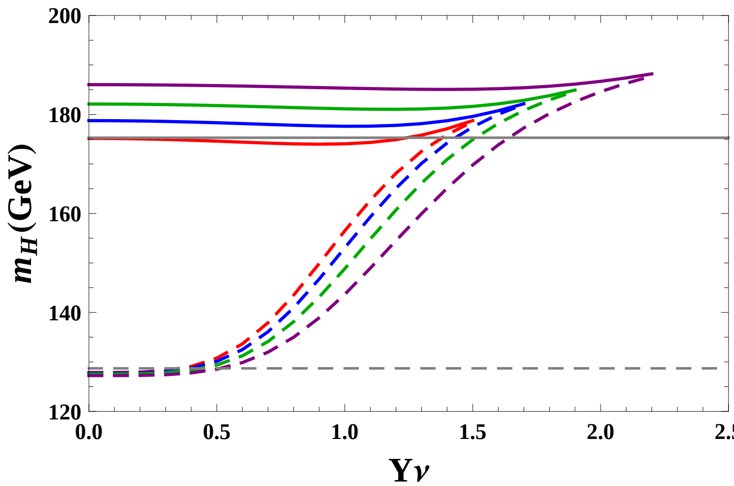

Figure 3.2: Perturbativity and vacuum stability bounds on Higgs boson mass versus Y_ν for various ξ and $M_R = 10^{13}$ GeV for type I seesaw. The red, blue, green and purple lines correspond to $\xi = 0, 10, 100$ and 10^3. The gray lines show the bounds in the SM case.

It is certainly interesting to consider more realistic cases which are compatible with the current neutrino oscillation data. The light neutrino mass matrix is diagonalized by a mixing matrix U_{MNS} such that

$$\mathbf{M}_\nu = \frac{v^2}{2M_R}\,\mathbf{S}_\nu = U_{MNS} D_\nu U_{MNS}^T, \tag{3.9}$$

with $D_\nu = \mathrm{diag}(m_1, m_2, m_3)$, where we have assumed, for simplicity, that the Yukawa matrix $\mathbf{Y}_\nu$ is real. We further assume that the mixing matrix has the so-called tri-bimaximal form [31],

$$U_{MNS} = \begin{pmatrix} \sqrt{\frac{2}{3}} & \sqrt{\frac{1}{3}} & 0 \\ -\sqrt{\frac{1}{6}} & \sqrt{\frac{1}{3}} & \sqrt{\frac{1}{2}} \\ -\sqrt{\frac{1}{6}} & \sqrt{\frac{1}{3}} & -\sqrt{\frac{1}{2}} \end{pmatrix}, \tag{3.10}$$

which is in very good agreement with the current best fit values of the neutrino oscillation data [32]. Let us consider two examples for the light neutrino mass spectrum, the hierarchical case and the inverted-hierarchical case. In the hierarchical case, we have

$$D_\nu \simeq \mathrm{diag}(0, \sqrt{\Delta m_{12}^2}, \sqrt{\Delta m_{23}^2}), \tag{3.11}$$

while for the inverted-hierarchical case, we choose

$$D_\nu \simeq \mathrm{diag}(\sqrt{-\Delta m_{12}^2 + \Delta m_{23}^2}, \sqrt{\Delta m_{23}^2}, 0). \tag{3.12}$$

We fix the input values for the solar and atmospheric neutrino oscillation data as [32]

$$\begin{aligned} \Delta m_{12}^2 &= 8.2 \times 10^{-5}\ \mathrm{eV}^2, \\ \Delta m_{23}^2 &= 2.4 \times 10^{-3}\ \mathrm{eV}^2. \end{aligned} \tag{3.13}$$

From Eqs. (3.9)-(3.13), we can obtain the matrix

$$\mathbf{S}_\nu = \mathbf{Y}_\nu^\dagger \mathbf{Y}_\nu = \mathbf{Y}_\nu^T \mathbf{Y}_\nu = \frac{2M_R}{v^2} U_{MNS} D_\nu U_{MNS}^T. \tag{3.14}$$

For a given value of M_R, we obtain a concrete 3×3 matrix at the M_R scale, which is used as an input in the RGE analysis. The windows for the Higgs boson pole mass for the hierarchical and inverted-hierarchical cases are shown in Figures 3.3 and 3.4,

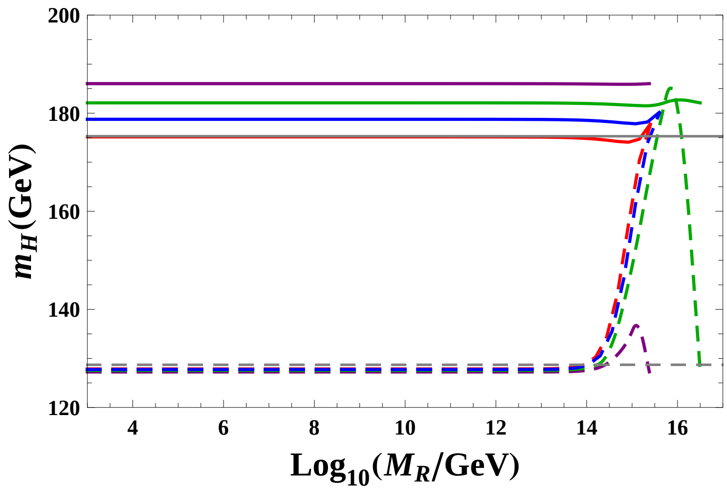

Figure 3.3: Perturbativity and vacuum stability bounds on Higgs boson mass versus M_R with a hierarchical mass spectrum for type I seesaw. The red, blue, green and purple lines correspond to $\xi = 0, 10, 100$ and 10^3. The gray lines show the bounds in the SM case.

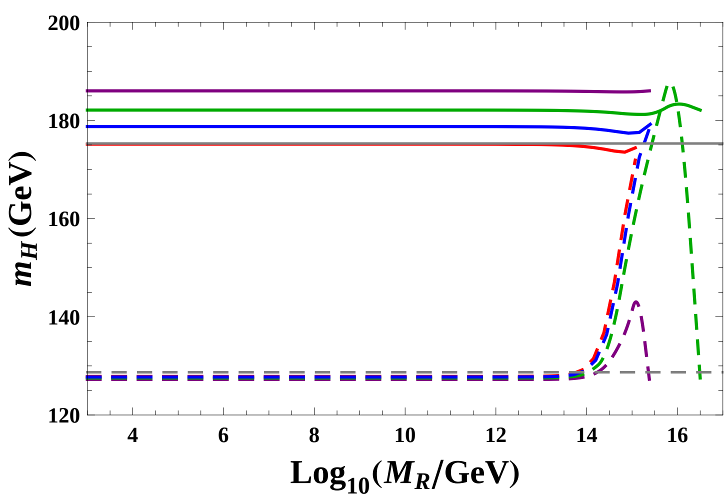

Figure 3.4: Perturbativity and vacuum stability bounds on Higgs boson mass versus M_R with an inverted hierarchical mass spectrum for type I seesaw. The red, blue, green and purple lines correspond to $\xi = 0, 10, 100$ and 10^3. The gray lines show the bounds in the SM case.

respectively. As M_R or equivalently the Yukawa couplings become large, the window for the Higgs boson mass becomes narrower and is eventually closed for a fixed ξ. In plots for large values of ξ, the Higgs boson mass window first narrows, but opens up again, as M_R is increased. This is because M_R becomes larger than Λ for a sufficiently large ξ.

3.3 Non-Minimal Gravitational Coupling and Type III Seesaw Extended Standard Model

The basic structure of type III seesaw is similar to type I seesaw, except that instead of the singlet right-handed neutrinos, three generations of fermions which transforms as $(\mathbf{3}, 0)$ under the electroweak gauge group $\mathrm{SU}(2)_L \times \mathrm{U}(1)_Y$ are introduced:

$$\psi_i = \sum_a \frac{\sigma^a}{2} \psi_i^a = \frac{1}{2} \begin{pmatrix} \psi_i^0 & \sqrt{2}\psi_i^+ \\ \sqrt{2}\psi_i^- & -\psi_i^0 \end{pmatrix}. \tag{3.15}$$

With canonically normalized kinetic terms for the triplet fermions, we replace the SM-singlet right-handed neutrinos of type I seesaw in Eq. (3.3) by these SU(2) triplet fermions. Assuming degenerate masses (M_R) for the three triplet fermions, the light neutrino mass matrix via type III seesaw mechanism is obtained as

$$\mathbf{M}_\nu = \frac{v^2}{8M_R} \mathbf{Y}_\nu^T \mathbf{Y}_\nu. \tag{3.16}$$

The analysis is analogous to the type I seesaw case. For $\mu \geq M_R$, the RGEs are modified as [28]

$$\begin{aligned} \beta_t^{(1)} &\to \beta_t^{(1)} + \frac{3}{4}\mathrm{tr}\left[\mathbf{S}_\nu\right], \\ \beta_\lambda^{(1)} &\to \beta_\lambda^{(1)} + 3\mathrm{tr}\left[\mathbf{S}_\nu\right]\lambda - \frac{5}{4}\mathrm{tr}\left[{\mathbf{S}_\nu}^2\right]. \end{aligned} \tag{3.17}$$

The RGE for $\mathbf{S}_\nu$ is given by

$$16\pi^2 \frac{d\mathbf{S}_\nu}{d\ln\mu} = \mathbf{S}_\nu \left[6y_t^2 + \frac{3}{2}\mathrm{tr}\left[\mathbf{S}_\nu\right] - \left(\frac{9}{10}g_1^2 + \frac{33}{2}g_2^2\right) + \frac{3+2s}{4}\mathbf{S}_\nu\right]. \tag{3.18}$$

In addition, in type III seesaw, the one-loop beta function coefficient of the SM SU(2) gauge coupling is modified as $-(39-s)/12 \to (9+s)/12$ in the presence of SU(2) triplet fermions.

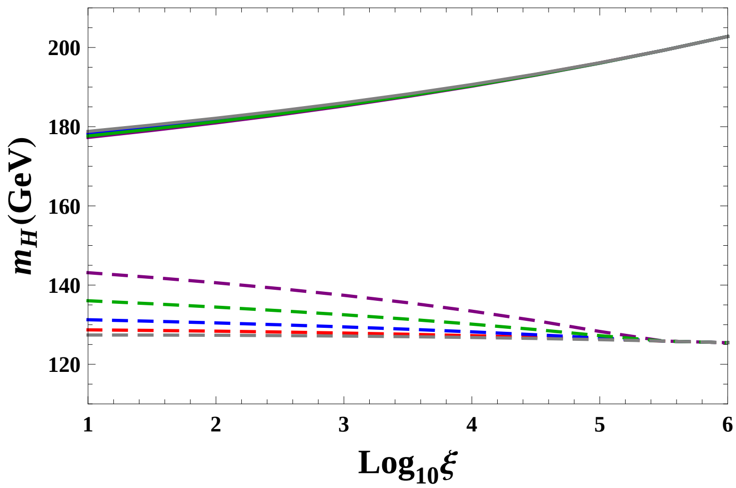

Figure 3.5: Perturbativity and vacuum stability bounds on Higgs boson mass versus ξ for various Y_ν and $M_R = 10^{13}$ GeV for type III seesaw. The gray lines correspond to $Y_\nu = 0$. The red, blue, green and purple lines correspond to $Y_\nu = 0.6, 0.8, 1.0$ and 1.2.

We first examine the toy model for type III seesaw with $M_R = 10^{13}$ GeV. The results are depicted in Figure 3.5, which corresponds to Figure 3.1 for type I seesaw. We can see results similar to those presented in Figure 3.1. The window for the Higgs boson mass between the vacuum stability and perturbativity bounds is shown in Figure 3.6 for various ξ values, corresponding to Figure 3.2 for type I seesaw.

In a more realistic case, we repeat the same analysis as in type I seesaw, except for a factor difference in the definition of the light neutrino mass matrix in type III seesaw, $\mathbf{M}_\nu = \frac{v^2}{8M_R}\,\mathbf{S}_\nu$. The windows for the Higgs boson pole mass for the hierarchical and inverted-hierarchical cases are shown in Figures 3.7 and 3.8, respectively. For large M_R, we can see behavior similar to Figures 3.3 and 3.4 for type I seesaw. However, note that for low M_R values, the Higgs boson mass bounds with type III seesaw are different from the SM ones and the range of the Higgs boson mass window is enlarged, as pointed out in [28] . In particular, a relatively light Higgs boson mass close to 120 GeV is now possible. This result can be qualitatively understood in the following way. The presence of the triplet fermions significantly alters the RGE running of the $\mathrm{SU}(2)_L$

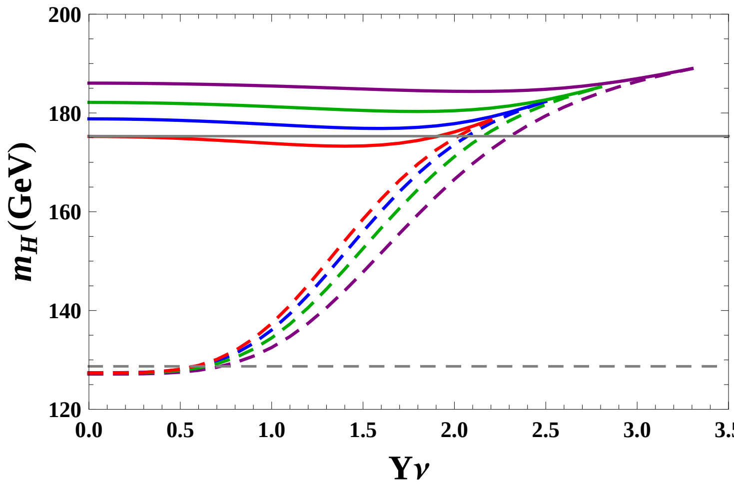

Figure 3.6: Perturbativity and vacuum stability bounds on Higgs boson mass versus Y_ν for various ξ and $M_R = 10^{13}$ GeV for type III seesaw. The red, blue, green and purple lines correspond to $\xi = 0, 10, 100$ and 10^3. The gray lines show the bounds in the SM case.

gauge coupling by making it asymptotically non-free, so that $g_2(\mu)$ for $\mu > M_R$ is larger than the SM value without type III seesaw. In the analysis of the stability bound, the Higgs quartic coupling is small, and the one-loop beta function of the Higgs quartic coupling can be approximated as (see Eq. (2.17))

$$\beta_\lambda^{(1)} \simeq \frac{1}{16\pi^2}\left[\frac{9}{4}\left(\frac{3}{25}g_1^4 + \frac{2}{5}g_1^2 g_2^2 + g_2^4\right) - 12y_t^4\right]. \tag{3.19}$$

Since the first term on the right hand side is larger in type III seesaw than in the SM case, the Higgs quartic coupling decreases more slowly than in the SM. Consequently, the stability bound on the Higgs boson mass is lowered. For the perturbativity bound, the Higgs quartic coupling is large and the one-loop beta function can be approximated by

$$\beta_\lambda^{(1)} \simeq \frac{1}{16\pi^2}\left[(3+9s^2)\lambda^2 - \left(\frac{9}{5}g_1^2 + 9g_2^2\right)\lambda + 12y_t^2\lambda - 12y_t^4\right]. \tag{3.20}$$

The beta function is smaller than the SM one due to the second term. Therefore, the evolution of the Higgs quartic coupling is slower, and as a result, the Higgs boson mass based on the perturbative bound is somewhat larger than the SM one.

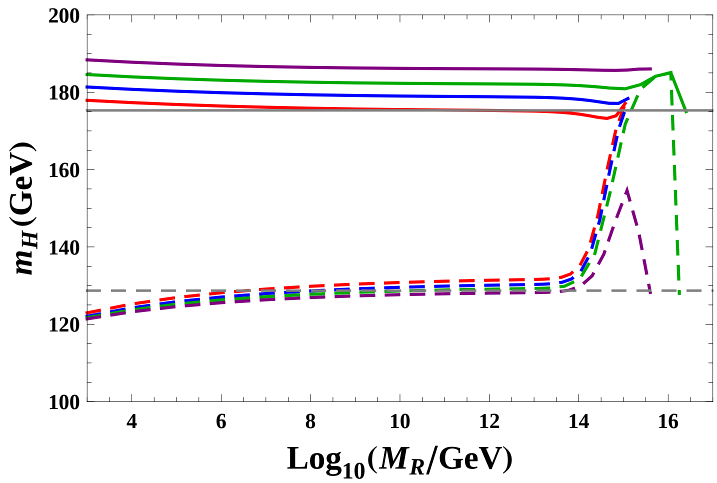

Figure 3.7: Perturbativity and vacuum stability bounds on Higgs boson mass versus M_R with a hierarchical mass spectrum for type III seesaw. The red, blue, green and purple lines correspond to $\xi = 0, 10, 100$ and 10^3. The gray lines show the bounds in the SM case.

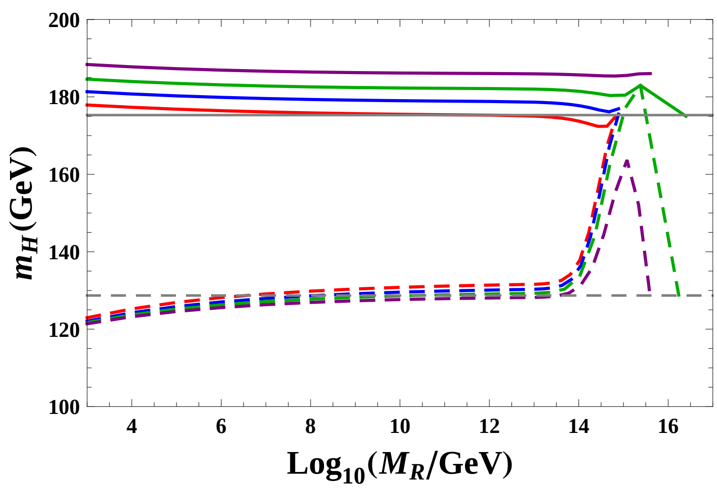

Figure 3.8: Perturbativity and vacuum stability bounds on Higgs boson mass versus M_R with an inverted hierarchical mass spectrum for type III seesaw. The red, blue, green and purple lines correspond to $\xi = 0, 10, 100$ and 10^3. The gray lines show the bounds in the SM case.

Finally, we note that with type III seesaw, the lower bound on the SM Higgs mass is approximately given by

$$m_H \geq 121.4 \text{ GeV} + 3.0 \text{ GeV}\left(\frac{M_t - 173.1 \text{ GeV}}{1.3 \text{ GeV}}\right) \\ -2.6 \text{ GeV}\left(\frac{\alpha_S(M_Z) - 0.1193}{0.0028}\right). \tag{3.21}$$

This is to be compared with a lower bound close to 128 GeV in the absence of type III seesaw.

3.4 Conclusion

We have considered the potential impacts of type I and III seesaw on the vacuum stability and perturbativity bounds on the Higgs boson mass in the presence of the non-minimal gravitational coupling, with an effective ultraviolet cutoff scale $\Lambda = m_P/\xi$ for $\xi \geq 1$. For energies higher than the seesaw scale, the heavy fermions introduced in type I and III seesaw are involved in loop corrections and the RGEs of the SM are modified. As a consequence, the vacuum stability and perturbativity bounds on the Higgs boson mass are altered. We have found that for a fixed ξ, as the neutrino Yukawa couplings are increased, the vacuum stability bound grows and eventually merges with the perturbativity bound. Therefore, the Higgs boson mass window is closed at some large Yukawa couplings with a fixed seesaw scale, or some high seesaw scale by fixing the light neutrino mass scale. For a fixed neutrino Yukawa coupling or a fixed seesaw scale, the Higgs boson mass window is enlarged as ξ is increased or equivalently the effective cutoff scale is lowered. A large neutrino Yukawa coupling or equivalently a large seesaw scale affects in similar ways the Higgs mass bounds in both type I and III seesaw. However, with type III seesaw, there is significant lowering of the Higgs mass due to modification of the RGE evolution of the $\mathrm{SU}(2)_L$ gauge coupling even if the neutrino Yukawa couplings are negligible. For a low seesaw scale, the Higgs boson mass window between the vacuum stability and perturbative bounds turns out to be wider than the SM one. This is in contrast with type I seesaw where the Higgs boson mass bounds in the SM are reproduced in the small Yukawa coupling limit. We have shown that in type III seesaw, the vacuum stability bound on Higgs mass can be close to the current Higgs mass lower bound of 114.4 GeV [29].

Chapter 4

HIGGS MASS IN NMSSM WITH INVERSE SEESAW

In this chapter we consider extensions of the next-to-minimal supersymmetric model (NMSSM) in which the observed neutrino masses are generated through a TeV scale inverse seesaw mechanism [44]. The new particles associated with this mechanism can have sizable couplings to the Higgs field which can yield a large contribution to the mass of the lightest CP-even Higgs boson. With this new contribution, a 126 GeV Higgs is possible along with order of 200 GeV masses for the stop quarks for a broad range of $\tan\beta$. The Higgs production and decay in the diphoton channel can be enhanced due to this new contribution. It is also possible to solve the little hierarchy problem in this model without invoking a maximal value for the NMSSM trilinear coupling and without severe restrictions on the value of $\tan\beta$.

4.1 Introduction

In 2012, the ATLAS and CMS Collaborations at the Large Hadron Collider (LHC) independently reported the discovery [45, 46] of a particle with production and decay modes that appear more or less consistent with the Standard Model (SM) Higgs boson of mass $m_h \approx 126$ GeV. In addition to the Higgs discovery, both experiments reported an excess in Higgs production and decay in the diphoton channel, around $1.4 - 2$ times larger than the SM expectations. These results nevertheless serve as strong motivation to investigate possible extensions of the SM where a possible signal in the diphoton channel could be enhanced compared to the SM.

The minimal supersymmetric standard model (MSSM) [47] can accommodate values of $m_h \sim 126$ GeV, but this requires either a very large, $\mathcal{O}(\text{few} - 10)$ TeV, stop quark mass [48], or a large soft supersymmetry breaking (SSB) trilinear A-term, with a stop quark mass of around a TeV [49]. Such a heavy stop quark leads to the so-called "little hierarchy" problem [50] because, in implementing radiative electroweak symmetry breaking, TeV scale quantities must conspire to yield the electroweak mass scale.

On the other hand, in the next-to-minimal supersymmetric standard model (NMSSM), the Higgs mass can be raised significantly through a tree level contribution to the Higgs potential [51]. Therefore, the NMSSM can alleviate the little hierarchy problem, and a 126 GeV Higgs mass can be realized with less fine-tuning. In Ref. [52] it was shown that in order to accommodate a 126 GeV Higgs mass with only a few percent fine-tuning, the NMSSM is pushed to the edge of its parameter space, with $\tan\beta \lesssim 2$ and $\lambda \sim 0.7$. Here $\tan\beta$ is the ratio of the vacuum expectation values (VEVs) of the up (H_u) and down (H_d) MSSM Higgs doublets. The parameter λ is the dimensionless coupling associated with the interaction $H_u H_d S$, where S is a MSSM gauge singlet field. Note that assuming non-universal gaugino masses at the GUT scale, one can also alleviate the little hierarchy problem [53], but we will not discuss this possibility.

Furthermore, in the framework of the NMSSM, Higgs production and decay in the diphoton channel can be enhanced with respect to the SM prediction due to the doublet-singlet mixing in the Higgs sector [52, 54]. It has been shown that to comply with the ATLAS and CMS results, a large stop mass still cannot be avoided. Besides, the couplings (λ, κ, y_t) are all of $\mathcal{O}(1)$ at the GUT scale, which are close to the Landau pole.[1] Here κ is the dimensionless coupling corresponding to the S^3 interaction and y_t is the top Yukawa coupling.

Inspired by recent studies on the NMSSM and the results from ATLAS and CMS, we consider an extension of the NMSSM which has previously been used to explain the origin of neutrino masses. In Ref. [56], in particular, it was shown that in the NMSSM the observed neutrino masses and mixings can be described in terms of

[1] The possible impact of non-perturbative couplings has also received attention. For an example, see Ref. [55].

dimension six, rather than dimension five, operators. All such operators respect the discrete Z_3 symmetries of the model. The new particles associated with the inverse seesaw mechanism [57] can have sizable couplings to the Higgs boson, even with the seesaw scale of around a TeV. This, as we will show, enables the Higgs boson mass to be 126 GeV, without invoking sizable contributions from the stop quark as well as keeping the λ and κ couplings relatively small. With relatively light stop quarks in the spectrum one can enhance the diphoton production relative to the SM prediction [58, 59, 60].

4.2 Higgs Boson Mass in MSSM and NMSSM

The NMSSM is obtained by adding to the MSSM a gauge singlet chiral superfield S (with even Z_2 matter parity) and including the following superpotential terms:

$$W \supset \lambda S H_u H_d + \frac{\kappa}{3} S^3, \tag{4.1}$$

where λ and κ are dimensionless constants, and H_u, H_d denote the MSSM Higgs doublets. A discrete Z_3 symmetry under which S carries a unit charge $\omega = e^{i2\pi/3}$ is introduced in order to eliminate terms from the superpotential that are linear and quadratic in S, as well as the MSSM μ term. We also need the Z_3 symmetry to forbid dangerous tadpole terms in the potential which can revive the gauge hierarchy problem in the theory. On the other hand, once the S field develops a VEV, the Z_3 symmetry is spontaneously broken which can cause the domain wall problem. In order to circumvent this problem, as pointed out in Ref. [61], suitable higher dimensional operators can be introduced in the superpotential which explicitly break the Z_3 symmetry, thereby lifting the degeneracy between three discrete vacua. Note that these Z_3 violating higher dimensional operators (S^7/M_{Pl}^4), where M_{Pl} denotes the Planck mass, are quite different in form from the effective seesaw operators which we will discuss. The higher dimensional operators which generate neutrino masses are Z_3 invariant.

In order to assign the Z_3 charges we require the presence of Yukawa couplings at the renormalizable level. There are several possible Z_3 charge assignments for the matter superfields presented in Ref. [56] that are consistent with this requirement. We consider those cases (see Table 4.1) which lead to the dimension six (inverse) seesaw operator for neutrinos. Later, we will briefly discuss the dimension seven seesaw operators and their implications for the Higgs boson mass. We employ the standard notation for the superfields in Table 4.1. Family indices are omitted for simplicity.

		Q	U^c	D^c	L	E^c	H_u	H_d	S
case I	Z_3	1	ω^2	ω^2	1	ω^2	ω	ω	ω
case II	Z_3	1	ω	1	ω^2	ω	ω^2	1	ω
case III	Z_3	1	1	ω	ω	1	1	ω^2	ω

Table 4.1: Z_3 charge assignments of the NMSSM superfields corresponding to dimension six operators for neutrino masses. Here $\omega = e^{i2\pi/3}$.

The Z_3 charge assignments presented in Table 4.1 lead to the following effective operator for neutrino masses and mixing:

$$\frac{LLH_uH_uS}{M_6^2}, \tag{4.2}$$

where M_6 denotes the appropriate seesaw mass scale. As we will show in the next section, this operator can be generated from the renormalizable superpotential by just integrating out the heavy ($\mathcal{O}$(TeV)) fields. In section 4.3.1 we consider the gauge singlet case, and in section 4.3.2 we replace the gauge singlet field with an $SU(2)_L$ triplet field. We will also show later that the new TeV scale fields will affect the lightest CP-even Higgs mass bound. Before studying this new contribution to the lightest CP-even Higgs boson mass, we briefly summarize the Higgs mass bound in the MSSM and NMSSM.

The upper limit on the lightest CP-even Higgs boson mass in the NMSSM is given by [62]

$$\begin{aligned}\left[m_h^2\right]_{NMSSM} &= M_Z^2\left(\cos^2 2\beta + \frac{2\lambda^2}{g_1^2+g_2^2}\sin^2 2\beta\right)\left(1-\frac{3}{8\pi^2}y_t^2 t\right)\\ &+ \frac{3}{4\pi^2}y_t^2 m_t^2\sin^2\beta\left[\frac{1}{2}\widetilde{X}_t + t + \frac{1}{(4\pi)^2}\left(\frac{3}{2}y_t^2 - 32\pi\alpha_s\right)\right.\\ &\times \left.\left(\widetilde{X}_t + t\right)t\right],\end{aligned} \tag{4.3}$$

where

$$t = \log\left(\frac{M_S^2}{M_t^2}\right), \ \widetilde{X}_t \ = \ \frac{2\widetilde{A}_t^2}{M_S^2}\left(1 - \frac{\widetilde{A}_t^2}{12M_S^2}\right), \ \widetilde{A}_t = A_t - \lambda\langle S\rangle \cot\beta. \tag{4.4}$$

A_t is the top trilinear soft term, and $\langle S\rangle$ denotes the vacuum expectation value (VEV) of the singlet field. Also, g_1 and g_2 denote the $U(1)_Y$ and the $SU(2)_L$ gauge couplings, $M_t = 173.2$ GeV is the top quark pole mass, $M_S = \sqrt{m_{\tilde{t}_L} m_{\tilde{t}_R}}$ denotes the SUSY scale, and $\tilde{t}_L$ and $\tilde{t}_R$ are the left and right handed stop quarks. Notice that we assume $\tan\beta < 50$, since for larger $\tan\beta$ values there can be additional contributions in Eq. (4.3) which may reduce the Higgs mass [51]. An approximate error of ± 3 GeV in the Higgs mass calculation is assumed, which largely arises from theoretical uncertainties [63] and simplifications in the calculation of the Higgs mass formula in Eq. (4.3). The upper bound on λ at the weak scale depends on $\tan\beta$. In general, it cannot be greater than ~ 0.7, if we require that λ remains perturbative up to the $M_{\rm GUT}$ scale [62].

Note that the main difference in the expression (see Eq. (4.3)) for the lightest CP-even Higgs mass between the NMSSM and the MSSM theory is the term $2\lambda^2 \sin^2(2\beta)/(g_1^2 + g_2^2)$. Therefore, the maximum value of the lightest CP-even Higgs mass in the NMSSM is obtained for smaller value of $\tan\beta$.

In Figure 4.1 we show our results in the m_h versus $\tan\beta$ planes. For comparison, we have chosen two different SUSY scales, $M_S = 1$ TeV (left panel) and $M_S = 200$ GeV (right panel), and the maximum value of the coupling λ is used. The red lines correspond to the NMSSM case, whereas the blue lines correspond to the MSSM case. The solid lines show the Higgs mass bounds for $\widetilde{X}_t = 6$, while the dashed lines show the bounds for $\widetilde{X}_t = 0$. The gray band shows the Higgs mass range of 126 ± 3 GeV. We can see that in order to obtain a 126 GeV Higgs in the MSSM, we need to have $M_S > 1$ TeV with maximal mixing. In the NMSSM, due to the additional contributions proportional to λ, for $\tan\beta = 2$ one can easily get a 126 GeV Higgs mass even for $M_S = 200$ GeV. However, without maximal mixing in the stop sector it is hard, even in the NMSSM, to generate a 126 GeV Higgs mass with $M_S < 1$ TeV.

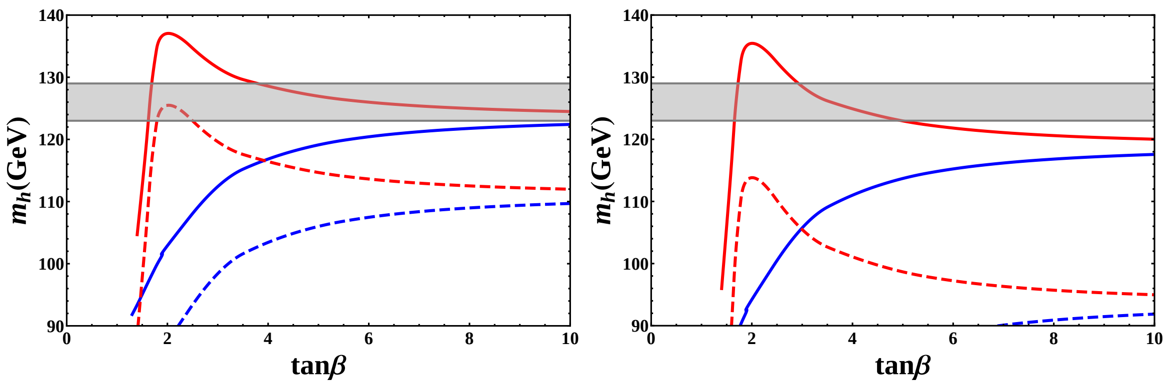

Figure 4.1: Upper bounds on the lightest CP-even Higgs boson mass versus $\tan\beta$, for $M_S = 1$ TeV (left panel) and $M_S = 200$ GeV (right panel). Maximum value of λ is used. Red lines correspond to the NMSSM, and blue lines correspond to the MSSM. The solid lines show the Higgs mass bounds for $\widetilde{X}_t = 6$, while the dashed lines show the bounds with $\widetilde{X}_t = 0$. The gray band shows the Higgs mass range of 126 ± 3 GeV.

4.3 Inverse Seesaw and Higgs Boson Mass

4.3.1 NMSSM + Gauge Singlet field

As shown in Ref. [56], one can incorporate the observed solar and atmospheric neutrino oscillations in the NMSSM by introducing an effective dimension six operator for neutrino masses and mixings. The simplest way to generate this operator is to introduce the gauge singlet chiral superfields $(N_n^c + N_n)$ in the NMSSM with charges listed in Table 4.2. This charge assignment corresponds to the so-called *case I* in Table 4.1. It is straightforward to find the Z_3 charge assignments for $N_n^c + N_n$ for other cases given in Table 4.1, but this will not lead to any new phenomena compared to *case I*. Because of this we will not consider here the other cases presented in Table 4.1. Since the new chiral superfields are gauge singlets, they will preserve gauge coupling unification which is one of the nice features of supersymmetry.

The renormalizable superpotential terms involving only the new chiral superfields are given by

$$W \supset y_{ni}^N N_n^c (H_u L_i) + \frac{\lambda_{N_{nm}}}{2} S N_n N_m + m_{nm} N_n^c N_m. \tag{4.5}$$

	$SU(3)_c$	$SU(2)_L$	$U(1)_Y$	Z_3	Z_2
N_n^c	1	1	0	ω^2	$-$
N_n	1	1	0	ω	$-$

Table 4.2: Charge assignments of $N_n^c + N_n$ superfields for *case I*. Here $\omega = e^{i2\pi/3}$, n denotes the number of gauge singlet $(N_n^c + N_n)$ pairs, and Z_2 is matter parity.

Here i runs from 1 to 3 and denotes the family index, while n and m denote the number of pairs of new fields which we consider, and can be from zero (just the NMSSM case) up to 3. For m_{nm} larger than the electroweak scale, we can integrate out the N_n^c and N_n fields and generate the effective non-renormalizable operators for neutrino masses presented in Eq. (4.2). Following the electroweak symmetry breaking, the neutrino Majorana mass matrix is generated:

$$m_\nu = \frac{(Y_N^T Y_N) {v_u}^2}{M_6} \times \frac{\lambda_N \langle S\rangle}{M_6}. \tag{4.6}$$

For simplicity, we take $m_{ij} = M_6 \delta_{ij}$, $Y_N \equiv y_{ij}$, and $(\lambda_N)_{ij} = \lambda_N \delta_{ij}$. v_u is the VEV of the H_u Higgs doublet and $\langle S\rangle$, the VEV of S field, is around the TeV scale.[2] Eq. (4.6) implies that even if $Y_N \sim \mathcal{O}(1)$ and $M_S \sim 1$ TeV, the correct mass scale for the light neutrinos can be reproduced by suitably adjusting λ_N.

From Eq. (4.5), the additional contribution to the lightest CP-even Higgs mass is given by

$$\left[m_h^2\right]_N = n \times \left[-M_Z^2 \cos^2 2\beta \left(\frac{1}{8\pi^2} Y_N^2 t_N \right) + \frac{1}{4\pi^2} Y_N^4 v^2 \sin^2\beta \left(\frac{1}{2} \widetilde{X}_{Y_N} + t_N \right) \right], \tag{4.7}$$

where

$$t_N = \log\left(\frac{M_S^2 + M_6^2}{M_6^2} \right), \quad \widetilde{X}_{Y_N} = \frac{4\widetilde{A}_{Y_N}^2 \left(3M_S^2 + 2M_6^2\right) - \widetilde{A}_{Y_N}^4 - 8M_S^2 M_6^2 - 10 M_S^4}{6\left(M_S^2 + M_6^2\right)^2}, \tag{4.8}$$

and

$$\widetilde{A}_{Y_N} = A_{Y_N} - Y_N \langle S\rangle \cot\beta. \tag{4.9}$$

[2] The smallness of M_6 can be understood using dimension 5 operator for mass generation. For an example, see Ref. [64].

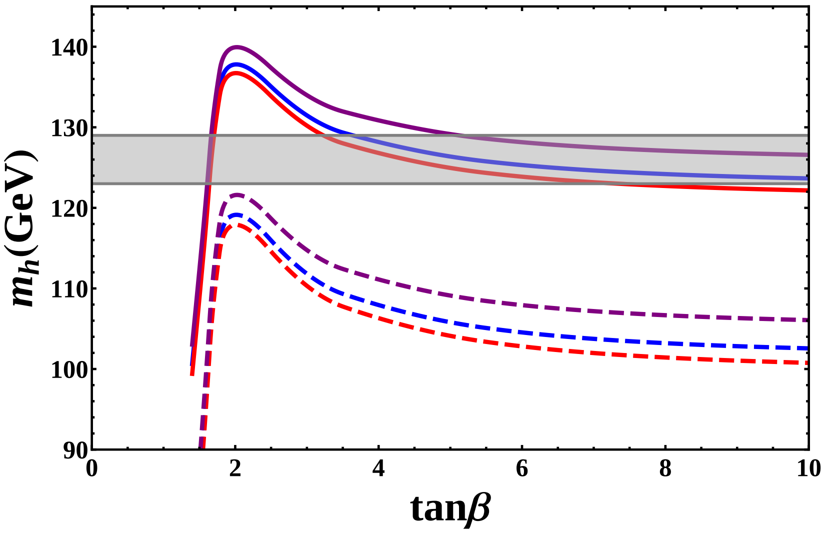

Figure 4.2: Upper bounds on the lightest CP-even Higgs boson mass versus $\tan\beta$, with $M_S = 300$ GeV, $M_6 = 3$ TeV, $\widetilde{X}_{Y_N} = 4$. Maximum value of λ is used. Red lines correspond to NMSSM, while blue lines correspond to NMSSM with one additional pair of $(N_n^c + N_n)$ singlets. Purple lines correspond to NMSSM with 3 additional pairs of $(N_n^c + N_n)$ singlets. In both cases $Y_N = 0.7$. The solid lines show the Higgs mass bounds with $\widetilde{X}_t = 6$, while the dashed lines show the bounds with $\widetilde{X}_t = 0$. For reference the gray band shows the Higgs mass range of 126 ± 3 GeV.

A_{Y_N} is the trilinear $N^c - L$ soft mixing parameter and n is the number of pairs of new singlets. $v = 174.1$ GeV is the electroweak VEV. Note that the expression in Eq. (4.5) is very similar to what was presented in Ref. [65].

To see how these new, $(N_n^c + N_n)$, singlets can affect the lightest CP-even Higgs mass, we plot the upper bounds on the lightest CP-even Higgs mass versus $\tan\beta$ for $n = 1$ and 3 in Figure 4.2. We choose $M_S = 300$ GeV for all cases in order to minimize the stop quark contribution to the Higgs boson mass. $M_6 = 3$ TeV and $Y_N = 0.7$ are used. Compared to the NMSSM bound, the Higgs mass can be increased by up to 5 GeV or so. To maximize the effect coming from the new field we choose the maximal value $\widetilde{X}_{Y_N} = 4$. For $n = 3$, the upper bound for the Higgs mass becomes as large as 140 GeV for $\tan\beta \approx 2$, and asymptotically approaches $m_h \approx 126$ GeV for large $\tan\beta$. This indicates that we are able to accommodate a Higgs mass of around 126 GeV even with

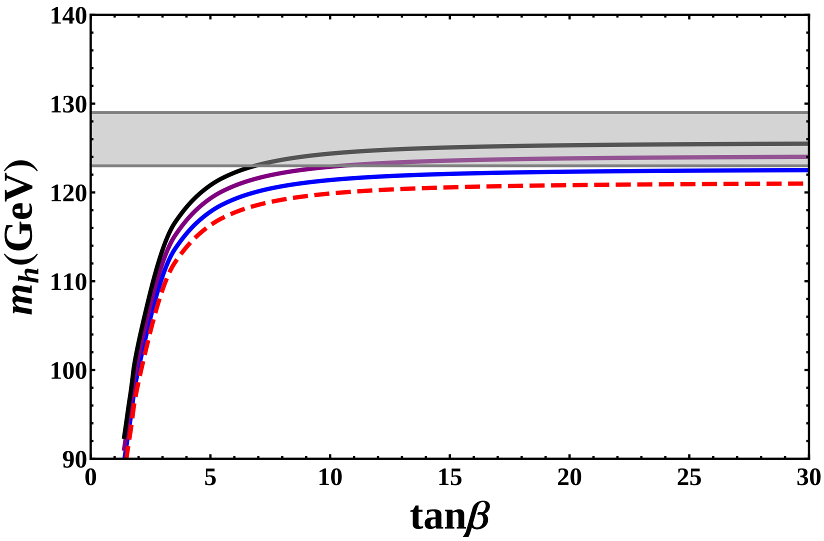

Figure 4.3: Upper bounds on the lightest CP-even Higgs boson mass versus $\tan\beta$, with $M_S = 300$ GeV, $M_6 = 3$ TeV, $\widetilde{X}_t = 6$, $\widetilde{X}_{Y_N} = 4$, $Y_N = 0.7$ and $\lambda = 0.1$. Red dashed line corresponds to NMSSM. Blue, purple and black solid lines (from bottom to top) correspond to NMSSM+singlets with n=1, 2 and 3. For reference the gray band shows the Higgs mass range of 126 ± 3 GeV.

relatively small values of λ and Y_N. Therefore, we can conclude that in the NMSSM with the inverse seesaw mechanism for neutrinos, we can have relatively light $\mathcal{O}(300)$ GeV stop quarks. This can be achieved without invoking maximal values for the λ or Y_N couplings, and without imposing severe restrictions on the values of $\tan\beta$.

In order to show how small the coupling λ can be, we consider the case with $\lambda = 0.1$, $M_S = 300$ GeV and $Y_N = 0.7$. The main reason for choosing $\lambda = 0.1$ is that in this case the contribution from λ to the lightest CP-even Higgs mass is negligible, and the results are applicable to the MSSM case as well. Figure 4.3 shows the upper bounds on the Higgs mass versus $\tan\beta$ for varying numbers of $N_n^c + N_n$ pairs. Note that in order to reproduce the neutrino oscillation data, we need to introduce at least two pairs of N_n^c and N_n. However, for completeness, we have shown the bounds with n =1, 2 and 3 in Figure 4.3. We can see from Figure 4.3 that in the MSSM and NMSSM, an inverse seesaw can make it very easy to generate $m_h = 126$ GeV. In this case we do not require very heavy stop quarks, or large value of λ, or a very restrictive value in the NMSSM of $\tan\beta \approx 2$.

Table 4.3 presents upper bounds on the Higgs masses for varying numbers of $(N_n^c + N_n)$ singlets. $n = 0$ corresponds to NMSSM/MSSM without inverse seesaw. The Higgs mass has been calculated using the input values $\tan\beta = 30$, $\lambda = 0.1$, $\widetilde{X}_t = 6$, $\widetilde{X}_{Y_N} = 4$, $Y_N = 0.7$ and $M_S = 300$ GeV.

	$n=0$	$n=1$	$n=2$	$n=3$
m_h(GeV)	121	123	124	126

Table 4.3: Higgs masses for varying numbers of $(N_n^c + N_n)$ singlets, with $n = 0$ corresponding to NMSSM/MSMM. The Higgs mass has been calculated using the input values $\tan\beta = 30$, $\lambda = 0.1$, $Y_N = 0.7$, $\widetilde{X}_t = 6$, $\widetilde{X}_{Y_N} = 4$ and $M_S = 300$ GeV.

As mentioned above, in order to have realistic neutrino masses and mixings, with TeV scale effective dimension six operators, we need to adjust the values for λ_N in Eq. (4.6). It turns out that λ_N should be order of 10^{-9} or so, which is possible but appears not natural. This can be resolved if we consider Z_3 charge assignment which allows dimension seven as the lowest possible operator for generating neutrino masses. One example of such a charge assignment is presented in Table 4.4.

	Q	U^c	D^c	L	E^c	H_u	H_d	S	N_n^c	N_n	N_m^0
Z_3	1	ω	ω	ω	ω	ω	ω	ω	ω	ω^2	1

Table 4.4: Z_3 charge assignments of the NMSSM with additional new superfields which correspond to dimension seven as lowest effective operator for neutrino masses. The new fields have Z_2 matter parity and $\omega = e^{i2\pi/3}$.

The relevant part of the renormalizable superpotential involving only the new chiral superfields is given by

$$W \supset Y_{nj} N_n^c (H_u L_j) + (\lambda_N)_{nm} S N_n N_m^0 + m_{nm} N_n^c N_m + \frac{1}{2} m'_{nm} N_n^0 N_m^0. \tag{4.10}$$

For simplicity, we set $m_{nm} = m'_{nm} = M_7\delta_{nm}$, $(\lambda_N)_{nm} = \lambda_N\delta_{ij}$ and $Y_N \equiv Y_{nj}$. Integrating out the new heavy chiral field and following the electroweak symmetry breaking, the light neutrino Majorana mass matrix is generated:

$$m_\nu = \frac{(Y_N^T Y_N)v_u^2}{M_7} \times \frac{\lambda_N^T \lambda_N \langle S\rangle^2}{M_7^2}. \tag{4.11}$$

We can see from this formula that the upper bound for seesaw scale is $M_7 \sim 10^6$ GeV, assuming all Yukawa coupling in Eq. (5.7) are $\mathcal{O}(1)$. It is clear from Eq. (4.11) that we can have $\mathcal{O}(1)$ Y_N couplings and the seesaw scale M_7 around TeV for $\lambda_N \sim 10^{-4}$ or so. In this case the value for λ_N is more natural compared to the dimension six case. Comparing Eq. (4.11) to Eq. (4.5), we can see that we have identical contributions to the lightest CP-even Higgs mass for effective dimension six and seven cases.

Having low ($\sim$TeV) scale for the inverse seesaw mechanism clearly makes the model accessible at the LHC. In Ref. [66] it is shown that regions of the parameter space of the inverse seesaw model can be tested at the LHC, while Ref. [67] shows that lepton flavor violation imposes strict constraints on these models.

4.3.2 NMSSM+Triplets

As pointed out in Ref. [56], another way for generating the dimension six operator is to introduce $SU(2)_L$ triplets with zero $(\Delta_0^c + \Delta_0)$ or with unit $(\Delta_n^c + \Delta_n)$ hypercharge. It was shown in Ref. [56] that two pairs $(n = 1, 2)$ of $(\Delta_n^c + \Delta_n)$ are needed in order to generate the effective dimension six operator for inverse seesaw mechanism. We will consider the case involving only $(\Delta_n^c + \Delta_n)$ as the additional fields. As an example we choose the charge assignments for the NMSSM fields shown as *case I* in Table 4.1. Accordingly, in order to generate effective dimension six operators (see Eq. (4.2)) for the light neutrinos, the Z_3 charges for $(\Delta_n^c + \Delta_n)$ fields are fixed, as given in Table 4.5. The additional contributions to the NMSSM superpotential in this case contain the following terms

$$\begin{aligned} W &\supset Y_{ij}(L_i\Delta_1 L_j) + Y_{H_u}(H_u\Delta_2 H_u) + \lambda_N S \,\mathrm{tr}\left[\bar{\Delta}_1\bar{\Delta}_2\right] + m_1 \,\mathrm{tr}\left[\bar{\Delta}_1\Delta_1\right] \\ &+ m_2 \,\mathrm{tr}\left[\bar{\Delta}_2\Delta_2\right], \end{aligned} \tag{4.12}$$

where Y_{ij}, Y_{H_u} and λ_N are dimensionless Yukawa couplings and m_1, m_2 are mass parameters. It is interesting to note that the interactions $(H_d \Delta_n H_d)$ and $(H_d \overline{\Delta}_n H_d)$, which can give significant contributions to the CP-even Higgs mass [68], are forbidden by Z_3 or $U(1)_Y$ symmetry.

	$SU(3)_c$	$SU(2)_L$	$U(1)_Y$	Z_3	Z_2
Δ_1	1	3	1	1	+
$\overline{\Delta}_1$	1	3	-1	1	+
Δ_2	1	3	-1	ω	+
$\overline{\Delta}_2$	1	3	1	ω^2	+

Table 4.5: Charge assignments of $(\Delta_n + \overline{\Delta}_n)$ superfields, where $n = 1, 2$. $\omega = e^{i2\pi/3}$ and Z_2 is matter parity.

The coupling $Y_H(H_u \Delta H_u)$ in Eq. (4.12) will generate a tree level contribution to the lightest CP-even Higgs boson mass given by [68]

$$\left[m_h^2\right]_\Delta = 4Y_{H_u}^2 v^2 \sin^4\beta. \tag{4.13}$$

We assume $\tan\beta \lesssim 50$ since for larger $\tan\beta$, there will be additional contribution in Eq. (4.13) which can reduce the Higgs mass [51]. To show the impact of $(\Delta_n + \overline{\Delta}_n)$ on the lightest CP-even Higgs mass, we plot in Figure 4.4 the upper bounds on the Higgs mass versus $\tan\beta$. We choose $M_S = 200$ GeV, $\widetilde{X}_t = 6$, $Y_{H_u} = 0.15$ and $m_1 = m_2 = 3$ TeV. The red dashed line corresponds to NMSSM. The blue solid line corresponds to NMSSM+ $(\Delta_n + \overline{\Delta}_n)$. For reference, the gray band corresponds to a Higgs mass of 126 ± 3 GeV. We see that there is no need for very large, $\mathcal{O}(1)$, value for the coupling Y_{H_u} in order to have a 126 GeV Higgs. As seen from Figure 4.4, $Y_{H_u} = 0.15$ already yields an upper bound on the Higgs mass above 126 GeV. The upper bound is 142 GeV for $\tan\beta \approx 2$, which asymptotically approaches $m_h \approx 130$ GeV for larger $\tan\beta$ values. We are able to realize a Higgs mass of around 126 GeV with relatively small values of λ and Y_{H_u}. We therefore conclude that in the NMSSM with the inverse seesaw mechanism for neutrinos, we can have relatively light, $\mathcal{O}(200)$ GeV or so, stop quarks

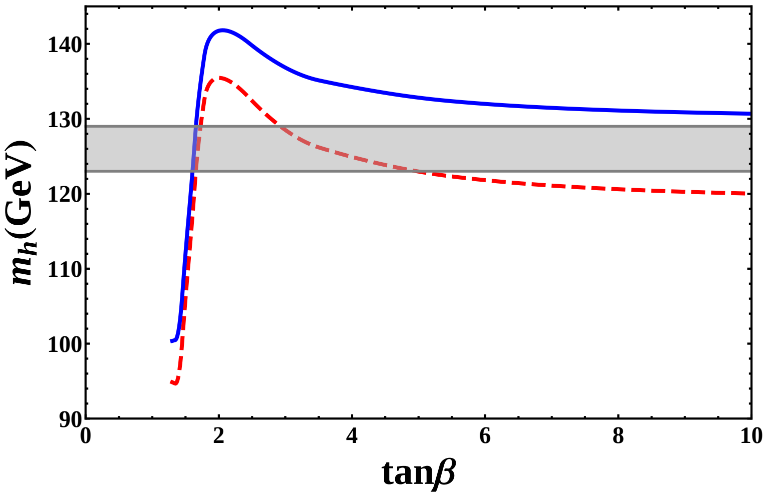

Figure 4.4: Upper bounds on the lightest CP-even Higgs boson mass versus $\tan\beta$, for $M_S = 200$ GeV, $\widetilde{X}_t = 6$, $Y_{H_u} = 0.15$, $m_1 = m_2 = 3$ TeV. Maximum value of λ is used. Red dashed line corresponds to NMSSM, and the blue solid line corresponds to NMSSM + $(\Delta_n + \overline{\Delta}_n)$. For reference, the gray band shows the Higgs mass range of 126 ± 3 GeV.

without invoking maximal values for λ or Y_{H_u}, and also without severely restricting $\tan\beta$.

Consider a case with relatively small value of λ. In Figure 4.5 we choose $\lambda = 0.3$ and $M_S = 200$ GeV. The red dashed line corresponds to the Higgs mass bound in NMSSM, while the blue and purple lines show the bounds with $Y_{H_u} = 0.15$ and $Y_{H_u} = 0.2$. One can see that it is fairly easy to increase the Higgs mass bound in NMSSM to 126 GeV, even with small values of λ and Y_{H_u}.

Notice that we can use a triplet with zero hypercharge to generate the inverse seesaw operator. In this case the superpotential looks exactly the same, with $(\Delta_0^c + \Delta_0)$ replacing $(N_n^c + N_n)$. The result will be similar to what we presented in section 4.3.1 when we consider 3 pairs of $(N_n^c + N_n)$. Given this similarity we do not extend our analysis to the case of an $SU(2)_L$ triplet with zero hypercharge.

The low scale triplet model has a very nice feature. A light triplet not only helps generate the inverse seesaw mechanism and provides significant contribution to

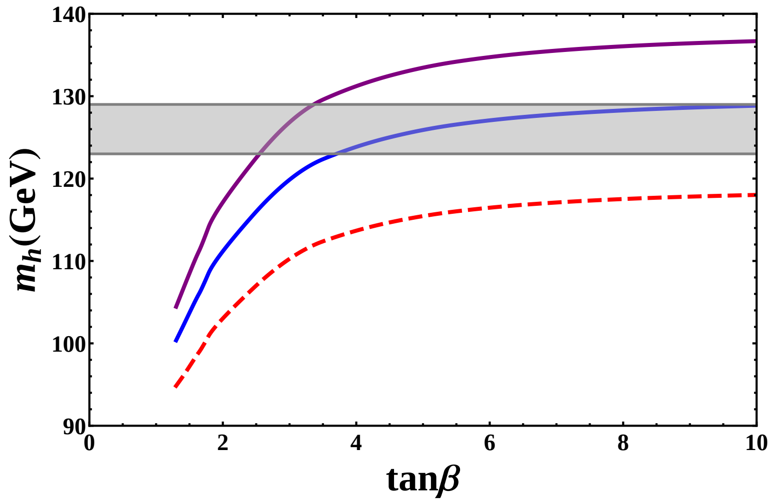

Figure 4.5: Upper bounds on the lightest CP-even Higgs boson mass versus $\tan\beta$, with $M_S = 200$ GeV, $\widetilde{X}_t = 6$, $m_1 = m_2 = 3$ TeV, and $\lambda = 0.3$. Red dashed line corresponds to the NMSSM, and blue and purple solid lines correspond to NMSSM + $(\Delta_n + \overline{\Delta}_n)$, with $Y_{H_u} = 0.15$ and 0.2. For reference, the gray band shows the Higgs mass range of 126 ± 3 GeV.

the CP-even Higgs boson mass, it also contributes to the enhancement of the Higgs production and decay in the diphoton channel. In order to have a sizable effect on the diphoton production, the coupling involving the triplet and the Higgs doublets has to be large [69], which makes the coupling non-perturbative below the Planck or GUT scale. On the other hand, as was shown in Ref. [56], we need one pair of $SU(2)_L$ triplets with zero hypercharge or two pairs of triplets with unit hypercharge. In both cases at least one of the gauge couplings becomes non-perturbative below the GUT scale. However, if the theory is still valid near the Landau pole all couplings will become large through the two and higher loop renormalization group equations (RGEs). The couplings can effectively merge together and we can have non-perturbative unification [70]. Another attractive feature of the light triplet extension of the NMSSM (MSSM) spectrum is that it can help resolve the little hierarchy problem [71] with a Higgs mass of around 126 GeV.

4.4 Conclusion

Following Ref. [56], we consider extensions of the next-to-minimal supersymmetric model (NMSSM) in which the observed neutrino masses are generated through TeV scale inverse seesaw mechanism. We have shown that the new particles associated with the inverse seesaw mechanism can have sizable couplings to the lightest CP-even Higgs field which can yield a large contribution to its mass. This new contribution makes it possible to have a 126 GeV Higgs with order of 200 GeV stop quarks mass and a broad range of $\tan\beta$ values. This can be exploited to enhance the Higgs production and decay in the diphoton channel as well.

Chapter 5

INVERSE SEESAW MECHANISM ON THE SPARTICLE SPECTRUM

In this chapter we study the implications of the inverse seesaw mechanism (ISS) on the sparticle spectrum in the Constrained Minimal Supersymmetric Standard Model (CMSSM) and Non-Universal Higgs Model (NUHM2) [72]. Employing the maximal value of the Dirac Yukawa coupling involving the up type Higgs doublet provides a 2-3 GeV enhancement of the lightest CP-even Higgs boson mass. This effect permits one to have lighter colored sparticles in the CMSSM and NUHM2 scenarios with LSP neutralino, which can be tested at LHC14. We present a variety of LHC testable benchmark points with the desired LSP neutralino dark matter relic abundance.

5.1 Introduction

The discovery of the Standard Model (SM)-like Higgs boson with mass $m_h \approx$ 126 GeV by the ATLAS [73] and CMS [74] experiments at the Large Hadron Collider (LHC) has sparked detailed examinations of viable regions of the parameter space of low scale supersymmetry. This is largely motivated by the fact that the Minimal Supersymmetric Standard Model (MSSM) predicts an upper bound on the mass of the lightest CP-even Higgs boson mass, $m_h \lesssim 135$ GeV [75]. The Higgs boson mass and the corresponding sparticle spectrum strongly depend on the soft supersymmetry breaking (SSB) parameters [49], which can be tested at the LHC (see, for instance [76, 48, 77]).

In low scale supersymmetry, a Higgs boson mass of around 125 GeV requires either a relatively large value, $\mathcal{O}(\text{few} - 10)$ TeV, for the geometric mean of top squark masses [48], or a large SSB trilinear A_t-term, with a geometric mean of the top squark masses of around a TeV [77]. The presence of heavy top squarks typically yields a heavy sparticle spectrum in gravity mediated supersymmetry breaking [78], if universality at

$M_{\rm GUT}$ of sfermion masses is assumed. It is especially hard in this case to achieve colored sparticles lighter than 2.5 TeV.

The current LHC lower bounds on the colored sparticle masses from LHC data are $m_{\tilde{g}} \gtrsim 1.5$ TeV (for $m_{\tilde{g}} \sim m_{\tilde{q}}$), and $m_{\tilde{g}} \gtrsim 0.9$ TeV (for $m_{\tilde{g}} \ll m_{\tilde{q}}$) [79, 80], and it is expected that the LHC14 can test squarks and gluinos with masses up to 3.5 TeV [81]. In order to be able to reduce the sparticle masses to more accessible values in models with universal sfermion and gaugino masses, we require additional contributions from new physics, which preserves gauge coupling unification.

Solar and atmospheric neutrino oscillation experiments have established that at least two neutrino states are massive [82]. On the theoretical side the nature of the physics responsible for neutrino masses and flavor properties remains largely unknown and is a subject of extensive investigations [83]. Since our goal is to lower the sparticle mass spectrum while preserving gauge coupling unification, we utilize in this chapter the inverse seesaw mechanism (ISS) for generating the light neutrino masses [84]. Introducing only SM singlet fields allows one to realize the ISS mechanism, and all new fields can be below the TeV scale. In addition, we can have $\mathcal{O}(1)$ Dirac Yukawa couplings involving the up type Higgs doublet. It has been shown in Refs. [85, 86] that the Dirac Yukawa coupling can impact the lightest CP-even Higgs boson mass through radiative corrections and increase it by 2-3 GeV when the additional new fields are SM singlets. The ISS mechanism can also be realized using $SU(2)_W$ weak triplets [85], and in this case the Higgs mass can be enhanced by more than 10 GeV.

In this chapter we restrict ourselves to the case of SM singlet fields since we do not want to disturb gauge coupling unification. An enhancement by 2-3 GeV of the CP-even SM-like Higgs boson mass, as we will show, can yield significant reductions of sparticle masses in the Constrained Minimal Supersymmetric Standard Model (CMSSM) [78] and Non-Universal Higgs Model with $m_{H_u}^2 \neq m_{H_d}^2$ (NUHM2) [87]. Here $m_{H_u}^2$ and $m_{H_d}^2$ denote the SSB mass square terms for the up and down type MSSM Higgs doublets respectively.

5.2 Inverse Seesaw Mechanism and Higgs Boson Mass

In order to explain non-zero neutrino masses and mixings by the ISS mechanism [84], we supplement the MSSM field content with three pairs of MSSM singlet chiral superfields $(N_i^c + N_i)$, $i = 1, 2, 3$, and a singlet chiral superfield S which develops a vacuum expectation value (VEV) comparable to or less than the electroweak scale. The part of the renormalizable superpotential involving only the new chiral superfields is given by

$$W \supset Y_{N_{ij}} N_i^c H_u L_j + \lambda_{N_{ij}} S N_i N_j + m_{ij} N_i^c N_j. \tag{5.1}$$

Here $Y_{N_{ij}}$ and $\lambda_{N_{ij}}$ are dimensionless couplings and m_{ij} is a mass term. A non-zero VEV for the scalar component of S generates the lepton-number-violating term $\mu_s N_i N_j \equiv \lambda_{N_{ij}} < S > N_i N_j$ and, as a result, Majorana masses for the observed neutrinos can be generated. The coupling $\lambda_{N_{ij}} S N_i N_j$ is preferred over the direct mass term $\mu N_i N_j$, with the former yielding the desired mass terms for the N fields with a non-zero $< S >$. A singlet chiral superfield S can make it easier to find extension of the SM gauge group with help from a suitable symmetry (see, for instance, Refs. [85, 88]), and avoid terms which otherwise may spoil the ISS mechanism.

The SSB terms pertaining to the fields N_i^c and N_i are given by

$$\begin{aligned} \mathcal{L}^{\text{soft}} \supset \;& m_{N^c}^2 \widetilde{N^c}^\dagger \widetilde{N^c} + m_N^2 \widetilde{N}^\dagger \widetilde{N} + \Big[A_\nu^{ij} \widetilde{L}_i \widetilde{N^c}_j H_u + B_m^{jk} \widetilde{N^c}_j \widetilde{N}_k + B_{\mu_N}^{jk} \widetilde{N}_j \widetilde{N}_k \\ + \;& \text{h.c.} \Big], \end{aligned} \tag{5.2}$$

where the SSB parameters are prescribed at the TeV SUSY breaking scale. In the ISS case there are regions of the SSB parameter space for which one of the sneutrinos can be the lightest supersymmetric particle (LSP). The phenomenology of models of this kind has been studied in Ref. [88]. In our present work we assume that the lightest neutralino is the LSP, and a spectrum of this nature can be realized both in the CMSSM and NUHM2 if we assume that all sfermions, including the N_i^c and N_i fields, have universal SSB mass terms at M_{GUT}.

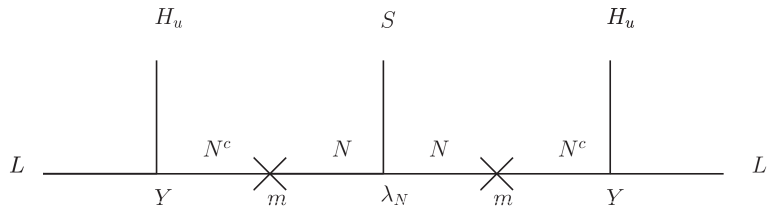

Figure 5.1: Supergraph leading to dimension six operator for neutrino masses.

According to the superpotential in Eq. (5.1), after integrating out the $(N_i^c + N_i)$ fields, the neutrino mass arises from the effective dimension six operator (Figure. 5.1):

$$\frac{LLH_uH_uS}{M_6^2}. \tag{5.3}$$

We assume here that $M_6\delta_{ij} \equiv m_{ij}$ is larger than the electroweak scale. Also, in Eq. (5.3) the family and $SU(2)_W$ gauge indices are omitted.

Following the electroweak symmetry breaking, the neutrino Majorana mass matrix is generated:

$$m_\nu = \frac{(Y_N^T Y_N){v_u}^2}{M_6} \times \frac{\lambda_N \langle S \rangle}{M_6}. \tag{5.4}$$

For simplicity, we set $Y_N \equiv Y_{N_{ij}}$ and $\lambda_N \equiv \lambda_{N_{ij}}$, and v_u, $\langle S \rangle$ are the VEVs of H_u, and the S field. Eq. (5.4) implies that even if we require $Y_N \sim \mathcal{O}(1)$ and $M_6 \sim 1$ TeV, the correct mass scale for the light neutrinos can be reproduced by suitably adjusting $\lambda_N \langle S \rangle$.

Keeping $Y_N \sim \mathcal{O}(1)$ will provide sizable contribution to the lightest CP-even Higgs mass, which is given by [89]

$$\left[m_h^2\right]_N = n \times \left[-M_Z^2 \cos^2 2\beta \left(\frac{1}{8\pi^2} Y_N^2 t_N\right) + \frac{1}{4\pi^2} Y_N^4 v^2 \sin^4 \beta \left(\frac{1}{2}\widetilde{X}_{Y_N} + t_N\right)\right], \tag{5.5}$$

where

$$t_N = \log\left(\frac{M_S^2 + M_6^2}{M_6^2}\right), \;\; \widetilde{X}_{Y_N} = \frac{4\widetilde{A}_{Y_N}^2 (3M_S^2 + 2M_6^2) - \widetilde{A}_{Y_N}^4 - 8M_S^2 M_6^2 - 10 M_S^4}{6\left(M_S^2 + M_6^2\right)^2}, \tag{5.6}$$

and

$$\widetilde{A}_{Y_N} = A_{Y_N} - Y_N \langle S \rangle \cot\beta. \tag{5.7}$$

Also, $A_{Y_N} \equiv A_\nu^{ij}$ is the SSB mixing parameter in Eq. (5.2), n is the number of pairs of new MSSM singlets, $M_S = \sqrt{m_{\tilde{t}_L} m_{\tilde{t}_R}}$ defines the SUSY scale, and $v = 174.1$ GeV is the electroweak VEV.

We incorporate the ISS mechanism in CMSSM and NUHM2 and scan the SUSY parameter space using the ISAJET 7.84 package [90]. We modify the code by including the additional contributions from Eq. (5.5) to the lightest CP-even Higgs boson mass.

5.3 Phenomenological constraints and scanning procedure

We employ the ISAJET 7.84 package [90] to generate sparticle spectrum over the fundamental parameter space. In this package, the weak scale values of the gauge, third generation Yukawa couplings, including the Yukawa coupling $N_i^c H_u L_j$ from ISS, are evolved to $M_{\rm GUT}$ via the MSSM renormalization group equations (RGEs) in the $\overline{DR}$ regularization scheme. With the boundary conditions given at $M_{\rm GUT}$, all of the SSB parameters, along with the gauge and Yukawa couplings, are evolved back to the weak scale $M_{\rm Z}$. The data points collected all satisfy the requirement of radiative electroweak symmetry breaking condition with the neutralino in each case being the LSP.

We have performed Markov-chain Monte Carlo (MCMC) scans for the following CMSSM parameter range:

$$\begin{aligned}
0 \leq m_0 &\leq 10\,\text{TeV}, \\
0 \leq m_{1/2} &\leq 5\,\text{TeV}, \\
-3 \leq A_0/m_0 &\leq 3, \\
3 \leq \tan\beta &\leq 60,
\end{aligned} \tag{5.8}$$

with $\mu > 0$ and $m_t = 173.3$ GeV [91]. We use $m_b^{\overline{DR}}(M_{\rm Z}) = 2.83$ GeV which is hard-coded into ISAJET. Here m_0 is the universal SSB mass parameter for MSSM sfermions, Higgs and additional N^c, N and S fields. $m_{1/2}$ is the gaugino mass parameter, $\tan\beta$ is the ratio of the VEVs of the two MSSM Higgs doublets, and A_0 is the MSSM universal SSB trilinear scalar coupling. In order to maximize the contribution from the ISS mechanism to the Higgs boson mass, we set $\tilde{X}_{Y_N} = 4$, following Ref. [85].

In the case of NUHM2, in addition to the above mentioned parameters we have two additional independent SSM mass parameters m_{H_d} and m_{H_u}. We use the following parameter range for them:

$$\begin{aligned} 0 &\leq m_{H_u} \leq 10\,\text{TeV}, \\ 0 &\leq m_{H_d} \leq 10\,\text{TeV}. \end{aligned} \tag{5.9}$$

To maximize the impact of ISS on the sparticle spectrum, we set $\lambda_N = 0.7$. This is the maximal value of λ_N at low scale that remains perturbative up to M_{GUT}. We also assume that M_6 is larger than M_S, in order that the neutralino rather than sneutrino is the LSP.

After collecting the data, we impose the mass bounds on all the particles [92] and use the IsaTools package [93] and Ref. [94] to implement the following phenomenological constraints:

$$m_h = 123 - 127 \text{ GeV} \qquad [95,\ 96] \tag{5.10}$$

$$0.8 \times 10^{-9} \leq \text{BR}(B_s \to \mu^+\mu^-) \leq 6.2 \times 10^{-9}\ (2\sigma) \qquad [97] \tag{5.11}$$

$$2.99 \times 10^{-4} \leq \text{BR}(b \to s\gamma) \leq 3.87 \times 10^{-4}\ (2\sigma) \qquad [98] \tag{5.12}$$

$$0.15 \leq \frac{\text{BR}(B_u \to \tau\nu_\tau)_{\text{MSSM}}}{\text{BR}(B_u \to \tau\nu_\tau)_{\text{SM}}} \leq 2.41\ (3\sigma) \qquad [99] \quad . \tag{5.13}$$

As far as the muon anomalous magnetic moment a_μ is concerned, we require that the benchmark points are at least as consistent with the data as the SM.

For the benchmark points presented in Table 5.1 and 5.2, we require that the LSP neutralino dark matter abundance lies in the interval $0.0913 \leq \Omega_{\text{CDM}} h^2 \leq 0.1363$ [100].

Finally we implement the following following bounds on the sparticle masses:

$$m_{\tilde{g}} \gtrsim 1.5\,\text{TeV (for } m_{\tilde{g}} \sim m_{\tilde{q}}) \quad \text{and} \quad m_{\tilde{g}} \gtrsim 0.9\,\text{TeV (for } m_{\tilde{g}} \ll m_{\tilde{q}}) \quad [79,\ 80]. \tag{5.14}$$

5.4 CMSSM and Inverse Seesaw

In this section we present our results for the CMSSM and the CMSSM with additional ISS contribution (CMSSM-ISS). The main idea behind the presentation of these results is to show that these two scenarios have quite distinct features as far as choice for the fundamental parameters of the models is concerned. In Figure 5.2, the left panels represent our results for the CMSSM, while the right panels display our results for the CMSSM-ISS. Here grey points satisfy REWSB and the LSP neutralino requirement. The orange points represent solutions which satisfy the mass bounds and B-physics bounds from Section 5.3. Solutions in blue color are a subset of orange points and satisfy the requirement $123\,\text{GeV} \lesssim m_h \lesssim 127\,\text{GeV}$. This figure clearly serves our purpose stated above.

For instance, the graph in $m_0 - m_{1/2}$ plane shows that for the CMSSM case, the Higgs mass bounds excludes simultaneously small values for m_0 and $m_{1/2}$, while in the CMSSM-ISS case, we can have relatively small values for $m_{1/2}$ ($<$ 800 GeV) and m_0 ($<$ 400 GeV), consistent with all constraints given in section 5.3. There is also noticeable difference between CMSSM and CMSSM-ISS in the $A_0/m_0 - m_0$ plane. In the CMSSM case, for instance, we find $m_0 \sim 700$ GeV for $A_0/m_0 = -3$, and for $A_0/m_0 = 3$ we have $m_0 \sim 1.3$ TeV. In CMSSM-ISS, on the other hand, the corresponding minimum m_0 values vary from 400 GeV to 1.1 TeV. In the $m_0 - \tan\beta$ plane too, considering the blue points, we see in the left panel that for a minimum value $m_0 \sim 700$ GeV, the corresponding $\tan\beta$ value is around 16. In the right panel, on the other hand, $\tan\beta$ is again around 16 but now the minimum value of m_0 is ~ 300 GeV.

In Figure 5.3 we show plots of m_0 versus μ. The color coding is the same as in Figure 5.2 with the left and right panels representing CMSSM and CMSSM-ISS respectively. This figure shows very distinct features of the two scenarios. Considering the orange points, in CMSSM-ISS we have solutions with $\mu \gtrsim 1$ TeV, in contrast with the CMSSM, where we have solutions with small, as well as large values of μ. The reason for this difference is that in CMSSM-ISS, $m_{H_u}^2$ gets new contribution from the loop induced by the coupling $N_i^c H_u L_j$ in addition to the top quark loop, which makes

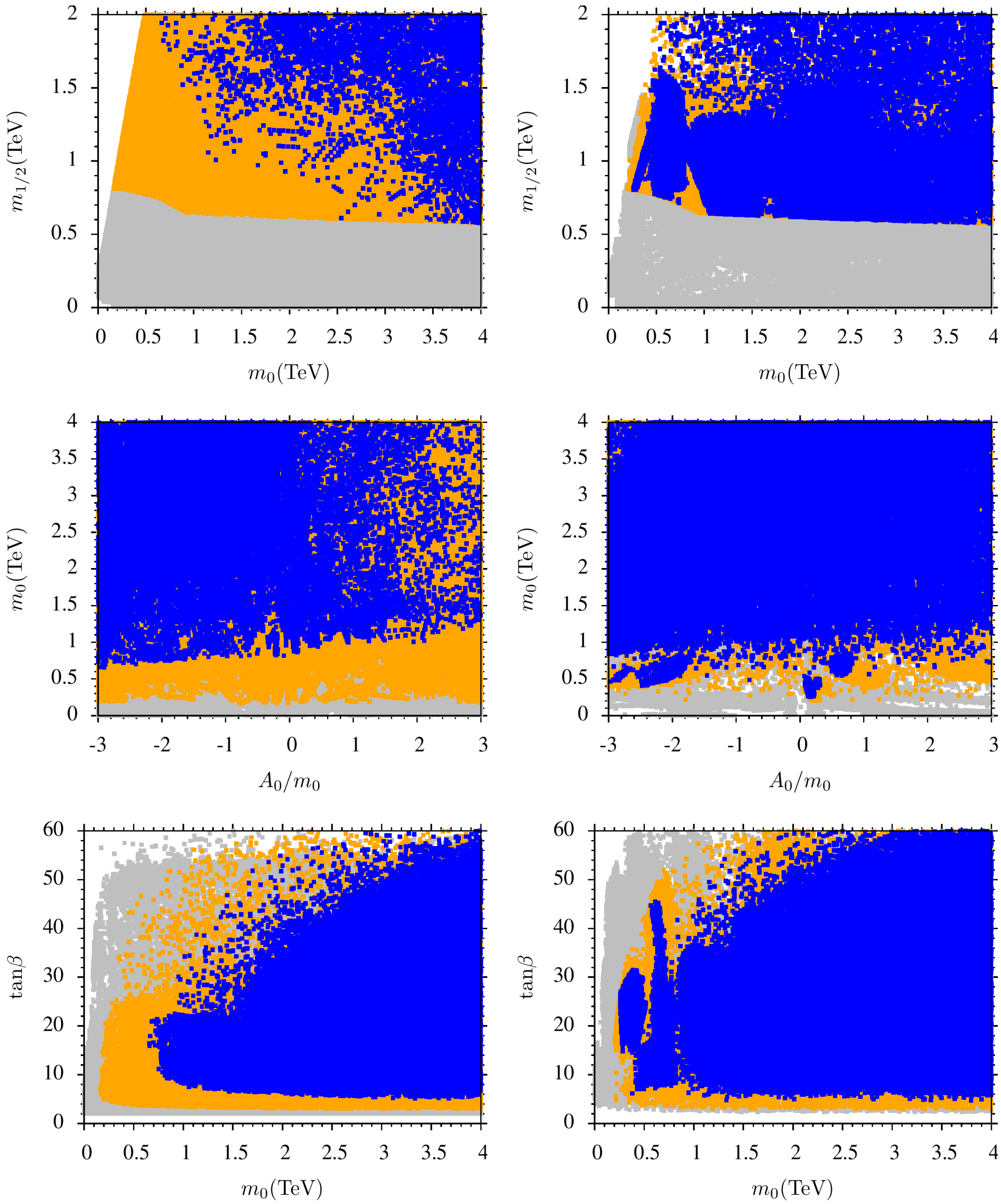

Figure 5.2: Plots in $m_0 - m_{1/2}$, $A_0/m_0 - m_0$ and $m_0 - \tan\beta$ planes for CMSSM (left panel) and CMSSM-ISS (right panel). Grey points satisfy REWSB and LSP neutralino conditions. Orange point solutions satisfy mass bounds and B-physics bounds given in Section 2. Points in blue are a subset of orange points and satisfy $123\,\text{GeV} \lesssim m_h \lesssim 127\,\text{GeV}$.

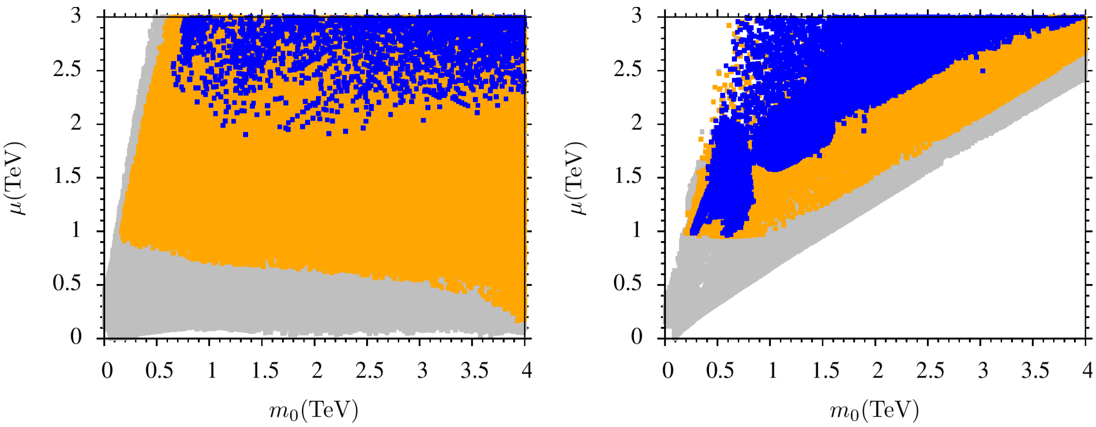

Figure 5.3: Plots in $m_0 - \mu$ plane for CMSSM (left panel) and CMSSM-ISS (right panel). Color coding is the same as in Figure 5.2.

μ relatively heavy. Thus, in the CMSSM-ISS case we do not have the so-called focus point/hyperbolic branch scenario [101, 102] while it is still a viable solution in the CMSSM case.

In Figure 5.4, we show graphs in $m_{\tilde{\chi}_1^0} - m_{\tilde{t}_1}$ and $m_{\tilde{\chi}_1^0} - m_{\tilde{\tau}_1}$ planes. The color coding is the same as in Figure 5.2, except that the solutions in red are a subset of solutions in blue and also satisfy the relic abundance bound $0.001 \leq \Omega h^2 \leq 1$. These graphs show that despite the fact that there are differences in the space of fundamental parameters, the mass spectrum for χ_1^0, $\tilde{t}_1$ and $\tilde{\tau}_1$ turn out to be more or less identical.

For instance, in the $m_{\tilde{\chi}_1^0} - m_{\tilde{t}_1}$ plane we see that we have NLSP $\tilde{t}_1$ in the mass range of $\sim 260-500$ GeV in both cases. Similar results were also reported in [103, 104] in the case of b-τ Yukawa coupling unification in CMSSM and $SU(5)$. It was shown in [105, 106] that the region of parameter space with stop-neutralino mass difference of 20% is ruled out for $m_{\tilde{t}_1} \lesssim 140$ GeV. In the $m_{\tilde{\chi}_1^0} - m_{\tilde{\tau}_1}$ plane, we note that NLSP $\tilde{\tau}_1$ has the same mass range in CMSSM and CMSSM-ISS. The reason why we have comparable intervals for $m_{\tilde{t}_1}$ and $m_{\tilde{\tau}_1}$ in CMSSM and CMSSM-ISS is that low values for both sparticle masses are acheived via fine tuning involving the trilinear SSB terms, while the addition of ISS to CMSSM mostly affects the first two generation sparticle masses.

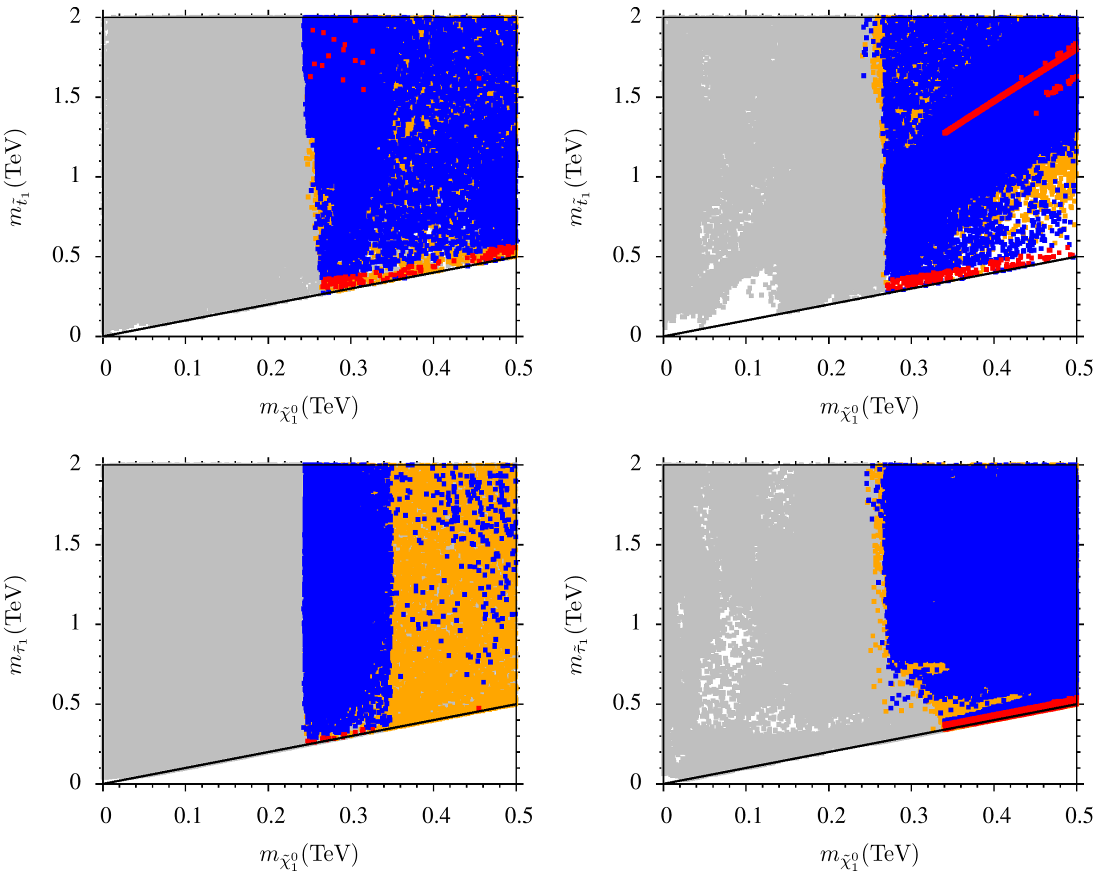

Figure 5.4: Plots in $m_{\tilde{\chi}_1^0} - m_{\tilde{t}_1}$ and $m_{\tilde{\chi}_1^0} - m_{\tilde{\tau}_1}$ planes for CMSSM (left panel) and CMSSM-ISS (right panel). The color coding is the same as in Figure 5.2 except that red points are a subset of blue point solutions and also satisfy bounds for relic abundance, $0.001 \leq \Omega h^2 \leq 1$.

In Figure 5.5, we present graphs in $m_{\tilde{\chi}_1^0} - m_A$ and $m_{\tilde{\chi}_1^0} - m_{\tilde{\chi}_1^\pm}$ planes, with color coding the same as in Figure 5.4. The graphs in $m_{\tilde{\chi}_1^0} - m_A$ plane show that we do not have the A-resonance solution [107], and the reason can be understood from the following equation:

$$m_A^2 = 2|\mu|^2 + m_{H_u}^2 + m_{H_d}^2. \tag{5.15}$$

In CMSSM, since we have universal scalar masses and we require $m_h \sim 123-127$ GeV, $m_{H_u}^2$ and $m_{H_d}^2$ are both large, and, as a result, m_A is also large. This can be seen in the $m_{\tilde{\chi}_1^0} - m_A$ graph in the left panel. The solid black line in the graph represents the condition $2m_{\tilde{\chi}_1^0} = m_A$ for the A-resonance solution [107].

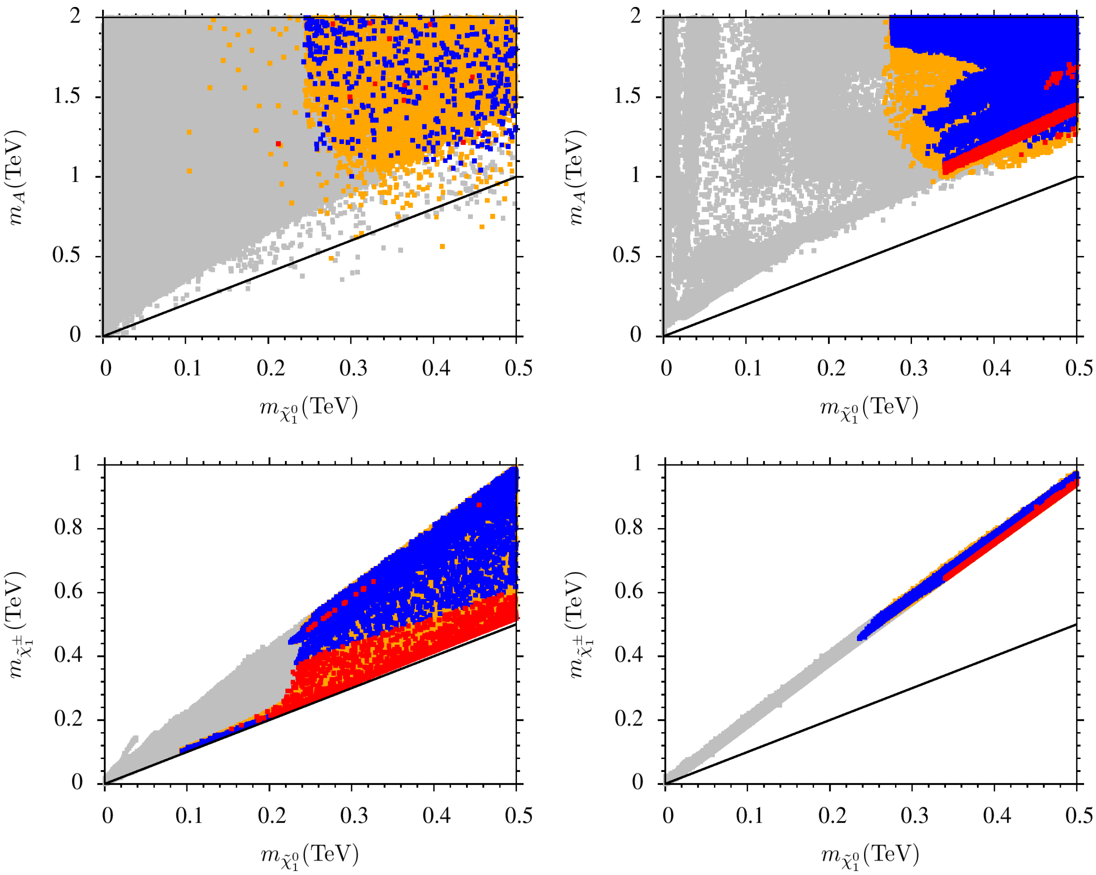

Figure 5.5: Plots in $m_{\tilde{\chi}_1^0} - m_A$ and $m_{\tilde{\chi}_1^0} - m_{\tilde{\chi}_1^\pm}$ planes for CMSSM (left panel) and CMSSM-ISS (right panel). The color coding is the same as in Figure 5.2 except that red points are subset of blue point solutions and also satisfy bounds for relic abundance, $0.001 \leq \Omega h^2 \leq 1$.

We note that the solutions in orange color lie around the solid black line, but if we apply the constraint 123 GeV $\lesssim m_h \lesssim$ 127 GeV, the relevant blue points lie further from the black line. In the right panel, which represents the CMSSM-ISS case, we note that both the orange and blue points are further away from the solid black line. This is because of two reasons. Firstly, as stated earlier, μ is larger because of extra contributions from the $N_i^c H_u L_j$ Yukawa coupling, and so the orange points move away from the solid black line. Secondly, as explained, in the CMSSM case the m_h constraint makes solutions move away from the solid black line as m_A becomes larger.

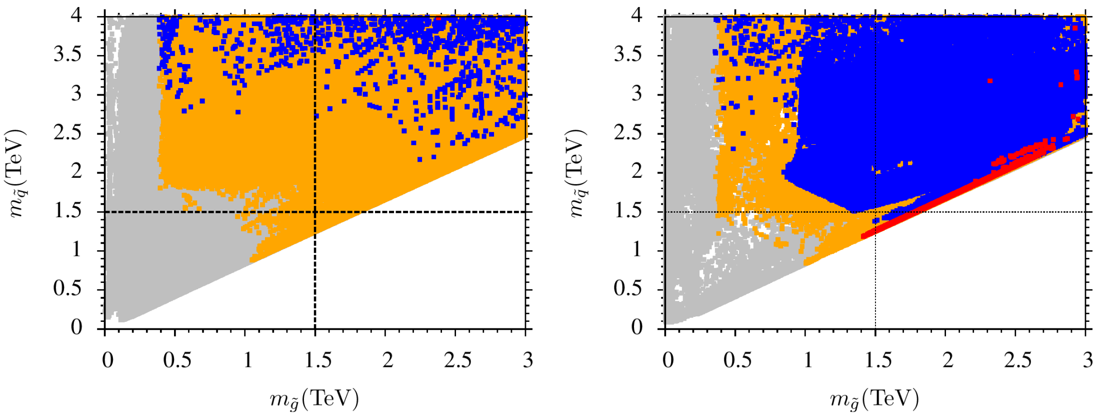

Figure 5.6: Plots in $m_{\tilde{g}} - m_{\tilde{q}}$ planes for CMSSM (left panel) and CMSSM-ISS (right panel). The color coding is the same as in Figure 5.2, except that orange points do not satisfy mass bounds for gluinos and first two generation squarks, and red points are a subset of blue point solutions and also satisfy bounds for relic abundance, $0.001 \leq \Omega h^2 \leq 1$. Dashed vertical and horizontal lines stand for current squark and gluino lower mass bounds respectively.

A more distinctive figure concerning the sparticle spectra in CMSSM and CMSSM-ISS is presented in the $m_{\tilde{\chi}_1^0} - m_{\tilde{\chi}_1^{\pm}}$ plane. In contrast to CMSSM (left panel), the figure for CMSSM-ISS is quite different. This is due to the fact that in CMSSM-ISS, the LSP neutralino is mostly a bino and the chargino mostly wino. Therefore, the ratio $m_{\tilde{\chi}_1^0}/m_{\tilde{\chi}_1^{\pm}}$ is close to the ratio of $U(1)$ and $SU(2)$ gauge couplings, $g_1/g_2 \approx 1/2$, and the points form a narrow strip.

In Figure 5.6 we show $m_{\tilde{q}}$ versus $m_{\tilde{g}}$ for CMSSM (left panel) and CMSSM-ISS (right panel). The color coding is the same as in Figure 5.2, except that the orange points do not include mass bounds for gluinos and the first two generation squarks. Dashed vertical and horizontal lines represent current squark and gluino mass bounds. We note that especially in the CMSSM the gluino mass bound excludes a significant portion of the parameter space which otherwise is consistent with the experimental data. The location of blue points relative to the orange points shows how the lower bounds on the squark and gluino masses are pushed up by m_h. It is interesting to observe that there are no red points with neutralino LSP dark matter within the reach

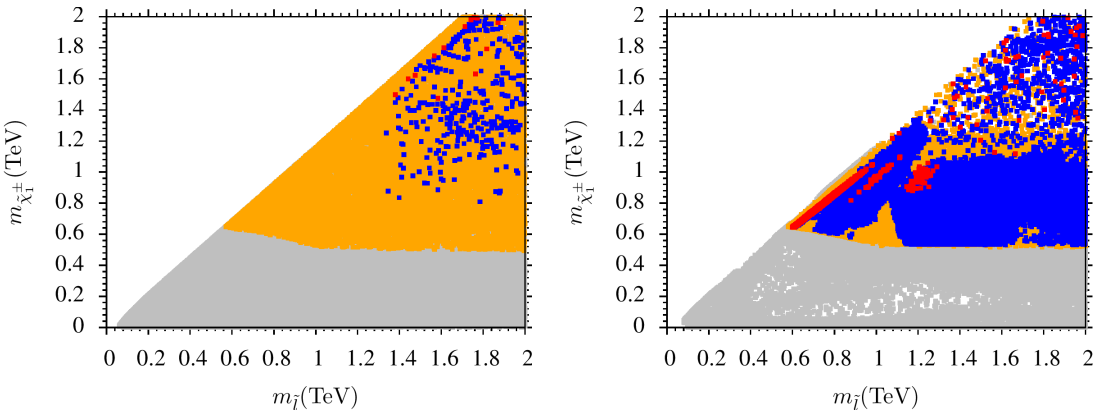

Figure 5.7: Plots in $m_{\tilde{l}} - m_{\tilde{\chi}_1^\pm}$ planes for CMSSM (left panel) and CMSSM-ISS (right panel). The color coding is the same as in Figure 5.2, except that red points are a subset of blue point solutions and also satisfy bounds for relic abundance, $0.001 \leq \Omega h^2 \leq 1$.

of LHC14. Comparing results from $m_{\tilde{g}} - m_{\tilde{q}}$ panel with the results from Figures 5.4 and 5.5, we conclude that in the CMSSM, the solution which yields the correct dark matter relic abundance predicts gluino and squarks masses that lie beyond the reach of the LHC14 [81].

On the other hand, comparison of left and right panels in Figure 5.6 shows the impact of the ISS mechanism on the sparticle masses. We can see from the $m_{\tilde{g}} - m_{\tilde{q}}$ plot in the right panel that plenty of blue points are left after we apply the Higgs mass constraint 123 GeV $\lesssim m_h \lesssim$ 127 GeV. This means that in the presence of the ISS mechanism, most points satisfying all experimental constraints lie in the Higgs mass range 123 GeV $\lesssim m_h \lesssim$ 127 GeV, which is very different from the CMSSM case. There are also red points in the right panel which shows that we can have LHC testable solutions with the correct relic abundance of dark matter.

In Figure 5.7 we display plots for $m_{\tilde{\chi}_1^\pm}$ versus $m_{\tilde{l}}$ in CMSSM (left panel) and CMSSM-ISS (right panel), with the color coding the same as in the previous figures. In the left panel we see from the blue points that $m_{\tilde{l}} > 1.4$ TeV, which may be difficult to test at the LHC. On the other hand, we see in the right panel solutions in blue and red colors around $m_{\tilde{l}} \simeq 500$ GeV, which provides a glimmer of hope that sleptons

	Point A	Point B
m_0	1020.3	3234
$M_{1/2}$	1091.1	684.6
A_0/m_0	-2.71	-2.97
$\tan\beta$	38	14.4
m_h	125	125
m_H	1602	4744
m_A	1592	4714
$m_{H^\pm}$	1604	4745
μ	1772	3727
$m_{\tilde{g}}$	2401	1705
$m_{\tilde{\chi}^0_{1,2}}$	**476**, 902	**312**, 608
$m_{\tilde{\chi}^0_{3,4}}$	1769, 1772	3724, 3724
$m_{\tilde{\chi}^\pm_{1,2}}$	905, 1773	614, 3733
$m_{\tilde{u}_{L,R}}$	2391, 2314	3492, 3476
$m_{\tilde{t}_{1,2}}$	1569, 1983	**347**, 2376
$m_{\tilde{d}_{L,R}}$	2392, 2305	3493, 3479
$m_{\tilde{b}_{1,2}}$	1940, 2035	2400, 3262
$m_{\tilde{\nu}_1}$	1248	3265
$m_{\tilde{\nu}_3}$	792	2024
$m_{\tilde{e}_{L,R}}$	1252, 1098	3261, 3245
$m_{\tilde{\tau}_{1,2}}$	**497**, 820	2040, 3027
σ_{SI}(pb)	1.57×10^{-11}	1.71×10^{-15}
σ_{SD}(pb)	5.05×10^{-9}	7.3×10^{-13}
$\Omega_{CDM}h^2$	0.114	0.092

Table 5.1: Masses (in GeV units) and other parameters for two CMSSM-ISS benchmark points satisfying all phenomenological constraints discussed in section 5.3. Points A and B are chosen from the stau-neutralino coannihilation and the stop-neutralino coannihilation regions respectively.

employing the CMSSM-ISS mechanism may be found at the LHC.

In Table 5.1 we display two benchmark points for the cMSM-ISS model that are consistent with constraints in Section 5.3. The LSP neutralino relic density in the two cases is in accord with the WMAP observations, and corresponds to stau-neutralino [108] (stop-neutralino [109]) coannihilation for point A (B). For point A, $m_{\tilde{\tau}_1} \approx 500$ GeV, $m_{\tilde{g}} \approx 2.4$ TeV, the first two generation squarks are close to 2 TeV, while slepton masses are around $1-2$ TeV. For point B, $m_{\tilde{t}_1} \approx 350$ GeV, $m_{\tilde{g}} \approx 1.7$ TeV, the first two generation squark masses are about 3.4 TeV, while slepton masses are around 3.2 TeV.

5.5 NUHM2 and Inverse Seesaw

In this section we present the results of our scan for NUHM2 with ISS contributions (NUHM2-ISS). In Figure 5.8 we present graphs in $m_0 - m_{1/2}$ and $m_0 - \mu$ planes, with color coding the same as in Figure 5.2. In the $m_0 - m_{1/2}$ plane we see that the results are similar to what we found in CMSSM-ISS. Again we can have solutions compatible with all experimental constraints presented in section 5.3. We note that the Higgs mass constraint $123\,\text{GeV} \lesssim m_h \lesssim 127\,\text{GeV}$ provides the lower bounds $m_{1/2} \approx 500$ GeV and $m_0 \approx 1$ TeV. Since μ is a free parameter in NUHM2, we can find solutions with any value of μ compatible with the experimental data (see $m_0 - \mu$ plot). As shown in [110], a relatively small μ term is necessary, but not sufficient, to be consistent with natural supersymmetry (little hierarchy problem) criteria. We find that it is hard to fully resolve the little hierarchy problem in this scenario.

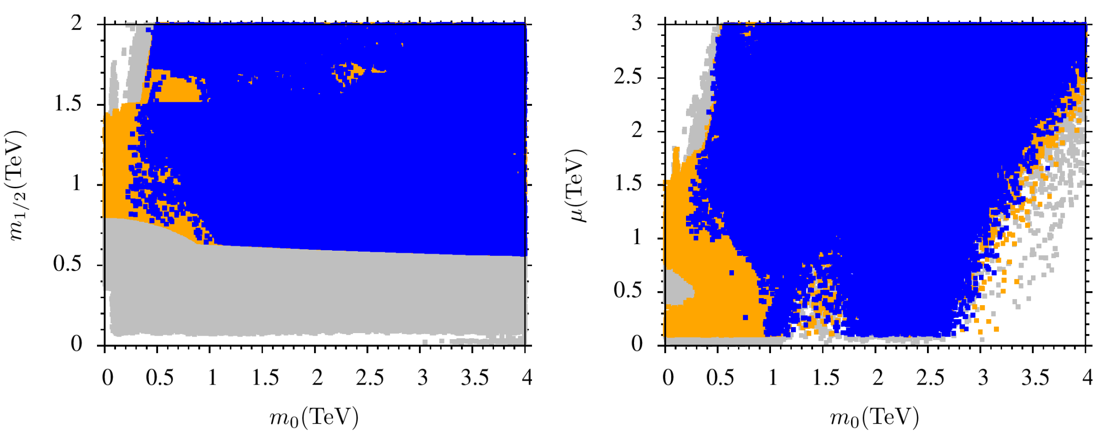

Figure 5.8: Plots in $m_0 - m_{1/2}$ and $m_0 - \mu$ planes for NUHM2-ISS. The color coding is the same as in Figure 5.2.

The sparticle spectrum for NUHM2-ISS is shown in Figure 5.9, with color coding the same as in the previous figures. The top left panel shows an NLSP $\tilde{t}_1$ in the mass range of 220 - 500 GeV, which can be tested at LHC14. The top panel on right shows

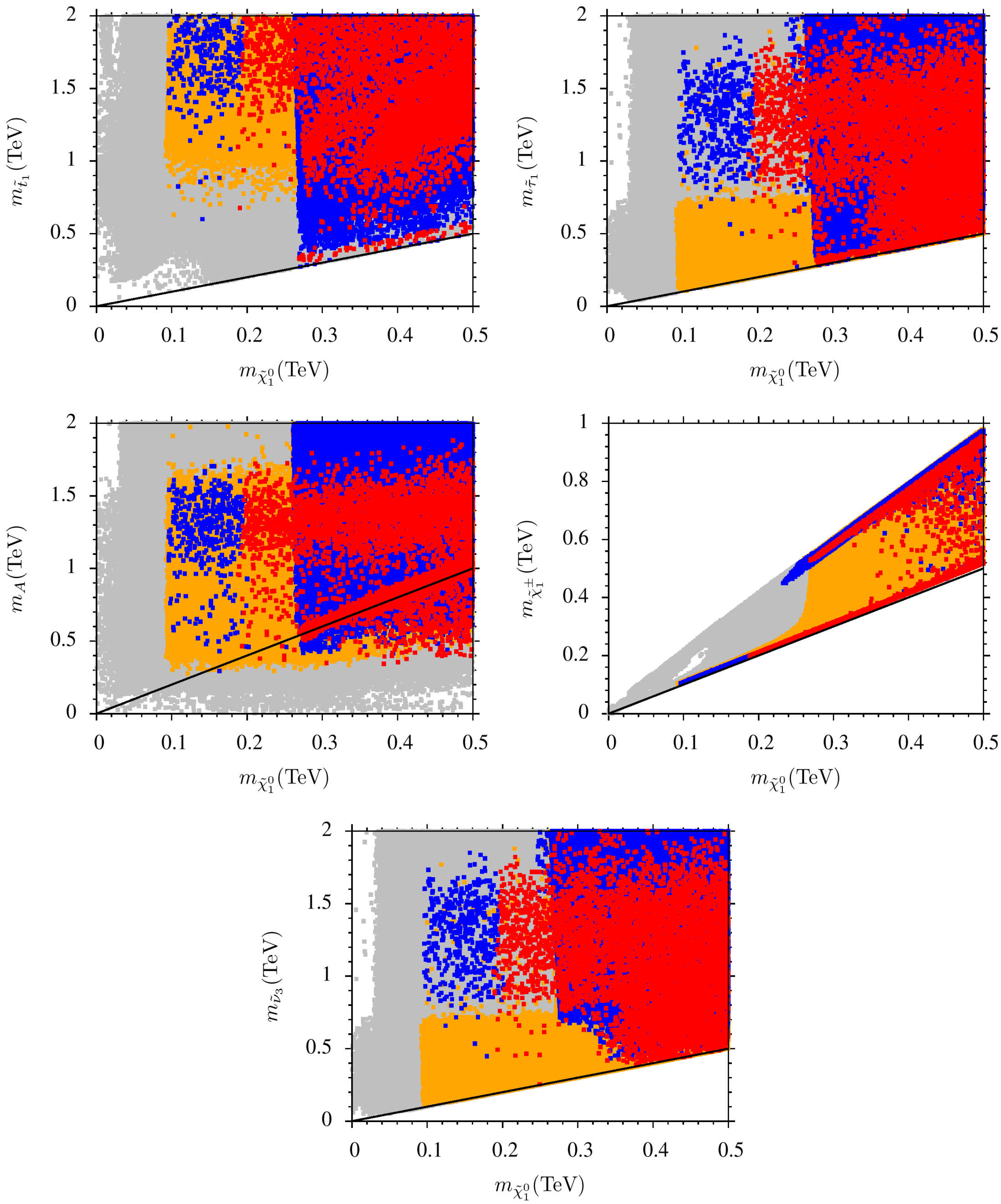

Figure 5.9: Plots in $m_{\tilde{\chi}_1^0} - m_{\tilde{t}_1}$, $m_{\tilde{\chi}_1^0} - m_{\tilde{\tau}_1}$, $m_{\tilde{\chi}_1^0} - m_A$, $m_{\tilde{\chi}_1^0} - m_{\tilde{\chi}_1^\pm}$ and $m_{\tilde{\chi}_1^0} - m_{\tilde{\nu}_3}$ planes for NUHM2-ISS. The color coding is the same as in Figure 5.2 except that red points are a subset of blue point solutions and also satisfy bounds for relic abundance, $0.001 \leq \Omega h^2 \leq 1$.

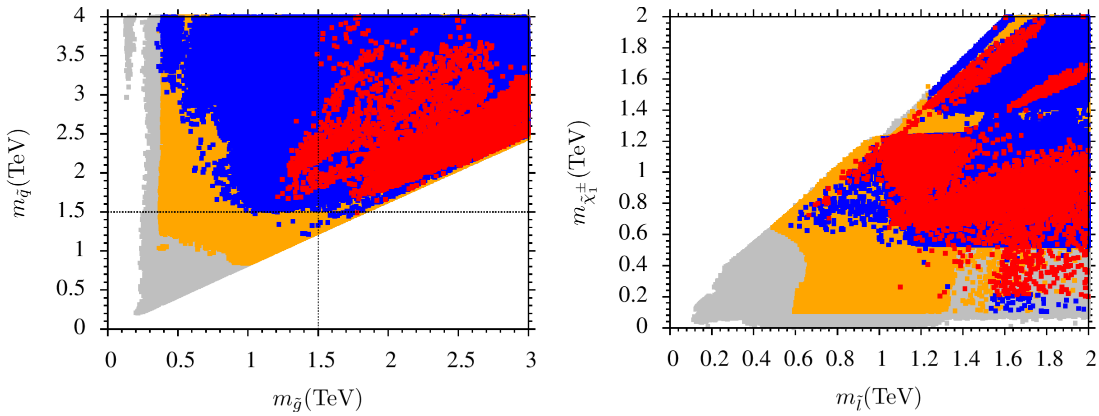

Figure 5.10: Plots in $m_{\tilde{g}} - m_{\tilde{q}}$ and $m_{\tilde{l}} - m_{\tilde{\chi}_1^{\pm}}$ planes for NUHM2. In the left panel orange points do not satisfy gluino and first two generation squark mass bounds and red points are a subset of blue point solutions and also satisfy bounds for relic abundance, $0.001 \leq \Omega h^2 \leq 1$. Dashed vertical and horizontal lines stand for current squark and gluino lower mass bounds respectively. Otherwise color coding is the same as in Figure 5.2.

that the NLSP $\tilde{\tau}_1$ can be as light as 250 GeV, which is somewhat lighter than in the CMSSM and CMSSM-ISS scenarios. The bottom left panel shows the presence of A-resonance solutions. This follows from the relatively low μ values in NUHM2 (Figure. 5.8), and with m_{H_u} and m_{H_d} (or equivalently μ and M_A) being independent parameters.

In the bottom right panel we plot $m_{\tilde{\chi}_1^{\pm}}$ versus $m_{\tilde{\chi}_1^0}$. This graph is very different from the corresponding one for CMSSM-ISS. In NUHM2-ISS scenario, because of low μ values, the chargino can be Higgsino-like, which yields bino-Higgsino mixed dark matter. This type of solution can be seen along the solid back line. In those cases where μ is heavy, the chargino will be wino-like as in the CMSSM-ISS case. Such solutions can are displayed in the second strip in the graph. We also display a plot in the $m_{\tilde{\chi}_1^0} - m_{\tilde{\nu}_3}$ plane where we show a minimum value $m_{\tilde{\nu}_3} \approx 250$ GeV, which is also consistent with the results reported in Ref. [111].

In Figure 5.10 we show graphs in $m_{\tilde{q}} - m_{\tilde{g}}$ and $m_{\tilde{\chi}_1^{\pm}} - m_{\tilde{l}}$ planes. In the left panel, the orange points do not satisfy the mass bounds for gluinos and first two generation squarks. The color coding otherwise is the same as in the previous figures. Dashed

	Point 1	Point 2	Point 3	Point 4	Point 5
m_0	2452.3	1742.2	1573.4	1301.9	3116
$M_{1/2}$	1333.4	1292.1	968.18	1293.1	857.6
A_0/m_0	-2.62	-2.49	-2.60	-2.82	-2.87
$\tan\beta$	53.42	12.54	26.25	22.67	18.89
m_{H_d}	4.5484	855.55	1.8117	1.7413	737.7
m_{H_u}	2.0939	3783.2	2661.3	3060.1	3972
m_h	125	125	125	125	126
m_H	1865	1253	**882**	658	2782
m_A	1853	1245	**876**	654	2765
$m_{H^\pm}$	1867	1256	886	664	2784
μ	3483	6455	1448	1006	3149
$m_{\tilde{g}}$	2971	2842	2188	2816	2054
$m_{\tilde{\chi}^0_{1,2}}$	**600**, 1139	**556**, 656	**423**, 805	**563**, 979	**388**, 748
$m_{\tilde{\chi}^0_{3,4}}$	3447, 3448	**657**, 1080	1445, 1450	1015, 1103	314, 314
$m_{\tilde{\chi}^\pm_{1,2}}$	1141, 3448	659, 1070	807, 1451	987, 1097	755, 3151
$m_{\tilde{u}_{L,R}}$	3565, 3492	3052, 3063	2479, 2483	2836, 2815	3515, 3576
$m_{\tilde{t}_{1,2}}$	2195, 2687	1180, 2302	1078, 1819	1374, 2185	**428**, 2303
$m_{\tilde{d}_{L,R}}$	3566, 3484	3053, 2943	2481, 2406	2837, 2720	3516, 3470
$m_{\tilde{b}_{1,2}}$	2628, 2776	2305, 2849	1804, 2153	2171, 2520	2329, 3160
$m_{\tilde{\nu}_1}$	2605	2021	1748	1627	3225
$m_{\tilde{\nu}_3}$	1503	804	818	**568**	1808
$m_{\tilde{e}_{L,R}}$	2606, 2502	2022, 1611	1749, 1502	1630, 1210	3222, 3012
$m_{\tilde{\tau}_{1,2}}$	**628**, 1501	824, 1536	824, 1201	588, 972	1823, 2693
σ_{SI}(pb)	1.80×10^{-12}	6.83×10^{-9}	5.11×10^{-11}	5.07×10^{-10}	2.35×10^{-13}
σ_{SD}(pb)	3.80×10^{-11}	1.00×10^{-5}	2.26×10^{-8}	2.56×10^{-7}	2.1×10^{-10}
$\Omega_{CDM}h^2$	0.108	0.093	0.113	0.103	0.122

Table 5.2: Masses (in GeV units) and ohter parameters for NUHM2-ISS benchmark points satisfying all phenomenological constraints discussed in section 5.3. Points 1-5 are chosen, respectively, from the stau-neutralino coannihilation, the bino-Higgsino mixed dark matter, the A-resonance, the sneutrino-neutralino coannihilation, and the stop-neutralino coannihilation regions.

vertical and horizontal lines display the current squark and gluino mass bounds.

Comparing results from Figures 5.10 and 5.7, we see very small changes on the lower mass bounds for the first two generation squarks, and sleptons as well as gluinos, which is what we expected. But there are many more red points in Figure 5.10, because in the NUHM2-ISS case, we have the additional $A-$resonance and bino-Higgsino dark matter solutions for the LSP neutralino relic abundance. As in the CMSSM-ISS case, we can have squarks and gluinos in a mass range which can be explored at LHC14.

In Table 5.2 we present five benchmark points for NUHM2-ISS case which satisfy the phenomenological constraints discussed in section 5.3. Points 1, 2, 3, 4 and 5 are chosen, respectively, from the stau-neutralino coannihilation region, the bino-Higgsino mixed dark matter region, the A-resonance region, the sneutrino-neutralino coannihilation region, and the stop-neutralino coannihilation region. In all the five benchmark points the first two generation squarks are in the mass range 2.4-3.5 TeV, while the first two generation sleptons lie around 1.6-3 TeV. Note that for the bino-Higgsino mixed dark matter point the spin independent cross section is 6.83×10^{-9} pb, which is below the current XENON100 bounds [112], but within the reach of XENON1T [113] and SuperCDMS [114].

5.6 Conclusions

The recent discovery at the LHC of a SM-like Higgs boson with mass $m_h \simeq 125$ GeV puts considerable stress on the MSSM. With $m_h \lesssim M_Z$ at tree level, large radiative corrections are required. Such corrections can be achieved in the MSSM either with multi-TeV stops, or with a large stop trilinear coupling and stop masses around 1 TeV. In models with universal sfermion masses at $M_{\rm GUT}$, such as CMSSM and NUHM2, this leads to heavy sleptons and 1st/2nd generation squarks which are near or beyond the ultimate LHC reach. Various MSSM extensions have been proposed to allow lighter sfermions via additional contributions to the lightest CP-even Higgs boson mass. In this paper we explored the impact of the inverse seesaw mechanism on the sparticle mass spectrum.

The ISS mechanism allows an increase of m_h by a few GeV, while simultaneously generating mass for neutrinos via dimension six operators. With a maximal value of the Dirac Yukawa coupling involving the up-type Higgs doublet, m_h is increased by 2-3 GeV. As we have shown, this effect allows one to have lighter colored sparticles in CMSSM and NUHM2 scenarios which can be tested at LHC14. For example, in CMSSM-ISS the minimal value of m_0 is $\sim$ 400 GeV, compared to CMSSM where $m_0 \gtrsim 800$ GeV. Furthermore, requiring neutralino LSP to be the cold dark matter (CDM) pushes m_0 to 10-20 TeV range in CMSSM, whereas in CMSSM-ISS values as low as $\sim$ 200 GeV are allowed. This means that squarks and gluinos in CMSSM-ISS lie within the reach of LHC14. Similarly, in NUHM2-ISS squarks and gluinos in 1.5-3 TeV range are consistent with neutralino CDM. We have presented several LHC testable benchmark points with the desired neutralino dark matter relic abundance.

REFERENCES

[1] S. Glashow, Nucl. Phys. **22** (1961) 579; S. Weinberg, Phys. Rev. Lett. **19** (1967) 1264; A. Salam, in Elementary Particle Theory, ed. N. Svartholm, Almqvist and Wiksells, Stockholm (1969) p. 367.

[2] P. W. Higgs, Phys. Rev. Lett. **13**, 508 (1964); F. Englert and R. Brout, Phys. Rev. Lett. **13**, 321 (1964); G. S. Guralnik, C. R. Hagen and T. W. B. Kibble, Phys. Rev. Lett. **13**, 585 (1964).

[3] A. Djouadi, arXiv:hep-ph/0503172.

[4] M. C. Gonzalez-Garcia, M. Maltoni, J. Salvado and T. Schwetz, JHEP **1212**, 123 (2012).

[5] S. Ray, arXiv:1005.1938[hep-ph].

[6] S. P. Martin, arXiv:hep-ph/9709356.

[7] G. Bertone, D. Hooper, J. Silk, Phys. Rep. **405**, 279 (2005).

[8] W. Marciano and S. Willenbrock, Phys. Rev. **D** 37 (1988) 2509; S. Dawson and S. Willenbrock, Phys. Rev. Lett. 62 (1989) 1232; L. Durand, B. A. Kniehl and K. Riesselmann, Phys. Rev. **D** 51 (1995) 5007; A. Ghinculov, Nucl. Phys. **B** 455 (1995) 21; A. Frink, B. Kniehl, D. Kreimer and K. Riesselmann, Phys. Rev. **D** 54 (1996) 4548; T. Binoth, A. Ghinculov and J.J. van der Bij, Phys. Rev. **D** 57 (1998) 1487.

[9] M. Veltman, Acta. Phys. Pol. **B** 8 (1977) 475; A. Ghinculov, Phys. Lett. **B** 337 (1994) 137 and (E) *ibid* **B** 346 (1995) 426; A. Frink, B. Kniehl and K. Riesselmann, Phys. Rev. Lett. 72 (1994) 2534 and (E) *ibid*. 74 (1995) 1699; V. Borodulin and G. Jikia, Phys. Lett. **B** 391 (1997) 434.

[10] T. Hambye and K. Riesselmann, Phys. Rev. **D** 55, 7255 (1997), ariXiv:hep-ph/9610272; J. Ellis, R. Espinosa, G. F. Giudice, A. Hoecker, and A. Riotto, Phys. Lett. **B** 679 (2009) 369, arXiv:0906.0954[hep-ph]

[11] S. Weinberg, Phys. Rev. Lett. **43**, 1566 (1979)

[12] P. Minkowski, Phys. Lett. B **67**, 421 (1977); T. Yanagida, in *Proceedings of the Workshop on the Unified Theory and the Baryon Number in the Universe* (O. Sawada and A. Sugamoto, eds.), KEK, Tsukuba, Japan, 1979, p. 95; M. Gell-Mann, P. Ramond, and R. Slansky, *Supergravity* (P. van Nieuwenhuizen et al. eds.), North Holland, Amsterdam, 1979, p. 315; S. L. Glashow, *The future of elementary particle physics*, in *Proceedings of the 1979 Cargèse Summer Institute on Quarks and Leptons* (M. Lévy et al. eds.), Plenum Press, New York, 1980, p. 687; R. N. Mohapatra and G. Senjanović, Phys. Rev. Lett. **44**, 912 (1980).

[13] G. Lazarides, Q. Shafi and C. Wetterich, Nucl. Phys. **B181**, 287 (1981); R. N. Mohapatra and G. Senjanović, Phys. Rev. **D 23**, 165 (1981); M. Magg and C. Wetterich, Phys. Lett. B **94**, 61 (1980); J. Schechter and J. W. F. Valle, Phys. Rev. D **22**, 2227 (1980).

[14] R. Foot, H. Lew, X. G. He and G. C. Joshi, Z. Phys. C **44**, 441 (1989).

[15] I. Gogoladze, B. He, Q. Shafi, Phys. Lett. B 690 (2010) 495.

[16] N. Cabibbo, L. Maiani, G. Parisi and R. Petronzio, Nucl. Phys. B **158**, 295 (1979); P. Q. Hung, Phys. Rev. Lett. **42**, 873 (1979); M.A.B. Beg, C. Panagiotakopoulos and A. Sirlin, Phys. Rev. Lett.52 (1984) 883; K. S. Babu and E. Ma, Phys. Rev. Lett. **55**, 3005 (1985); M. Lindner, Z. Phys. C **31**, 295 (1986); M. Sher, Phys. Rept. **179**, 273 (1989); G. Altarelli and G. Isidori, Phys. Lett. B **337**, 141 (1994); J. A. Casas, J. R. Espinosa and M. Quiros, Phys. Lett. B **342**, 171 (1995); Phys. Lett. B **382**, 374 (1996); J. R. Espinosa and M. Quiros, Phys. Lett. B **353**, 257 (1995); P. Q. Hung and G. Isidori, Phys. Lett. B **402**, 122 (1997);

[17] I. Gogoladze, N. Okada and Q. Shafi, Phys. Rev. D **78**, 085005 (2008).

[18] N. Haba, S. Matsumoto, N. Okada and T. Yamashita, JHEP **0602**, 073 (2006); I. Gogoladze, N. Okada and Q. Shafi, Phys. Lett. B **655**, 257 (2007); I. Gogoladze, N. Okada and Q. Shafi, Phys. Lett. B **659**, 316 (2008); Y. Hosotani, N. Maru, K. Takenaga and T. Yamashita, Prog. Theor. Phys. **118**, 1053 (2007).

[19] U. Amaldi, W. de Boer, P. H. Frampton, H. Furstenau and J. T. Liu, Phys. Lett. B **281**, 374 (1992); J. L. Chkareuli, I. G. Gogoladze and A. B. Kobakhidze, Phys. Lett. B **340** (1994) 63; J. L. Chkareuli, I. G. Gogoladze and A. B. Kobakhidze, Phys. Lett. B **376**, 111 (1996); D. Choudhury, T. M. P. Tait and C. E. M. Wagner, Phys. Rev. D **65**, 053002 (2002); D. E. Morrissey and C. E. M. Wagner, Phys. Rev. D **69**, 053001 (2004).

[20] G. Barenboim, F. J. Botella and O. Vives, Nucl. Phys. B **613**, 285 (2001); D. Choudhury et al. in ref [5].

[21] L. Lavoura and J.P. Silva, Phys. Rev. D **47**, 2046 (1993); N. Maekawa, Phys. Rev. D **52**, 1684 (1995).

[22] C. Amsler *et al.* [Particle Data Group], Phys. Lett. B **667**, 1 (2008).

[23] M. E. Machacek and M. T. Vaughn, Nucl. Phys. B **222**, 83 (1983); Nucl. Phys. B **236**, 221 (1984); Nucl. Phys. B **249**, 70 (1985); C. Ford, I. Jack and D. R. T. Jones, Nucl. Phys. **B387** (1992) 373, [Erratum-ibid. **B504** (1997) 551]; H. Arason, D. J. Castano, B. Keszthelyi, S. Mikaelian, E. J. Piard, P. Ramond and B. D. Wright, Phys. Rev. D **46**, 3945 (1992); V. D. Barger, M. S. Berger and P. Ohmann, Phys. Rev. D **47**, 1093 (1993); M. X. Luo and Y. Xiao, Phys. Rev. Lett. **90**, 011601 (2003).

[24] See, for example, H. Arason, D. J. Castano, B. Keszthelyi, S. Mikaelian, E. J. Piard, P. Ramond and B. D. Wright, Phys. Rev. D **46**, 3945 (1992); H. E. Haber, R. Hempfling and A. H. Hoang, Z. Phys. C **75**, 539 (1997).

[25] See, for example, F. Jegerlehner, M. Y. Kalmykov and O. Veretin, Nucl. Phys. B **641**, 285 (2002); Nucl. Phys. B **658**, 49 (2003); F. Jegerlehner and M. Y. Kalmykov, Nucl. Phys. B **676**, 365 (2004).

[26] A. Sirlin and R. Zucchini, Nucl. Phys. B **266** (1986) 389.

[27] See for instance, P. Nath and P. Fileviez Perez, Phys. Rept. **441**, 191 (2007).

[28] J. A. Casas, V. Di Clemente, A. Ibarra and M. Quiros, Phys. Rev. D **62**, 053005 (2000); I. Gogoladze, N. Okada and Q. Shafi, Phys. Lett. B **668**, 121 (2008).

[29] R. Barate *et al.* [LEP Working Group for Higgs boson searches], Phys. Lett. B **565**, 61 (2003).

[30] See for instance, J. R. Espinosa, G. F. Giudice and A. Riotto, JCAP **0805**, 002 (2008).

[31] P. F. Harrison, D. H. Perkins, W. G. Scott, Phys. Lett. **B530** 167 (2002).

[32] B. T. Cleveland *et.al*, Astrophys.J. **496** 505 (1998); Super-Kamiokande Collaboration, Phys. Lett. **B539** 179 (2002); Super-Kamiokande Collaboration, Phys. Rev. **D71** 112005 (2005); M. Maltoni, T. Schwetz, M.A. Tortola, J.W.F. Valle New J.Phys. **6** 122 (2004); A. Bandyopadhyay *et al*, Phys. Lett. **B608** 115 (2005); G. L. Fogli *et al*, Prog. Part. Nucl. Phys. **57** 742 (2006); For a recent review, see, for example, H. Nunokawa, S. J. Parke and J. W. F. Valle, Prog. Part. Nucl. Phys. **60**, 338 (2008).

[33] B. He, N. Okada, Q. Shafi, Phys. Lett. B 695 (2011) 219.

[34] F. L. Bezrukov, arXiv:0810.3165 [hep-ph]; F. L. Bezrukov and M. Shaposhnikov, Phys. Lett. B **659**, 703 (2008) [arXiv:0710.3755 [hep-th]]; F. L. Bezrukov, A. Magnin and M. Shaposhnikov, Phys. Lett. B **675**, 88 (2009) [arXiv:0812.4950 [hep-ph]]; F. Bezrukov, D. Gorbunov and M. Shaposhnikov, JCAP **0906**, 029

(2009) [arXiv:0812.3622 [hep-ph]]; F. Bezrukov and M. Shaposhnikov, JHEP **0907**, 089 (2009) [arXiv:0904.1537 [hep-ph]]; F. Bezrukov, A. Magnin, M. Shaposhnikov and S. Sibiryakov, arXiv:1008.5157 [hep-ph].

[35] A. O. Barvinsky, A. Y. Kamenshchik and A. A. Starobinsky, JCAP **0811**, 021 (2008) [arXiv:0809.2104 [hep-ph]]; A. O. Barvinsky, A. Y. Kamenshchik, C. Kiefer, A. A. Starobinsky and C. Steinwachs, arXiv:0904.1698 [hep-ph]; A. O. Barvinsky, A. Y. Kamenshchik, C. Kiefer, A. A. Starobinsky and C. F. Steinwachs, arXiv:0910.1041 [hep-ph].

[36] A. De Simone, M. P. Hertzberg and F. Wilczek, Phys. Lett. B **678**, 1 (2009) [arXiv:0812.4946 [hep-ph]].

[37] S. C. Park and S. Yamaguchi, JCAP **0808**, 009 (2008) [arXiv:0801.1722 [hep-ph]].

[38] T. E. Clark, B. Liu, S. T. Love and T. ter Veldhuis, Phys. Rev. D **80**, 075019 (2009) [arXiv:0906.5595 [hep-ph]].

[39] N. Okada, M. U. Rehman and Q. Shafi, arXiv:0911.5073 [hep-ph].

[40] M. B. Einhorn and D. R. T. Jones, JHEP **1003**, 026 (2010) [arXiv:0912.2718 [hep-ph]]; S. Ferrara, R. Kallosh, A. Linde, A. Marrani and A. Van Proeyen, arXiv:1004.0712 [hep-th]; arXiv:1008.2942 [hep-th].

[41] C. P. Burgess, H. M. Lee and M. Trott, JHEP **0909**, 103 (2009); J. L. F. Barbon and J. R. Espinosa, Phys. Rev. D **79**, 081302 (2009); M. P. Hertzberg, arXiv:1002.2995 [hep-ph].

[42] J. A. Casas, J. R. Espinosa, M. Quiros and A. Riotto, Nucl. Phys. B **436**, 3 (1995) [Erratum-ibid. B **439**, 466 (1995)].

[43] For a recent analysis, see J. Ellis, J. R. Espinosa, G. F. Giudice, A. Hoecker and A. Riotto, Phys. Lett. B **679**, 369 (2009) [arXiv:0906.0954 [hep-ph]]; I. Gogoladze, B. He, and Q. Shafi, Phys. Lett. B **690**, 495 (2010) [arXiv:1004.4217 [hep-ph]].

[44] I. Gogoladze, B. He, Q. Shafi, Phys. Lett. B 718 (2013) 1008.

[45] F. Gianotti, CERN Seminar, "Update on the Standard Model Higgs searches in ATLAS", July, 4 2012. ATLAS-CONF-2012-093

[46] J. Incandela, CERN Seminar, "Update on the Standard Model Higgs searches in CMS", July, 4 2012. CMS-PAS-HIG-12-020.

[47] See for instance S. P. Martin, hep-ph/9709356 and references therein.

[48] M. A. Ajaib, I. Gogoladze, F. Nasir and Q. Shafi, Phys. Lett. B **713**, 462 (2012).

[49] For a review see A. Djouadi, Phys. Rept. **459**, 1 (2008) and reference therein.

[50] P. H. Chankowski, J. R. Ellis and S. Pokorski, Phys. Lett. B **423**, 327 (1998); P. H. Chankowski, J. R. Ellis, M. Olechowski and S. Pokorski, Nucl. Phys. B **544**, 39 (1999); G. L. Kane and S. F. King, Phys. Lett. B **451**, 113 (1999); G. L. Kane, J. D. Lykken, B. D. Nelson and L. T. Wang, Phys. Lett. B **551**, 146 (2003).

[51] For a review see U. Ellwanger, C. Hugonie and A. M. Teixeira, Phys. Rept. **496**, 1 (2010); M. Maniatis, Int. J. Mod. Phys. A **25**, 3505 (2010) and reference therein.

[52] U. Ellwanger, JHEP **1203**, 044 (2012): L. J. Hall, D. Pinner and J. T. Ruderman, JHEP **04**, 131 (2012); Z. Kang, J. Li and T. Li, arXiv:1201.5305 [hep-ph]; U. Ellwanger, G. Espitalier-Noel and C. Hugonie, JHEP **1109**, 105 (2011); T. Cheng, J. Li, T. Li, X. Wan, Y. k. Wang and S. -h. Zhu, arXiv:1207.6392 [hep-ph]; K. Schmidt-Hoberg and F. Staub, arXiv:1208.1683 [hep-ph]; M. Perelstein and B. Shakya, arXiv:1208.0833 [hep-ph]; J. Cao, Z. Heng, J. M. Yang, Y. Zhang and J. Zhu, arXiv:1202.5821 [hep-ph]; J. Cao, Z. Heng, J. M. Yang and J. Zhu, arXiv:1207.3698 [hep-ph].

[53] H. Abe, T. Kobayashi and Y. Omura, Phys. Rev. D **76**, 015002 (2007); I. Gogoladze, M. U. Rehman and Q. Shafi, Phys. Rev. D **80**, 105002 (2009); D. Horton and G. G. Ross, Nucl. Phys. B **830**, 221 (2010); J. E. Younkin and S. P. Martin, Phys. Rev. D **85**, 055028 (2012); S. Antusch, L. Calibbi, V. Maurer, M. Monaco and M. Spinrath, arXiv:1207.7236 [hep-ph].

[54] J. F. Gunion, Y. Jiang and S. Kraml, Phys. Lett. B **710**, 454 (2012); S. F. King, M. Muhlleitner and R. Nevzorov, Nucl. Phys. B **860**, 207 (2012); D. A. Vasquez, G. Belanger, C. Boehm, J. Da Silva, P. Richardson and C. Wymant, arXiv:1203.3446 [hep-ph]; U. Ellwanger and C. Hugonie, arXiv:1203.5048 [hep-ph]; E. Gabrielli, K. Kannike, B. Mele, A. Racioppi and M. Raidal, arXiv:1204.0080 [hep-ph]; J. Rathsman and T. Rossler, arXiv:1206.1470 [hep-ph].

[55] E. Hardy, J. March-Russell and J. Unwin, arXiv:1207.1435 [hep-ph].

[56] I. Gogoladze, N. Okada and Q. Shafi, Phys. Lett. B **672**, 235 (2009).

[57] R. N. Mohapatra, Phys. Rev. Lett. **56** (1986) 561; R. N. Mohapatra and J. W. F. Valle, Phys. Rev. D **34**, 1642 (1986).

[58] A. Djouadi, Phys. Lett. B **435**, 101 (1998); R. Dermisek and I. Low, Phys. Rev. D **77**, 035012 (2008); I. Low and S. Shalgar, JHEP **0904**, 091 (2009). I. Low, R. Rattazzi and A. Vichi, JHEP **1004**, 126 (2010); I. Low and A. Vichi, Phys. Rev. D **84**, 045019 (2011).

[59] N. Desai, B. Mukhopadhyaya and S. Niyogi, arXiv:1202.5190 [hep-ph]; D. Carmi, A. Falkowski, E. Kuflik and T. Volansky, arXiv:1202.3144 [hep-ph]; N. D. Christensen, T. Han and S. Su, arXiv:1203.3207 [hep-ph]; R. Benbrik, M. G. Bock, S. Heinemeyer, O. Stal, G. Weiglein and L. Zeune, arXiv:1207.1096 [hep-ph];

N. Arkani-Hamed, K. Blum, R. T. D'Agnolo and J. Fan, arXiv:1207.4482 [hep-ph]; A. Joglekar, P. Schwaller and C. E. M. Wagner, arXiv:1207.4235 [hep-ph]; M. R. Buckley and D. Hooper, arXiv:1207.1445 [hep-ph]; Z. Kang, T. Li, J. Li and Y. Liu, arXiv:1208.2673 [hep-ph].

[60] M. A. Ajaib, I. Gogoladze and Q. Shafi, arXiv:1207.7068 [hep-ph].

[61] C. Panagiotakopoulos and K. Tamvakis, Phys. Lett. B **446**, 224 (1999); C. Panagiotakopoulos and A. Pilaftsis, Phys. Rev. D **63**, 055003 (2001).

[62] G. K. Yeghian, hep-ph/9904488; U. Ellwanger and C. Hugonie, Eur. Phys. J. C **25**, 297 (2002).

[63] G. Degrassi, S. Heinemeyer, W. Hollik, P. Slavich and G. Weiglein, Eur. Phys. J. C **28**, 133 (2003).

[64] Z. Kang and T. Li, arXiv:1111.7313 [hep-ph]

[65] K. S. Babu, I. Gogoladze and C. Kolda, hep-ph/0410085; K. S. Babu, I. Gogoladze, M. U. Rehman and Q. Shafi, Phys. Rev. D **78**, 055017 (2008).

[66] P. S. B. Dev, R. Franceschini and R. N. Mohapatra, arXiv:1207.2756 [hep-ph]. A. Das and N. Okada, arXiv:1207.3734 [hep-ph]; P. Bandyopadhyay, E. J. Chun, H. Okada and J. -C. Park, arXiv:1209.4803 [hep-ph].

[67] M. Hirsch, W. Porod, L. Reichert and F. Staub, arXiv:1206.3516 [hep-ph]; A. Abada, D. Das, A. Vicente, and C. Weiland, arXiv:1206.6497 [hep-ph].

[68] J. R. Espinosa and M. Quiros, Phys. Rev. Lett. **81**, 516 (1998).

[69] A. Delgado, G. Nardini and M. Quiros, arXiv:1207.6596 [hep-ph].

[70] L. Maiani, G. Parisi and R. Petronzio, Nucl. Phys. B **136** (1978) 115; N. Cabibbo and G. R. Farrar, Phys. Lett. B **110** (1982) 107.

[71] K. Agashe, A. Azatov, A. Katz and D. Kim, Phys. Rev. D **84**, 115024 (2011); T. Basak and S. Mohanty, arXiv:1204.6592 [hep-ph]; K. Agashe, Y. Cui and R. Franceschini, arXiv:1209.2115 [hep-ph].

[72] I. Gogoladze, B. He, A. Mustafayev, S. Raza, Q. Shafi, JHEP 05 (2014) 078.

[73] G. Aad *et al.* [ATLAS Collaboration], Phys. Lett. B **716**, 1 (2012).

[74] S. Chatrchyan *et al.* [CMS Collaboration], Phys. Lett. B **716**, 30 (2012).

[75] M. S. Carena and H. E. Haber, Prog. Part. Nucl. Phys. **50**, 63 (2003) and references therein.

[76] I. Gogoladze, Q. Shafi and C. S. Un, JHEP **1208**, 028 (2012); N. Karagiannakis, G. Lazarides and C. Pallis, J. Phys. Conf. Ser. **384**, 012012 (2012); A. Anandakrishnan and S. Raby, Phys. Rev. Lett. **111**, 211801 (2013); M. Adeel Ajaib, I. Gogoladze, Q. Shafi and C. S. Un, JHEP **1307**, 139 (2013); M. Badziak, M. Olechowski and S. Pokorski, JHEP **10**, 088 (2013).

[77] H. Baer, V. Barger, P. Huang and A. Mustafayev, Phys. Rev. D **84** (2011) 091701; H. Baer, V. Barger and A. Mustafayev, Phys. Rev. D **85**, 075010 (2012); A. Arbey, M. Battaglia, A. Djouadi, F. Mahmoudi and J. Quevillon, *Phys. Lett.* **B 708** (2012) 162; M. Carena, S. Gori, N. R. Shah and C. E. M. Wagner, *J. High Energy Phys.* **1203** (2012) 014; S. Akula, B. Altunkaynak, D. Feldman, P. Nath and G. Peim, *Phys. Rev.* **D 85** (2012) 075001; M. Kadastik, K. Kannike, A. Racioppi and M. Raidal, *J. High Energy Phys.* **1205** (2012) 061; O. Buchmueller, R. Cavanaugh, A. De Roeck, M. J. Dolan, J. R. Ellis, H. Flacher, S. Heinemeyer and G. Isidori *et al.*, *Eur. Phys. J.* **C 72** (2012) 2020; J. Cao, Z. Heng, D. Li and J. M. Yang, *Phys. Lett.* **B 710** (2012) 665; K. A. Olive, *J. Phys. Conf. Ser.* **384** (2012) 012010; L. Roszkowski, E. M. Sessolo and Y. L. Tsai, Phys. Rev. D **86**, 095005 (2012).

[78] A. H. Chamseddine, R. L. Arnowitt and P. Nath, Phys. Rev. Lett. **49**, 970 (1982); R. Barbieri, S. Ferrara, and C. A. Savoy, Phys. Lett. B **119**, 343 (1982); L. J. Hall, J. D. Lykken, and S. Weinberg, Phys. Rev. D **27**, 2359 (1983); E. Cremmer, P. Fayet, and L. Girardello, Phys. Lett. B **122**, 41 (1983); N. Ohta, Prog. Theor. Phys. **70**, 542 (1983).

[79] G. Aad *et al.* [ATLAS Collaboration], Phys. Rev. D **87**, 012008 (2013).

[80] S. Chatrchyan *et al.* [CMS Collaboration], JHEP **1210**, 018 (2012).

[81] CMS Collaborations, CMS NOTE -2012/006

[82] M. C. Gonzalez-Garcia, M. Maltoni, J. Salvado and T. Schwetz, JHEP **1212**, 123 (2012).

[83] R. N. Mohapatra *et al.*, Rept. Prog. Phys. **70**, 1757 (2007) [hep-ph/0510213].

[84] R. N. Mohapatra, Phys. Rev. Lett. **56**, 561 (1986); R. N. Mohapatra and J. W. F. Valle, Phys. Rev. D **34**, 1642 (1986).

[85] I. Gogoladze, N. Okada and Q. Shafi, Phys. Lett. B **672**, 235 (2009) [arXiv:0809.0703 [hep-ph]]; I. Gogoladze, B. He and Q. Shafi, Phys. Lett. B **718**, 1008 (2013) [arXiv:1209.5984 [hep-ph]].

[86] J. Guo, Z. Kang, T. Li and Y. Liu, arXiv:1311.3497 [hep-ph].

[87] J. Ellis, K. Olive and Y. Santoso, *Phys. Lett.* **B 539** (2002) 107; J. Ellis, T. Falk, K. Olive and Y. Santoso, *Nucl. Phys.* **B 652** (2003) 259; H. Baer, A. Mustafayev, S. Profumo, A. Belyaev and X. Tata, *J. High Energy Phys.* **0507** (2005) 065.

[88] P. S. B. Dev and R. N. Mohapatra, Phys. Rev. D **81**, 013001 (2010); S. Khalil, Phys. Rev. D **82**, 077702 (2010). Z. Kang, J. Li, T. Li, T. Liu and J. Yang, arXiv:1102.5644 [hep-ph]; S. Khalil, H. Okada and T. Toma, JHEP **1107**, 026 (2011); F. -X. Josse-Michaux and E. Molinaro, Phys. Rev. D **84**, 125021 (2011); H. An, P. S. B. Dev, Y. Cai and R. N. Mohapatra, Phys. Rev. Lett. **108**, 081806 (2012); P. S. Bhupal Dev, S. Mondal, B. Mukhopadhyaya and S. Roy, JHEP **1209** (2012) 110; L. Basso, O. Fischer and J. J. van der Bij, Phys. Rev. D **87**, no. 3, 035015 (2013); S. Banerjee, P. S. B. Dev, S. Mondal, B. Mukhopadhyaya and S. Roy, JHEP **1310**, 221 (2013).

[89] K. S. Babu, I. Gogoladze, M. U. Rehman and Q. Shafi, Phys. Rev. D **78**, 055017 (2008); S. P. Martin, Phys. Rev. D **81**, 035004 (2010) [arXiv:0910.2732 [hep-ph]].

[90] H. Baer, F. E. Paige, S. D. Protopopescu and X. Tata, hep-ph/0001086.

[91] [Tevatron Electroweak Working Group and CDF Collaboration and D0 Collab], arXiv:0903.2503 [hep-ex].

[92] J. Beringer *et al.* [Particle Data Group Collaboration], Phys. Rev. D **86**, 010001 (2012).

[93] H. Baer and M. Brhlik, *Phys. Rev.* **D 55** (1997) 4463; H. Baer, M. Brhlik, D. Castano and X. Tata, *Phys. Rev.* **D 58** (1998) 015007.

[94] D. Eriksson, F. Mahmoudi and O. Stal, *J. High Energy Phys.* **0811** (2008) 035.

[95] G. Aad *et al.* [ATLAS Collaboration], Phys. Lett. B **716**, 1 (2012).

[96] S. Chatrchyan *et al.* [CMS Collaboration], Phys. Lett. B **716**, 30 (2012) and arXiv:1303.4571 [hep-ex].

[97] R. Aaij *et al.* [LHCb Collaboration], Phys. Rev. Lett. **110**, 021801 (2013).

[98] Y. Amhis *et al.* [Heavy Flavor Averaging Group Collaboration], arXiv:1207.1158 [hep-ex].

[99] D. Asner *et al.* [Heavy Flavor Averaging Group Collaboration], arXiv:1010.1589 [hep-ex].

[100] G. Hinshaw *et al.* [WMAP Collaboration], arXiv:1212.5226 [astro-ph.CO].

[101] J. L. Feng, K. T. Matchev and T. Moroi, Phys. Rev. Lett. **84**, 2322 (2000) and Phys. Rev. D **61**, 075005 (2000); J. L. Feng, K. T. Matchev and F. Wilczek, Phys. Lett. B **482**, 388 (2000).

[102] K. L. Chan, U. Chattopadhyay and P. Nath, Phys. Rev. D **58**, 096004 (1998).

[103] H. Baer, I. Gogoladze, A. Mustafayev, S. Raza and Q. Shafi, JHEP **1203**, 047 (2012).

[104] I. Gogoladze, S. Raza and Q. Shafi, Phys. Lett. B **706**, 345 (2012).

[105] M. A. Ajaib, T. Li and Q. Shafi, Phys. Rev. D **85**, 055021 (2012).

[106] B. He, T. Li and Q. Shafi, JHEP **1205**, 148 (2012).

[107] M. Drees and M. M. Nojiri, Phys. Rev. D **47** (1993) 376; H. Baer and M. Brhlik, Phys. Rev. D **53** (1996) 597 and Phys. Rev. D **57** (1998) 567; H. Baer, M. Brhlik, M. A. Diaz, J. Ferrandis, P. Mercadante, P. Quintana and X. Tata, Phys. Rev. D **63** (2001) 015007; A. B. Lahanas, D. V. Nanopoulos and V. C. Spanos, Mod. Phys. Lett. A **16** (2001) 1229; A. B. Lahanas and V. C. Spanos, Eur. Phys. J. C **23** (2002) 185.

[108] J. R. Ellis, T. Falk and K. A. Olive, Phys. Lett. B **444** (1998) 367; J. R. Ellis, T. Falk, K. A. Olive and M. Srednicki, Astropart. Phys. **13** (2000) 181 [Erratum-ibid. **15** (2001) 413]; R. Arnowitt, B. Dutta and Y. Santoso, Nucl. Phys. B **606** (2001) 59; M. E. Gómez, G. Lazarides and C. Pallis, Phys. Rev. D **D61** (2000) 123512; Phys. Lett. **B487** (2000) 313; Nucl. Phys. B **B638** (2002) 165; T. Nihei, L. Roszkowski and R. Ruiz de Austri, JHEP **0207** (2002) 024.

[109] C. Boehm, A. Djouadi and M. Drees, Phys. Rev. D **62**, 035012 (2000); J. R. Ellis, K. A. Olive and Y. Santoso, Astropart. Phys. **18**, 395 (2003); J. Edsjo, M. Schelke, P. Ullio and P. Gondolo, JCAP **0304**, 001 (2003); J. L. Diaz-Cruz, J. R. Ellis, K. A. Olive and Y. Santoso, JHEP **0705**, 003 (2007).

[110] H. Baer, V. Barger, P. Huang, D. Mickelson, A. Mustafayev and X. Tata, Phys. Rev. D **87**, no. 3, 035017 (2013); I. Gogoladze, F. Nasir and Q. Shafi, Int. J. Mod. Phys. A **28**, 1350046 (2013).

[111] N. Okada, S. Raza and Q. Shafi, arXiv:1307.0461 [hep-ph].

[112] E. Aprile *et al.* [XENON100 Collaboration], Phys. Rev. Lett. **109**, 181301 (2012).

[113] The XENON Dark Matter Project `http://xenon.astro.columbia.edu/talks/aprile_ucla_dm2010.pdf/`

[114] `http://cdms.berkeley.edu/APS_Panofsky_130413_Cabrera.pdf/`

Appendix

PERMISSION TO REPRINT PUBLISHED MATERIAL

A.1 Reprint Permission of Content in Chapters 2, 3 and 4

Dear Bin,

Thank you for your e-mail.

Permission is covered by the rights you retain as an Elsevier journal author as outlined at http://www.elsevier.com/about/company-information/policies/copyright# Author%20rights which include Inclusion in a thesis or dissertation, provided that proper acknowledgement is given to the original source of publication. Should you require any further clarification, please let me know.

Best of luck with your thesis.

Laura

Laura Stingelin

Permissions Helpdesk Associate

Elsevier

1600 John F. Kennedy Boulevard

Suite 1800

Philadelphia, PA 19103-2899

T: (215) 239-3867

F: (215) 239-3805

E: l.stingelin@elsevier.com

A.2 Reprint Permission of Content in Chapter 5

This is a License Agreement between Bin He ("You") and Springer ("Springer") provided by Copyright Clearance Center ("CCC"). The license consists of your order details, the terms and conditions provided by Springer, and the payment terms and conditions.

License Number	3645781420431
License date	Jun 11, 2015
Licensed content publisher	Springer
Licensed content publication	Journal of High Energy Physics
Licensed content title	Effects of neutrino inverse seesaw mechanism on the sparticle spectrum in CMSSM and NUHM2
Licensed content author	I. Gogoladze
Licensed content date	Jan 1, 2014
Volume number	2014
Issue number	5
Type of Use	Thesis/Dissertation
Portion	Full text
Number of copies	10
Author of this Springer article	Yes and you are a contributor of the new work
Order reference number	None
Title of your thesis/dissertation	Higgs Phenomenology and New Physics beyond the Standard Model
Expected completion date	Jun 2015
Estimated size(pages)	104
Total	0.00 USD

Table A.1: Springer License Agreement